



Dibris



UNIVERSITÀ DEGLI STUDI DI GENOVA

**Department of Informatics, Bioengineering, Robotics and
Systems Engineering**

Curriculum: Bionanotechnology

**Fabrication of biomedical devices through
electro-fluid-dynamic-based techniques**

PhD student:

Cataldo Pignatelli

Supervisor:

Athanassia Athanassiou

**XXX cycle
(2014-2017)**

Contents

Introduction	1
1. Techniques of fabrication	7
1.1. Electrospinning and Electrospray.....	7
1.1.1 History of EFD-based techniques.....	8
1.2. Basics of EFD-based techniques	10
1.2.1. Taylor cone	10
1.2.2. Jet.....	11
1.2.3. Whipping jet	11
1.2.4. Coulomb fission phase.....	12
1.2.5. Collection	12
1.3. Working parameters	12
1.3.1. Solution or materials parameters.	13
1.3.2. Processing parameters	16
1.3.3. Ambient parameters.....	18
1.4. Versatility of electrospinning and electrospray.....	18
1.5 Characteristics of electrospun fibrous materials.....	19
1.5.1 Characteristics of electrospun fibers applied to the biomedicine	21
1.5.2 Polymeric electrospun fibers	22
1.6. Characteristics of electrosprayed particles	28
1.6.1. Polymeric electrosprayed particles	29
1.7. Bibliography	32
2. Electrospinning of ECA to fabricate aligned surfaces to control cells adhesion.....	42
2.1. Cyanoacrylate adhesives	42
2.1.1. Usage of the cyanoacrylate as biomedical adhesives	45

2.1.2. Poly-ECA coatings through the electrospinning	46
2.2 Organization of skeletal muscle tissue	46
2.2.1 Strategies for skeletal muscle regeneration	48
2.3 Fabrication of aligned ECA coating for myoblast cells alignment	49
2.4. Experimental section	49
2.4.1. PECA electrospinning	49
2.4.2. Fibers characterization.....	50
2.4.3. Cells viability.....	50
2.4.4. Optical and confocal microscope analysis.....	51
2.4.5. Statistical methods	52
2.5. Results and discussion.....	53
2.5.1. Fibers characterization.....	53
2.5.2. Evaluation of coating biocompatibility and cell morphology	54
2.6. Conclusions	58
2.7. Bibliography	60
3. Electrospun silk fibroin fibers for human platelets lysate release.....	65
3.1. Silk fibroin.....	65
3.2. Silk fibroin as biomaterials.....	66
3.3. Platelet-derived proteins	69
3.4. Fabrication of electrospun silk fibroin fibers encapsulating hPL.....	71
3.5. Experimental section	72
3.5.1. Fibroin regeneration.....	72
3.5.2. Fibers fabrication and water vapor treatment	72
3.5.3. Fibers Characterization	74
3.5.4. Drug release assessment	75
3.5.5. Evaluation of the hPL biological activity released from the fibers	76
3.5.6. Statistical methods	78
3.6. Results and discussion.....	79
3.6.1. Fibers characterization.....	79
3.6.2. Evaluation of FITC-albumin release	83
3.6.3. Evaluation of the biological activity of the hPL released the fibers.....	84

3.7 Conclusions	92
3.8 Bibliography	94
4. Polysaccharides-based formulation for oral delivery of curcumin	101
4.1. Curcumin	101
4.2. Oral delivery systems for curcumin	104
4.2.1 Functional, medical and excipient food.....	105
4.2.2 Excipient food-base systems.....	106
4.3. Polysaccharides-based system for improving curcumin bioaccessibility	107
4.4. Experimental section	108
4.4.1. Analysis of the interaction CS/curcumin and Alg/curcumin.....	108
4.4.2. Particles preparation	109
4.4.3. Particles characterization	110
4.4.4. Drug release study	111
4.4.5. Statistical methods	112
4.5. Results and discussion.....	112
4.5.1. Dispersion of curcumin in CS and Alg solutions	112
4.5.2. Particles characterization	113
4.5.3. Curcumin encapsulation	116
4.5.4. Curcumin release characterization.....	117
4.5.5. Acid vapors treatment.....	119
4.5.6. Curcumin release from treated particles	121
4.6. Conclusions	122
4.7 Bibliography	124
5. Conclusions	129
5.1 Final remarks	129

Introduction

Electrospinning and electrospray are techniques used to fabricate respectively fibrous or particles-shaped materials. Both processes are based on the electro-fluid-dynamic (EFD) fundamentals. Both techniques revolve around the application of a high voltage at the tip of a spinneret of a pumped polymeric solution that is able to stretch the droplet that is formed. When conditions like voltage and viscosity of the solution are optimized, a jet leaves the drop, taking the form of a fiber and the technique is called electrospinning; other parameters result in the break of the jet into small droplets, in which case the technique is called electrospray. In both the situations, fibers or particles are accumulated on a grounded collector, after solvent evaporation.

Electrospinning is a technique that dates back in the first years of the 1900 and that recently has been rediscovered to produce fibrous materials with nanoscale structure. Other techniques used to create fibrous materials like wet spinning, melt spinning, dry spinning and gel spinning resulted in fibers with macro and microscale. Thanks to their nanosized structure,

electrospun materials have very interesting characteristics: large surface area, high porosity, wide interconnectivity and small pore size. All these features have been resulted suitable for different technological fields, mainly in biomedicine, filtration, clothing and protective devices. In particular, electrospun fibrous materials had a great impact in biomedical field, because they can mimic the characteristics of the extracellular matrix (ECM), providing scientists with a great tool and enabling applications such as scaffold for tissue engineering and for tissue regeneration. Furthermore, the versatility of electrospinning set up can provide fibrous materials with specific orientation and disposition. A specific topography can control the cell disposition, leading them to arrange and organize themselves in structure that mimic the *in vivo* conditions. Electrospun materials have been also used also as wound dressing, because they allow the transpiration of the wound thanks to their porosity; they can protect the injured site from bacteria which are blocked by the small pore size; they are able to absorb wound exudate, due to the large surface area. Finally, electrospinning can be used to encapsulate drugs with high loading and encapsulation efficiency, a very useful ability, especially for drugs difficult to be loaded on a pharmaceutical carrier.

Electrospray process is currently used in mass spectrometry analysis as a method for producing ions from macromolecules. Recently, electrospray was adapted as a method for the fabrication of polymeric particle-shaped systems. Electrospray can produce, in one step and with a high yield, monodisperse and micro or nanometric particles, with a precise morphology. Such particle systems are self-dispersing in space, due to their highly unipolar charges that induce the repulsion of the particles, preventing their aggregation. Other techniques are used to produce polymeric micro and nanoparticles, such as coacervation, emulsions technique and spray drying. However, few particulate devices have been translated in clinic, due to the shortfalls related to their methods of fabrication. For instance, emulsions are characterized by issues concerning the stability of molecules in presence of solvents.

Moreover, emulsions-based techniques produce particles with broad size distribution, contributing to their lack of reproducibility in molecules release. In fact, obtaining a homogenous particulate formulation would allow a better control on the release kinetics of drugs. As the electrospinning, the electrospray is characterized by high loading capacity and encapsulation efficiency. Therefore, the encapsulation of drugs, independently from their nature (hydrophobic or hydrophilic), is granted.

The advantages of using the electrospinning and the electrospray as methods of fabrication, derive also from the possibility to tune the size and/or the morphology of the materials obtained. By changing the working parameters during the fabrication, the size and the morphology of the systems can be controlled. Then, both the techniques are able to process a wide range of polymers, synthetic and natural, such to exploit their properties (mechanical, different degradation rate, biological activity) in fibrous or particle shaped materials.

In this thesis, both the techniques were used to fabricate biomedical devices. Particularly, electrospinning was used to (1) produce a scaffolds and coatings with a specific topography, able to induce the cells to acquire a precise disposition on the substrate. Furthermore, the electrospinning was exploited to (2) encapsulate a complex pool of growth factors, extracted from the human platelets, namely human platelets lysate (hPL), with the aim to obtain a wound dressing. Finally, the electrospray was applied to (3) fabricate particles systems to encapsulate curcumin for its oral delivery, in order to increase its absorption at the intestinal tract and increase its bioavailability.

In Chapter 1, the electrospinning and electrospray techniques are presented and described, as well as its basics and all the parameters involved in the fibers and particles fabrication. Then, the characteristics and the advantages of the electrospun fibers and electrosprayed particles, especially for biomedical application, are discussed. Successively, some of the synthetic and natural polymers, which can be used in the fabrication techniques are presented.

Chapter 2 shows how the electrospinning technique was exploited to fabricate surfaces with oriented topography. Particularly, a variant of the electrospinning set-up includes a rotating collector on which the fibers were aligned during the deposition. Herein, the highly aligned fibers obtained thanks to this set up, were used to modify surfaces by creating a topography with a preferential alignment. This surface property was exploited as a strategy to control cell disposition. In fact, by controlling the cell disposition, it was possible to mimic the organizations of some tissues and help their growth and *in vitro*. Skeletal muscle tissue is characterized by aligned structures that derive from myoblasts (musculoskeletal cells precursors) differentiation. During this process, myoblasts start to get into line and fuse their plasmatic membranes, leading to the formation of myotubes. They will form the muscle fibers that internally have aligned structures that is functional to the contraction and relaxation of the muscle. Therefore, by aligning myoblasts, *in vitro* functional skeletal muscle tissues can be obtained and, successively, implanted in damage site of patients. Ethyl-2-cyanoacrylate (ECA) was used to produce aligned fibers by using a rotating collector. The aligned fibers were used to modify glass surfaces through a thermal treatment. Upon a melting process, the aligned fibers created a coating characterized by aligned topography which derived from the electrospun fibers arrangement. Myoblast cells were used to evaluate the effect on the viability and morphology of the coatings. Thanks to these experiments, the aligned coatings resulted biocompatible and able to induce the alignment of the cells.

Chapter 3 shows how electrospinning was applied to fabricate fibers by using silk fibroin, in order to encapsulate human platelets lysate (hPL). hPL is a pool of cytokines and growth factors involved in physiological process of the wound healing. Currently, they are used in chronic wounds therapy as a gel. Although the hPL gel is able to release the platelets derived proteins, it is characterized by several limits. The preparation, the application and the handleability of the gel result difficult and are feasible only by qualified personnel. In

addition, since they are sensitive molecules, they can be subjected to degradative processes. Therefore, by encapsulating them within electrospun fibers, it should overcome the limits of hPL gel. In particular, silk fibroin was used because it is a protein characterized by tunable physical and chemical properties and it has the ability to protect the activity of sensitive molecules. Such properties were exploited for controlling the release kinetics of the hPL and preserve its growth factors activity, improving the shelf life of the fabricated device. The characterization of the release of the proteins from the fibrous mats was carried out using FITC-albumin, since Albumin is a component of hPL. Then, the activity of the hPL after the fabrication and after a thermal stress to simulate ageing was evaluated, such to investigate the preserving activity of fibroin toward the hPL growth factors. The investigations have shown that the fibrous patch was able to control the release of proteins and to preserve their biological activity, even after a thermal stress.

Chapter 4 describes how the electrospray has been exploited to produce particles able to encapsulate curcumin. Curcumin is a nutraceutical molecule with antioxidant, anti-inflammatory and anticancer activity that has also a very low bioavailability when it is orally administrated. This is due its insolubility in water, poor absorption at intestinal tract and rapid metabolism of the phase I and II enzymes at intestinal and liver level. To increase curcumin bioavailability, two approaches can be adopted: increase its absorption or inhibiting the metabolism of the phase I and II enzymes. Herein, a polysaccharide-based formulation has been designed in order to increase the absorption of curcumin at the intestinal tract. In particular, cornstarch (CS), alginate (Alg) and low methoxy pectin (LMP) were used in order to increase the bioaccessible concentration of curcumin at intestinal tract. LMP, which is a polysaccharide gastro-resistant, was used as principal polymer for fabricating the system. CS and Alg were used for their ability to act as dispersing agents toward the curcumin, as proved in this chapter. Thanks to the ability of LMP to be cross-linked with Ca^{2+} , CS/curcumin and

Alg/curcumin solutions were encapsulated by electrospraying the polysaccharidic solutions. They were collected in a water bath with calcium chloride. The characterization of the release kinetics was performed by using two different buffers, one simulating the gastric fluid and the other the intestinal fluid. Their usage intended to mimic the passage through the gastrointestinal tract. The results showed that, respect to the LMP:CS formulations, LMP:Alg allowed a higher encapsulation efficiency of the curcumin, a minimum loss of curcumin in the simulated gastric medium, upon a vapors acid treatment, and a better control of the release in the simulated intestinal medium, ensuring a sustained delivery of curcumin.

In chapter 5, final remarks are discussed. They are focused on highlighting the ability of the EFD-based techniques (electrospinning and electrospray) to produce biomedical application with particular topography, and to encapsulate bioactive molecules (hPL through the electrospinning and curcumin through the electrospray). Future investigations are also discussed, and they are about the further development and characterization of the biomedical device obtained.

Chapter 1

Techniques of fabrication

1.1 Electrospinning and Electrospray

Electrospinning and the related process of the electrospray have been widely investigated as techniques for fabrication of biomedical devices¹. Electrospinning is a process in which ultrathin fibers can be obtained, while, through the electrospray particle-shaped systems can be obtained. Particularly, electrospun fibrous systems are used as scaffold for regenerating tissues or as wound dressing, since their particular features are suitable for such kind of biomedical applications^{2,3}. Furthermore, both electrospinning and electrospray can be used as methods to encapsulate poorly water-soluble drugs or bioactive molecules difficult to be loaded into pharmaceutical carriers, with high efficiency^{4,5}.

They are processes based on identical electro-fluid-dynamic (EFD) phenomena that can be reproduced by using the same equipment¹. Their set up consists of a syringe pump, a syringe with a needle, which connected to a power supply, and a grounded collector placed at a

certain distance. A polymeric solution is allowed to flow out from the needle, forming a drop which is stretched by the electrostatic field. In the electrospinning, from the drop, a jet takes the shape of a fiber and, during the flight toward the collector, the solvent tends to evaporate. At the end, the solid fibers are gathered on the collector plate⁶. In the case of the electrospray, after its formation, the jet can be broken such to create droplets, which can be deposited on the collector after the solvent evaporation^{5,7}.

1.1.1 History of EFD-based techniques

Electrospinning and electrospray are dependent on the same physical mechanism, therefore, milestones in their discovery as methods of fabrication are common in some points. The intuition of such processes was based by observing the behavior of liquid subjected to electrical forces. The EFD phenomena were observed for the first time by Sir William Gilbert in the XVI century. He was trying to demonstrate the differences between the electrostatic and the magnetic attractions. He observed that a piece of amber, rubbed with a diamond, was able to exert an attractive force on a water drop, placed on a dry surface. The drop acquired a cone shape and very small droplets were ejected from the tip of this cone. This was the first recorded observation of the electrospray⁸.

Later, in 1745, the professor George M. Bose created an aerosol spray through the application of a high potential to a liquid at the end of a glass capillary tube⁹. Then, Giovanni B. Beccaria, in the 1753, observed that charged liquids evaporate faster than the uncharged ones¹⁰. In 1882, Lord Rayleigh performed some investigations on the stability of electrically charged water drops. He was able to calculate the theoretical charge useful to induce the burst of a drop into smaller droplets¹¹. Moreover, he observed that a moderate electrical charge is able to stabilize an ascending jet of water and if the electrical charge is too high, the stability of the jet is lost¹².

John F. Cooley was the first that intuited the potentiality of the EFD processes, such to exploit them as method of fibrous material fabrication. In fact, in the first of the XX-century, he filed two electrospinning patents^{13,14}. He proposed four type of electrospinning set-ups and also a method to recover the solvent after the electrospinning¹⁵. He had recognized three fundamentals of the electrospinning, which later resulted true also for the electrospray: the fluid should have a suitable viscosity; the solvent should be volatile enough to evaporate and leave the polymer solid; the electric field strength should be in a suitable range to have the deposition on the collector of the materials¹³. In the same period, James W. Morton in 1903 patented a system able to disperse liquid using high voltage source^{10,15}.

In 1917 John Zeleny published a work about the behavior of a fluid at the end of a metal capillary. He photographed and described the electrospray phenomena, and he was the first to attempt to mathematically model the behavior of fluids under electrostatic forces¹⁶.

Anton Formhals from the 1934 to 1944 filed a series of patents. He contributed to the developments of the electrospinning technique toward the commercialization of the process to fabricate textile yarns⁶. In 1938, Natalya D. Rozenblum and Igor V. Petryanov-Sokolov produced electrospun fibers as smoke filter materials for gas masks, which led to the establishment of a factory¹⁷.

The theoretical background of EFD phenomena was finally established by Sir Geoffrey I. Taylor between 1964 and 1969. He contributed to mathematically model the shape of the cone of a water drop under an electrostatic field. Today, this particular shape is known as Taylor cone^{18,19}. In the same period (1968), the electrospray process was introduced by Malcolm Dole as a method for generating gas phase ions in order to determine the mass of polystyrene macromolecules²⁰. The ability of the electrospray to create ions was exploited by Masamichi Yamashita and John B. Fenn to improve the mass spectrometry analysis. In 1984, they published a work in which described for the first time an electrospray ionization mass

spectrometer (ESI-MS)²¹. While the electrospray found its application in mass spectrometry, in the early 1990s, the electrospinning was re-discovered thanks to the work of Doshi and Reneker. They proposed the electrospinning as a potential instrument to produce materials in the nanoscale^{6,19}. Numerous works were published in those years, demonstrating that many organic polymers could be electrospun into nanofibers. Moreover, other studies were also focused on the comprehension and the modeling of electrostatic and fluid-dynamic forces involved in the process²²⁻²⁴. Finally, more recently (in 2005), also the electrospray has been rediscovered as a method for fabricating particles in micro and nanoscale or thin film as well, by electrospaying polymeric solution²⁵⁻²⁸.

1.2 Basics of EFD-based techniques

Electrospinning and electrospray processes can be divided in four stages. Taylor cone, the jet, whipping jet and the collection for the electrospinning (Figure 1.2a)¹⁹; Taylor cone, jet, Coulomb fission phase and collection for the electrospray (Figure 1.2b)^{5,7}.

1.2.1 Taylor cone

This phase is common for electrospinning and electrospray. When a droplet of a charged polymer is at a tip of a needle and an electric field is applied, electrostatic charges are accumulated on top of the droplet. When the repulsion of the charges becomes stronger, the shape of the droplet changes to a cone, called Taylor cone. The cone is the results of the equilibrium between the surface tension of the droplet and the repulsion of electrostatic forces. When the intensity of the electric field is increased, this equilibrium is going to be broken, due to the repulsion of the charges, allowing to a fine and charged jet to leave the tip of the cone.

1.2.2 Jet

In both electrospinning and electrospray, the polymer solution is driven by the electrical stress toward the grounded collector. In this stage, the repulsion of the electrical charges needs to be resisted by the viscosity of the solution in order to have well-formed fibers, otherwise the jet can be broken in droplets, as explained below in the coulomb fission phase. The viscosity during the path toward the collector changes because of the evaporation of the solvent and the change of the temperature. The charges of the jet allow the travel toward the collector in order to close the circuit. The speed of the jet increases as it moves away from the needle. It can be faster with the increase of the applied voltage.

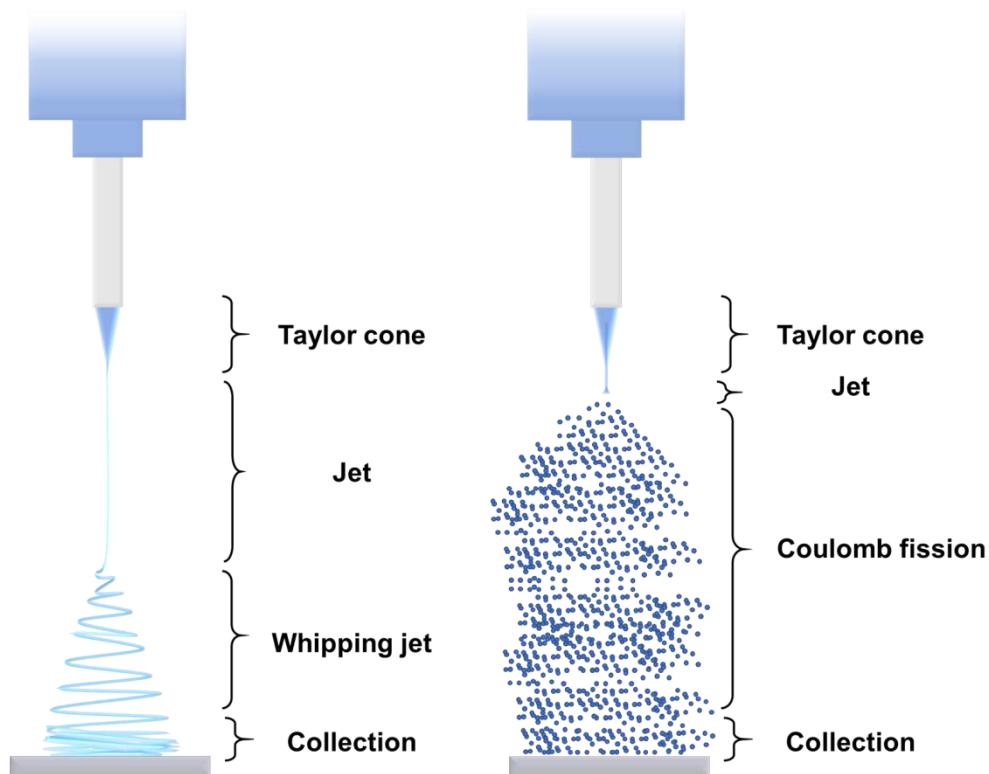


Figure 1.2 The stages that characterize the electrospinning (on the left) and electrospray (on the right) processes

1.2.3 Whipping jet

This phase is present only in the electrospinning. In this step, the jet tends to be bended because of the Coulomb repulsion forces. Therefore, the jet starts to create an irregular coil

but, at the same time, it continues to elongate and to increase its diameter. Due to this mechanism, the solvent completely evaporates, leaving the polymer fiber solid.

1.2.4 Coulomb fission phase

This phase is characteristic of the electrospray process. The jet loses its stability and it is broken in droplets, because the surface tension is very high, and the viscosity cannot equilibrate such forces. During the droplets formation, the solvent starts to evaporate, decreasing the size of the particles that result highly charged. At this step, such particles can be subjected to the Coulomb fission, since the charges tend to repulse each other's, generating further smaller droplets.

1.2.5 Collection

After the solvent evaporation, the fibers or the particles are deposited on a grounded collector, such as an aluminum foil. Sometimes, a water bath can be used to collect the electrospun fibers or electrosprayed particles.

1.3 Working parameters

An optimized protocol of electrospinning or electrospray should be characterized by a stable Taylor cone and should continuously produce fibers or particles^{5,6,29}. Furthermore, in the case of the electrospinning, the fibers should be smooth and beads free, while, for the electrospray, the particles should be smooth at the surface and highly monodispersed. Working parameters play a crucial role in protocol optimization. They consist of all the physical forces that take part of the electrospinning and electrospray processes (surface tension, viscosity, applied voltage, humidity etc.). They need to be balanced such to reach an optimal equilibrium that induces the correct fibers or particles formation. However, once the process is optimized,

working parameters can be manipulated in order to change the morphology and the dimension of the fibers or of the particles^{5,6}. Several studies, about the influence of the working parameters on both the processes, are reported^{5,7,35-44,17,45-54,19,55-57,29-34}. They were divided into three categories⁶:

1. solution properties including viscosity, conductivity, solvent, concentration and molecular weight of the polymer;
2. processing parameters including flow rate, electric field strength, needle-to-collector distance, collector geometry;
3. ambient parameters including temperature, humidity and air flow.

1.3.1 Solution or materials parameters.

The polymer solution is one of the most important variable which affects the electrospinning or the electrospray, and it is the first parameters that needs to be optimized.

a) Concentration

Four critical concentrations have been reported: at very low concentration, the process is not continuous and polymeric particles can be obtained, through the electrospray. This is caused by the high surface tension of the solution³⁹. As the concentration is little increased, fibers with pearl necklace structures are obtained. This structure consists of fibers and beads mixture²⁹⁻³¹. At optimal concentration for the electrospinning, fibers with well-defined morphology and beads-free are obtained²⁹⁻³¹. Finally when the concentration is very high, the process is not continuous and the fibers obtained are micro-ribbons³².

Therefore, to have the production of particles, the concentration should be relatively low. Conversely, to electrospin the polymeric solution, the solution should be concentrated enough to have fibers formation. Both the electrospinning and the electrospray occur in specific range of concentration. If the concentration is changed within such ranges, the dimension of the

fibers or of the particles can be controlled. For instance, by increasing the concentration, the dimension of the fibers or particles is increased^{5,52}.

b) Molecular weight

Molecular weight of the polymer affects the electrospinning and the electrospray processes. In the electrospinning, low molecular weight polymers result in fibers with beads. Contrarily, high molecular weight polymers can produce fibers with larger diameter^{33,58}. In the electrospray, low molecular weight polymers result in not defined particles, while, increasing the molecular weight, well-formed particles can be obtained with a round shape and smooth surface⁵⁹.

The influence of the molecular weight on the processes is due to the increase of the entanglement of polymer chains in solutions, namely solution viscosity, that plays a crucial role both in electrospinning and electrospray.

c) Viscosity

Solution viscosity determines the morphology and the size of the electrospun fibers. At low viscosity beaded fibers are obtained, while, at very high viscosity, the electrospinning process results in hard ejection of the jet from the solution³⁴⁻³⁷. For this reason, a suitable viscosity needs to be found in order to obtain well-formed fibers.

For the electrospray, very low viscous solutions are suitable to obtain particles. In fact, at very low viscosity the surface tension prevails, inducing the formation of particles. If the viscosity becomes too high, the risk is to obtain fibers instead of particles. Therefore, as for the electrospinning, for the electrospray a range of viscosity needs to be found such to produce round shaped and smooth particles.

The viscosity can be tuned by changing the concentration or the molecular weight of the polymer.

d) Solvent

The solvent used to dissolve the polymer can also affect the electrospinning and the electrospray. The solvent characterizes the surface tension of the solution. A previous study investigated the influence of the solvent on the fibers morphology. At fixed concentration, by changing the solvent in order to induce a decreasing in surface tension, smooth fibers were obtained³².

In the electrospray the solvent should be highly volatile such to have dry particles. However, too high volatile solvents can generate undesired particles morphology⁵. If the evaporation occurs rapidly, the polymer chains in the droplets cannot have the time to rearrange, leading to the formation of polydisperse particles with porous or hollow morphology⁵.

e) Conductivity

For the electrospinning, the conductivity of the solution can change the dimension of the fibers. It can be dependent on polymer, on solvent or on salt. Natural polymers generally present charges that help the stabilization of the jet and the fibers formation, unlike the synthetic polymers that are poorly charged⁵³. In addition, ionic materials can be added to the solution in order to increase its conductivity. By increasing the conductivity of the solution, smaller fibers can be obtained, and beads formation can be suppressed³⁸.

As for the electrospinning, also for the electrospray the conductivity affects the size of the particles. In fact, higher conductivity allows the fabrication of smaller particles. However, very high conductivity results in unstable electrospray process and elongated particles. On the other hand, too low conductivity impedes the solution to be sensible to the electrostatic forces⁵.

1.3.2 Processing parameters

a) Applied voltage

The applied voltage is indispensable to have the electric field, which generates the EFD processes. During the electrospinning, when the applied voltage surpasses a threshold voltage, it induces the formation of the Taylor cone and the ejection of the fiber. The influence of the applied voltage on the fibers morphology is not univocal, as for the other parameters. Previously, different works have shown that increasing the strength of the electric field resulted in beads formation³⁹⁻⁴¹, in thinner⁴² or even thicker⁴³ fibers. Contrarily, other studies have showed no influence on the fibers size¹⁹. Overall, the influence of the applied voltage can depend on the nature of the polymer solution and on the distance between the tip and the collector⁴⁴.

Also for the electrospray, the electrostatic field is important to induce the formation of the Taylor cone and the formation of particles⁵. By increasing the applied voltage, the particles are more elongated⁵⁴. While, low voltage results in a non-continuous jet which produce large and irregular particles. Therefore, a “working” range needs to be individuated such to have a stable electrospray process⁵.

b) Flow rate

The flow rate of the polymer solution in the syringe pump is another parameter to be considered for the optimization of the electrospinning and electrospray. For the electrospinning, the flow rate should be low enough to allow the polymer in the Taylor cone to respond to the electric field, such to be electrospun. Upon the increase of the flow rate, the fibers can be thicker. However, the system can result unstable, inducing the formation of beads¹⁷.

Similarly, the flow rate during the electrospray should be slow for permitting the evaporation of the solvent. By increasing the flow rate, the particles result larger and the size distribution become broader⁵⁵.

c) Needle-collector distance

The distance between the tip of the needle and the collector is important to have well-formed electrospun fibers³⁶. Too short distances can prevent the complete evaporation of the solvent, whereas too long distance can induce the formation of pearl necklace structures. Nevertheless, in some previous work, increasing the distance can promote the formation of thinner fibers⁴². Therefore, to obtain dry and well-formed fibers, a suitable distance between the needle and the collector needs to be found.

During the electrospray, shorter distances increase the strength of the electrostatic field, obtaining smaller particles. However, it can impede the total evaporation of the solvent. On the other hand, increasing the distance, the system has more time to complete the evaporation, but the applied voltage needs to be consequentially increased, resulting in larger particles⁵.

d) Collectors

The collector is the target where the fibers or the particles are deposited. It has to be a conductive material and, usually, it is an aluminum foil. Since the fibers can adhere on the aluminum foil, other kind of collector can be used, such as parallel bars⁴⁵, wire mesh⁴⁶, grids⁴⁷ and liquid bath⁴⁸. Furthermore, a rotating collector allows the fibers to be aligned⁴⁵. The alignment of the fibers occurs due to the rotation of the collector, which forces their deposition in only one direction. The rotation speed of the collector can affect the alignment degree and, generally, higher rotation speed increases the alignment. Then, by increasing the velocity, the fibers can result thinner because of the stretching forces of the rotating collector⁴⁹.

The electrospray can have an aluminum foil, as for the electrospinning. Very often, a liquid bath is used to collect the particles, in which different solvent or aqueous solutions can be used^{56,57}.

1.3.3 Ambient parameters

The temperature and the relative humidity are the ambient parameters. The temperature is critical because can change the viscosity of the solution, obtaining smaller fibers and smaller particles^{5,50}. In the electrospinning, the relative humidity can intervene in the rate of the solvent evaporation. Low relative humidity induces a rapid and total evaporation of the solvent; high relative humidity retards the solvent evaporation obtaining thicker fibers and changes in the single fiber surface. The latter effect is investigated to increase the already large surface area of the electrospun fibers⁵¹.

1.4 Versatility of electrospinning and electrospray

One of the advantage of the EFD-based techniques is their versatility in obtaining fibers or particles with particular structures, such as core-shell, bicomponent and hollow systems. This kind of materials can be obtained by using specific needle, changing the solvent or the ambient conditions⁶⁰.

To obtain systems with core-shell structure, a coaxial needle is used. Basically, the process of fabrication is the same, but it is modified at the needle which is coaxial. It consists of one spinneret inside another one, through which two different polymeric solutions can flow. Therefore, two syringe pumps work individually. In this way, it is possible to have fibers or particles made up of two different polymers. These structures are mostly used as systems for releasing drugs that can be encapsulated in the two phases^{5,61}.

Hollow fibers or particles can be obtained using the same set-up with the coaxial. The core of fibers can be selectively dissolved in a solvent, in which the shell polymer component is not soluble. Therefore, removing the core part, hollow fibers can be produced. Hollow particles can be obtained by using only a solvent in the core phase that evaporates during the spray, leaving the internal part empty⁶². Hollow systems are useful for fluidics, energy conversion or drug delivery^{9,63}.

Electrospinning is used to produce fibers starting from an emulsion, both water-in-oil and oil-in-water. With the emulsions, the single nozzle spinneret is used. Depending on the property of the emulsion, core-shell fibers can be obtained⁶⁴. However, if the conditions are not optimal for producing core-shell structures, the emulsion can be electrospun fabricating fibers with dispersed phases⁶¹. Emulsions can be electrospayed as well, by using a single nozzle spinneret. Particles can be obtained with dispersed phases⁶⁵.

1.5 Characteristics of electrospun fibrous materials

Electrospun fibrous materials are nanometric systems with size ranged from 50 and 500 nm⁶⁶. However, depending on the working parameters and on the polymers used, fibers in microscale can be obtained as well. The small diameter of the fibers provide electrospun fibers with increased surface to volume ratio of 1000 times respect the microscale systems⁶⁷. They are characterized by a high molecular alignment, which derives from the very large spin draw ratio, induced by the stretching of the fibers⁵³. In addition, such materials can be chemically functionalized modifying their surface, or by adding, directly to the solution, doping agents, before the fibers fabrication⁶⁷.

Generally, the traditional fibrous materials (in the microscale), such as carbon, glass and Kevlar fibers, are used as reinforcement for composite materials. Electrospun nanofibrous materials have shown to ensure for composite materials better mechanical properties (e.g.

stiffness and tensile strength) than microfibers. For instance, electrospun Nylon-4,6 nanofiber non-woven membrane was used to fabricate nanocomposites with epoxy matrix. The nanocomposites resulted in a significant increase of stiffness and strength respect to the epoxy matrix without Nylon nanofibers. However, few works are about the use of electrospun materials as mechanical reinforcement, since they have non-woven mesh and a limited amount of low uniaxial and continuous fibers, which do not grant significant mechanical improvement⁶⁸. In addition, they can fail the integration with the surrounding materials of the composite^{58,67}.

Electrospun fibrous materials have found wide application as filtration means, because they showed to increase filtration efficiency^{67,69}. In fact, their high interconnectivity, high porosity and the small pore size allow high volume permeability, a better withstand fouling and filtration of submicron particles⁵⁸. Another strategy to increase the filtration efficiency is the modification of the fibers surface, such to have molecular filters. Therefore, the chemical modification of the high surface area of the fibers can be exploited to improve the detection of chemical and biological agents^{70,71}. Electrospun fibrous materials are also used in dust filters. They can consist of three overlapped layers, in whose mid-layer nonwoven nanofibers are used. Polyacrylonitrile membranes have been developed with this aim⁵⁸. The same three-overlapped-layers structures have been adopted as protective devices. In fact, their ability in filtering nanometer substances was exploited in development of protective clothing^{72,73}. Moreover, their low impedance to the moisture provides electrospun materials with advantages on the activated carbon, currently used as protective devices, which are poorly permeable to the water vapor⁵⁸.

Finally, the high surface area of the electrospun fibers can be exploited in conductive devices, because the electrochemical reactions occur with a rate that is proportional to the available surface of the electrode. Therefore, electrospun materials are used to design high performant

batteries⁷⁴. Conductive (in terms of electrical, ionic and photoelectric) nanofibrous materials also have potential for applications including electrostatic dissipation, corrosion protection, electromagnetic interference shielding, photovoltaic device, etc^{75,76}.

1.5.1 Characteristics of electrospun fibers applied to the biomedicine

The success of the electrospun materials in biomedical application is related to their good interaction with the cells and the physiological environment. This is because of their properties^{3,77-79}. The fibrous structure can mimic the ECM, which consists of fibrillar glycoproteins and polysaccharides. *In vivo*, the cells are attached to the ECM thanks to which they can grow, proliferate, differentiate and migrate. Furthermore, the fibrous shape of electrospun materials lends a higher surface area to them, allowing more adhesion of the cells on the substrate. Their intrinsic porosity allows the nutrients to pass through the materials, reaching the cells attached on the substrate. Moreover, the porosity permits the gas exchange and transpiration of the site covered by the fibers, which is useful when they are used as wound dressing. The surface roughness or the topography of the fibrous materials can be exploited, especially when the fibers are aligned. Such oriented surfaces can be used to force the cells to acquire a specific orientation. This effect can be useful for mimicking the cells disposition of some tissues^{80,81}. In addition aligned fibers have also shown that are more tolerated than the random ones, because their topography was able to minimize the response against the scaffold *in vivo*⁸².

Electrospun fibers can be loaded with drugs during the electrospinning, obtaining high drug loading (up to 60%) and encapsulation efficiency (up to 100%)⁸³. Different drugs have been encapsulated in fibrous devices, both hydrophilic and hydrophobic. Particularly, the electrospinning is used when the drug is difficult to be embedded in a releasing system. This is possible because during the fabrication the drug is forced to remain on the fibers after the

evaporation of the solvent. Moreover, by encapsulating two or more drugs, electrospun fibers allow their simultaneous release^{4,61,84}.

Finally, electrospun fibrous materials are characterized by cost-effectiveness and ease fabrication. Therefore, their usage as biomedical device, should decrease the cost of the therapies.

1.5.2 Polymeric electrospun fibers

Generally, the materials for the biomedical application, need to be biocompatible and no toxic. In addition, they should be biodegradable and the secondary products, derived from their degradation, need to be well tolerated and eliminated or resorbed by the organism. In some cases, the materials should have specific mechanical properties, which should be as similar as the mechanical properties of the injured site⁸⁵. These guidelines are also valid for the fabrication of electrospun materials aimed to biomedical application. Therefore, beside the ability to be electrospun, polymers should have these characteristics.

Synthetic and natural polymers are both used to produce electrospun fibers for wound healing, drug delivery and tissue engineering. The choice depends on the final application.

- **Synthetic polymeric fibers**

Synthetic polymers have been the first type of polymers used in the electrospinning because they are easier to be electrospun with the solvent and were more available than the natural polymers, when the electrospinning was re-discovered^{6,38}. Synthetic polymers became attractive for medical application because their mechanical and physical properties can be modified, depending on the monomers unit or upon the polymerization of co-polymers⁸⁶. Synthetic polymers can be also chemically modified in order to further change their characteristics⁸⁷. For this reason, they are considered flexible and their characteristics

adjustable. Moreover, since the polymerization and functionalization methods are mostly established and well-known, their processability and usage result easy⁸⁷.

Synthetic polymer, such as poly(lactide-co-glycolide) (PLGA), poly(L-lactide) (PLLA), polycaprolactone (PCL) or polyurethanes (PU), can be subjected to degradation through hydrolysis^{88,89}. Polymer hydrolysis processes occur through the same mechanisms, independently from the patient, in which they are used^{88,90-92}. So, their behavior *in vivo* can be anticipated and studied. For instance, PLLA polymer degrades hydrolytically into lactic acid, which is a human metabolite. So, it is broken down into water and carbon dioxide via the citric acid cycle⁹³. However, in several cases, as the PLGA, the hydrolytic degradation produces acidic secondary products that can alter the pH of the surrounding environment⁸⁸. Other polymers, as poly(trimethylene carbonate) (PTMC), polyphosphoesters and poly(alkyl cyanoacrylate) (PACA) can be subjected to both the degradation mechanisms⁹⁴⁻⁹⁶. In any case, the immunogenicity of the secondary products should be investigated before to use them for the biological application⁹⁷.

The degradation rate of the polymers can make them suitable for one application or for another. Generally, polymers which have fast degradation (from minutes to few days) are used for drug delivery and/or wound healing, whereas polymers with slow degradation (one month to at least one year) are applied as scaffold for tissue engineering. For instance, the rate of degradation of PCL is rather slow (2–3 years), such to be extensively investigated as scaffolds for tissue engineering. On the other hand, PLLA, PLGA or PTMC were widely investigated as materials for drug delivery system, since their fast degradation rate *in vivo*⁸⁸. There are also synthetic polymers that are resistant to the biodegradability but kept their biocompatibility. This kind of polymers can be used for application where permanent polymeric supports are required, such as dental, corneal or articular cartilage implants⁹⁸.

For some kind of synthetic polymers, the degradation rate can be modified. The ratio between the monomers, which constitute the PLGA (lactic and glycolic acid), can affect the degradation rate, resulting in different releasing system, by using the same polymer⁹⁹. Decreasing the molecular weight of PTMC, its degradation rate is accelerated⁹⁶. For PLLA, by increasing its crystallinity, slower degradation rate is obtained⁸⁸.

Synthetic polymers are characterized by different mechanical properties. Sometimes, there is the necessity to use a specific mechanical property, depending on the application. For instance, poly-alkyl-cyanoacrylate (PACA) are a group of polymers with important adhesives. Among them, poly(ethyl-2-cyanoacrylate) (PECA) is used as a fixative for bone tissue, due to its high strength bond, while poly(octyl-2-cyanoacrylate) (POCA) as a tool for wound closure because can ensure flexibility to the site^{100,101}.

Synthetic polymers showed several disadvantages, which can limit their use in biomedicine. Part of the synthetic polymers, such as PCL, PLGA, PLA, PACA, are insoluble in water; therefore, they need to be process with organic solvents. The possibility to find traces of solvents in the electrospun fibers, after the fabrication, can make more difficult their application in the biomedicine¹⁰². In addition, water-based polymers are better tolerated by the organism, and this can improve the cell adhesion and allow the delivery of drugs in aqueous environment¹⁰³. In addition, hydrophobic synthetic polymers lack domains able to facilitate the adhesion of cell or their migration. Plasma treatment or functionalization with poly-lysine can be performed to support the cells dissemination^{104–106}. Another strategy for increasing the cells adhesion is to fabricate blends of synthetic polymers with proteins or proteins domains. Tripeptide arginine-glycine-aspartate (RGD) is the binding domain of the fibronectin recognized by the cells *in vivo*. Addition of RGD tripeptide or protein of the ECM, such as collagen or elastin, is a strategy used to support the cells attachment^{107–109}. However, the addition of proteins with the synthetic polymers can alter the protein folding, since the solvent

used in the electrospinning process are mostly organic. Therefore, using water-based polymers, such as poly(ethylene oxide) (PEO), poly(vinyl alcohol) (PVA) or natural ones, can make easier the integration with proteins¹¹⁰⁻¹¹².

- **Natural polymeric fibers**

Natural polymeric fibers are produced using proteins or polysaccharides present in the human or extracted from animal or plants source. Using natural polymer for biomedical application allows the possibility to fabricate device which mimic as much as possible the property and the composition of the ECM. Generally, these polymers have in nature fibrillar structure. Therefore, during the process they easily self-assemble in fibrous structures, such to obtain systems with improved ability in ECM mimicking¹¹³. Moreover, several natural polymer present intrinsic biological properties, such as anti-inflammatory or antibacterial, which can be exploited in biomedicine.

Among these polymers, components of the ECM were used as materials to fabricate biomedical devices. Collagen, for instance, is the most abundant protein of the ECM, especially in skin and musculoskeletal tissues⁸⁸. It has structural role and supports the cells in adhesion and proliferation processes. Moreover, it has also hemostatic activity, because is one of the primary initiators of the coagulation cascade. Therefore, electrospun scaffold or wound dressing are collagen-based in order to exploit its biological activity⁸⁸. Hyaluronic acid (HA) is another components of the ECM and it is used as biomaterial^{88,114}. HA is a polysaccharide which is prevalently present in the ECM of connective tissues. Besides having a structural role, it can be involved in cell migration, proliferation and metabolism, as well as in metastasis, wound healing and inflammation¹¹⁵.

Contrary to the synthetic polymers, the processability of these kind of natural polymers by the electrospinning is poor and less versatile^{9,116}. In fact, to improve the electrospinnability of collagen, organic solvents such as hexafluoro-2-propanol (HFIP), is preferred, although

concerns have been arisen on the safety and possible effects on protein denaturation^{114,116}. In fact, HFIP helps the solubility of natural polymer due to strong hydrogen-bonding properties and its ability to break hydrophobic interactions^{17,102}. Another possibility is to add to the natural polymers solution, synthetic polymers (PEO, PCL, PVA). In this case, the fibers result in a blend of synthetic and natural polymers⁹.

Polymers of the ECM, when used as biomaterials in biomedical devices, are subjected to degradation, mostly via enzymes. Collagen are processed by the collagenase and metalloprotease which are present in human tissue. HA are degraded by metalloprotease, but also by free radical and nitric oxide^{117,118}. Strategies in getting slower the degradation of HA, include its cross-linking – by using diepoxy, carbodiimide-mediated, aldehyde, divinyl sulfone, and photo-crosslinking – that induces the formation of hydrogel¹¹⁹.

Beside their numerous advantages, polymers of the ECM have problem of safety, concerning their extraction, which can make difficult their usage. In fact, collagen and HA are obtained from animal source (bovine, porcine or rooster) which can create problem of immunogenicity⁸⁸. In the case of collagen, the purification of allogeneic material has high cost and can have the risk to transmit infection⁸⁸. Therefore, new strategies are currently under development: use of bacteria to synthesize this kind of polymer is a solution to bypass their safety problems^{88,120}.

Other example of natural polymers, existing in human organism, for fabricating fibers, are elastin and fibrinogen. Elastin is a protein of the vascular and lung tissue, which is responsible of the impressive elasticity of this tissues⁸⁸. It is a highly crosslinked insoluble polymer, which derives from the assembling of its precursor, the tropoelastin. Allogeneic elastin have shown to induce the immune response¹²¹. Therefore, elastin resulted poorly available for producing fibers. To surpass these limits, elastin obtained by the assembling of recombinant

tropoelastin is used^{121,122}. As for the collagen, its electrospinning occurs by using HFIP solvent¹²².

Fibrinogen is a blood protein, involved in coagulation cascade. Its lysis results in formation of the fibrin fibers, which are insoluble, leading to the clotting formation^{88,114}. Fibrinogen promotes cells adhesion and migration thanks to the presence of the RGD binding domain for cells¹²³. Also for the fibrinogen, HFIP is used to obtain fibers through the electrospinning¹²⁴. However, its high solubility makes the polymer difficult to be used. By crosslinking it, through glutaraldehyde or genipin, the stability in aqueous environment can be increased¹²³.

Natural polymers derived from animal or plant source are also used to fabricate electrospun fibers. Chitosan is a polysaccharide obtained from the deacetylation of the chitin extracted from the exoskeleton of the arthropod or from the fungi cell wall¹²⁵. Depending on the acetylation degree, the properties of the chitosan can change: high deacetylated chitosan is characterized by slow degradation rate *in vivo*¹²⁶. Chitosan is soluble at weakly acid pH resulting in formation of cationic polymers. The presence of the positive charge provides the chitosan with mucoadhesion property and antibacterial activity^{127,128}. Moreover, it has shown to stimulate macrophages and to be chemoattractive toward the neutrophils¹²⁹. Due to its solubility at acid pH, the electrospinning of chitosan is performed with acid solutions, such as diluted hydrochloric acid, acetic acid, formic acid and trifluoroacetic acid (TFA)^{130,131}. TFA is prevalently used because it is more volatile¹²⁵. However, the viscosity and the surface tension resulted too high to form fibers, because of the strong repulsive forces among the positively charged chains^{125,132}. Therefore, it was electrospun by adding HFIP solvent or other synthetic polymers, such as PVA and PEO,^{125,131}.

Alginic acid is another polysaccharide used to fabricate electrospun devices. It is extracted from the brown algae or it can be synthesized by some bacteria¹³³. It is mostly used as sodium alginate which is negatively charged and therefore water soluble. However, the aqueous

solution results highly viscous¹¹⁴. As for chitosan, the addition of PEO or PVA can decrease the repulsive forces among the polyanionic alginate chains, such to facilitate the electrospinning process and obtain continuous fibers¹¹⁴. Due to its high solubility in water, alginate cannot be used in biomedical application. Therefore, cross-linking of alginate with Ca^{2+} decreases its solubility in aqueous solutions, resulting more stable¹¹⁴.

Silk fibroin is a structural protein extracted from the cocoons of silkworms¹³⁴. Naturally, fibroin is not soluble in water due to the presence of hydrophobic amino acids in its sequence, which self-assemble in hydrophobic β -sheets secondary structure¹³⁴. Fibroin is characterized by low immunogenicity and good mechanical properties, such as elasticity, strength and toughness. Its degradation rate is slow *in vivo*, but it can be controlled through the manipulation of its crystallinity^{102,135}. Protocol to extract fibroin from the cocoons have been optimized, providing water soluble fibroin, through the denaturation of the protein chains¹³⁶. PEO is added to the fibroin, in order to reach a suitable viscosity and facilitate the electrospinning process¹³⁷. However, silk fibroin fibers are also obtained by using HFIP or TFA^{35,137–139}.

1.6 Characteristics of electrosprayed particles

Electrosprayed particles are mainly used as system for releasing drugs. Their usage as carriers is possible because they can have an elevated encapsulation efficiency ($\approx 100\%$). When a water bath is used as collector, the encapsulation efficiency decreases, but remains high if compared to other methods for fabricating particles (coacervation, emulsion)⁷.

The kinetic release of pharmaceutical systems depends on the materials used, but also on their dimension and morphology⁷. The particles obtained from an optimized electrospray process can result in the microscale or nanoscale^{5,7}. Moreover, they are highly monodispersed and round shaped¹⁴⁰. The properties of the electrosprayed particles are functional to have a fine

control on the drug release, in order to have reproducible release profiles¹⁴¹. This can be granted by the monodispersion of particles obtained from the optimized electrospray process. Furthermore, decreasing the particles dimensions, the surface to volume ratio increases, allowing a higher release of the loaded drug respect to formulation in the macroscale^{5,7,52}. Finally, the round morphology allows the possibility to better control the release of drugs⁷. In fact, wrinkled particles can have a considerable burst release, due to their porosity¹⁴², while round shape particles have a more controlled and sustained release, due to the erosion which occur at the particles surface. However, as mentioned above, the kinetic release can be affected by the properties of electrosprayed particles, but the it is principally dependent on the polymer type used in the fabrication as well as the nature of the drug⁷.

1.6.1 Polymeric electrosprayed particles

Polymers used to produce particles for drug release application need to be biocompatible. To release drugs, polymers need to be subjected to hydrolytic or enzymatic degradation. In addition, for electrosprayed particles, the polymers should be suitable for being electrosprayed. As for the electrospinning, the electrospray can be used a wide range of polymers. However, since it is more recent than the electrospinning, only few polymers have been used to produce particles for drug release.

- **Synthetic polymeric particles**

The most frequently polymer used in electrospray is PLGA⁷. As explained before, it can be subjected to hydrolytic degradation and thanks to the possibility to manipulate its composition, the degradation rate can be tuned, such to control the delivery of encapsulated drugs¹⁴³. However, its acidic degradation provokes the acidification of the surrounding environment or can lead to the alteration of the bioactivity of the drug¹⁴⁴. Nevertheless, the PLGA remains the most common polymer to produce electrosprayed particles^{142,145-149}.

PLA polymers have been also used to fabricate particles through the electrospray. PLA allows a slower degradation, due to its higher crystallinity¹⁵⁰. In a previous work, it was used as shell for a PLGA core, such to have a more controlled release^{150,151}.

PCL was also electrosprayed such to obtain particles. PCL can be highly permeable toward small drug molecules. Moreover, it is subjected to hydrolytic degradation, but without the formation of acid compounds. However, the degradation rate is too slow *in vivo*⁸⁹. In addition, the hydrophobicity of the PCL precludes the encapsulation to hydrophilic bioactive molecules, and makes difficult the loading of hydrophilic ones such as proteins, growth factors or enzymes¹⁵². To overcome such limitations, co-polymers of PCL with hydrophilic blocks (polyamino ethyl ethylene phosphate, PPE-EA), was synthesized, with the aim to decrease its hydrophobicity and accelerate its degradation rate¹⁵³.

Polyvinylpyrrolidone (PVP) is a water-soluble polymer, which was used to fabricate particles in the nanoscale. Through the electrospray of the PVP, several drugs were encapsulated: quercetin¹⁵⁴ and ketoprofen¹⁵⁵. However, their release resulted very fast (less than 1 minute)^{7,154,155}. To prevent the fast release of the drug, PVP was electrosprayed with surfactant, such to avoid the immediate release^{156,157}, or with other polymers, such as PLGA or PCL¹⁵⁸.

- **Natural polymeric particles**

Protein and polysaccharides polymers were electrosprayed, such to obtain particles systems. Elastin-like protein was electrosprayed in order to control the release of drug. The solubility of such protein is dependent on the pH. Therefore, the release of the drug occur in a pH-dependent manner¹⁵⁹.

Chitosan was also used to produce electrosprayed particles. As mentioned for the electrospinning, the degradation rate of chitosan depends on its deacetylation¹²⁶. Chitosan is subjected to enzymatic degradation *in vivo*, and its resulting metabolites are resorbed by the

organism¹⁶⁰. Chitosan was used to encapsulate ampicillin¹⁶⁰, doxorubicin⁵⁴ and insulin¹⁶¹. Chitosan particles can be also obtained by using a water bath as collector, containing tripolyphosphate (TPP), which is able to cross-link the chitosan^{54,162}.

Alginate particles are obtained by electro spraying its solution in a water bath with CaCl₂^{163,164}. In this way the alginate is cross-linked, forming the particles. Alginate cannot be enzymatically degraded *in vivo* but can response to pH change. In particular, swelling of alginate particles occurs at basic pH inducing the release of drugs, while, at acid pH the particles can be shrunk preventing the release and protecting the encapsulated drugs. Thanks to these properties, electro sprayed alginate particles were used for oral delivery of protein and vaccines^{163,164}. Alginate was also used to encapsulate through the electro spray enzymes¹⁶⁵, adenovirus-based vector for human gene therapy¹⁶⁶ and even cells, for cell therapy¹⁶⁷.

1.7 Bibliography

1. Rodríguez-Tobías, H., Morales, G. & Grande, D. in *Nanofiber Research - Reaching New Heights* (InTech, 2016). doi:10.5772/63470
2. Lannutti, J., Reneker, D., Ma, T., Tomasko, D. & Farson, D. Electrospinning for tissue engineering scaffolds. *Mater. Sci. Eng. C* **27**, 504–509 (2007).
3. Zahedi, P., Rezaeian, I., Ranaei-Siadat, S.-O., Jafari, S.-H. & Supaphol, P. A review on wound dressings with an emphasis on electrospun nanofibrous polymeric bandages. *Polym. Adv. Technol.* **21**, 77–95 (2010).
4. Hu, X. *et al.* Electrospinning of polymeric nanofibers for drug delivery applications. *J. Control. Release* **185**, 12–21 (2014).
5. Nguyen, D. N., Clasen, C. & Van den Mooter, G. Pharmaceutical Applications of Electrospinning. *J. Pharm. Sci.* **105**, 2601–2620 (2016).
6. Doshi, J. & Reneker, D. H. Electrospinning process and applications of electrospun fibers. *J. Electrostat.* **35**, 151–160 (1995).
7. Bock, N., Dargaville, T. R. & Woodruff, M. A. Electrospinning of polymers with therapeutic molecules: State of the art. *Prog. Polym. Sci.* **37**, 1510–1551 (2012).
8. Gilbert, W. & Thompson, S. P. C. N.-Q. . G. 1900a. *On the magnet. The Collector's series in science* (1958).
9. Greiner, A. & Wendorff, J. H. Electrospinning: A fascinating method for the preparation of ultrathin fibers. *Angewandte Chemie - International Edition* **46**, 5670–5703 (2007).
10. Morton W.J., M. of D. F. Method of Dispersing Fluids. *US Pat. 705, 691*, (1902).
11. Rayleigh, Lord. XX. On the equilibrium of liquid conducting masses charged with electricity. *Philos. Mag. Ser. 5* **14**, 184–186 (1882).
12. Fell, G. The influence of electricity on protoplasm. *Amer. Mon. Microsc. Journal.* **28**, 1–34 (1890).
13. Cooley, J. F. Apparatus for electrically dispersing fluids. US Patent 692,631. *US Patent 692,631* 1–6 (1900).
14. Cooley, J. F. Electrical method of dispersing fluids. US Patent 745,276. *US Patent 745,276* 1–5 (1903).
15. Tucker, N., Stanger, J., Staiger, M., Razzaq, H. & Hofman, K. The History of the Science and Technology of Electrospinning from 1600 to 1995. *J. Eng. Fiber. Fabr.* **7**, 63–73 (2012).
16. Zeleny, J. The electrical discharge from liquid points, and a hydrostatic method of measuring the electric intensity at their surfaces. *Phys. Rev.* **3**, 69–91 (1914).
17. Bhardwaj, N. & Kundu, S. C. Electrospinning: A fascinating fiber fabrication technique. *Biotechnology Advances* **28**, 325–347 (2010).
18. Taylor, G. Disintegration of Water Drops in an Electric Field. *Proc. R. Soc. A Math. Phys. Eng. Sci.* **280**, 383–397 (1964).

19. Reneker, D. H. & Chun, I. Nanometre diameter fibres of polymer, produced by electrospinning. *Nanotechnology* **7**, 216–223 (1996).
20. Dole, M. *et al.* Molecular Beams of Macroions. *J. Chem. Phys.* **49**, 2240–2249 (1968).
21. Yamashita, M. & Fenn, J. B. Electrospray ion source. Another variation on the free-jet theme. *J. Phys. Chem.* **88**, 4451–4459 (1984).
22. Spivak, A. F., Dzenis, Y. A. & Reneker, D. H. Model of steady state jet in the electrospinning process. *Mech. Res. Commun.* **27**, 37–42 (2000).
23. Reneker, D. H. & Yarin, A. L. Electrospinning jets and polymer nanofibers. *Polymer* **49**, 2387–2425 (2008).
24. Bellan, L. M., Craighead, H. G. & Hinstroza, J. P. Direct measurement of fluid velocity in an electrospinning jet using particle image velocimetry. *J. Appl. Phys.* **102**, 094308 (2007).
25. Salata, O. Tools of Nanotechnology: Electrospray. *Curr. Nanosci.* **1**, 25–33 (2005).
26. Jaworek, A. Electrostatic micro- and nanoencapsulation and electroemulsification: A brief review. *Journal of Microencapsulation* **25**, 443–468 (2008).
27. Ciach, T. Application of electro-hydro-dynamic atomization in drug delivery. *Journal of Drug Delivery Science and Technology* **17**, 367–375 (2007).
28. Jaworek, A. & Sobczyk, A. T. Electro spraying route to nanotechnology: An overview. *J. Electrostat.* **66**, 197–219 (2008).
29. Fong, H., Chun, I. & Reneker, D. H. Beaded nanofibers formed during electrospinning. in *Polymer* **40**, 4585–4592 (Elsevier, 1999).
30. Eda, G. & Shivkumar, S. Bead-to-fiber transition in electrospun polystyrene. *J. Appl. Polym. Sci.* **106**, 475–487 (2007).
31. Lee, K. H., Kim, H. Y., Bang, H. J., Jung, Y. H. & Lee, S. G. The change of bead morphology formed on electrospun polystyrene fibers. *Polymer (Guildf)*. **44**, 4029–4034 (2003).
32. Yang, Q. *et al.* Influence of solvents on the formation of ultrathin uniform poly(vinyl pyrrolidone) nanofibers with electrospinning. *J. Polym. Sci. Part B Polym. Phys.* **42**, 3721–3726 (2004).
33. Koski, A., Yim, K. & Shivkumar, S. Effect of molecular weight on fibrous PVA produced by electrospinning. *Mater. Lett.* **58**, 493–497 (2004).
34. Larrondo, L. & St. John Manley, R. Electrostatic fiber spinning from polymer melts. I. Experimental observations on fiber formation and properties. *J. Polym. Sci. Polym. Phys. Ed.* **19**, 909–920 (1981).
35. Sukigara, S., Gandhi, M., Ayutsede, J., Micklus, M. & Ko, F. Regeneration of Bombyx mori silk by electrospinning - Part 1: Processing parameters and geometric properties. *Polymer (Guildf)*. **44**, 5721–5727 (2003).
36. Ki, C. S. *et al.* Characterization of gelatin nanofiber prepared from gelatin-formic acid solution. *Polymer (Guildf)*. **46**, 5094–5102 (2005).
37. Ding, B. *et al.* Preparation and characterization of a nanoscale poly(vinyl alcohol) fiber

- aggregate produced by an electrospinning method. *J. Polym. Sci. Part B Polym. Phys.* **40**, 1261–1268 (2002).
38. Huang, C. *et al.* Electrospun polymer nanofibres with small diameters. *Nanotechnology* **17**, 1558–1563 (2006).
 39. Deitzel, J. ., Kleinmeyer, J., Harris, D. & Beck Tan, N. . The effect of processing variables on the morphology of electrospun nanofibers and textiles. *Polymer (Guildf)*. **42**, 261–272 (2001).
 40. Buchko, C. J., Kozloff, K. M. & Martin, D. C. Surface characterization of porous, biocompatible protein polymer thin films. *Biomaterials* **22**, 1289–1300 (2001).
 41. Demir, M. M., Yilgor, I., Yilgor, E. & Erman, B. Electrospinning of polyurethane fibers. *Polymer (Guildf)*. **43**, 3303–3309 (2002).
 42. Yuan, X. Y., Zhang, Y. Y., Dong, C. & Sheng, J. Morphology of ultrafine polysulfone fibers prepared by electrospinning. *Polym. Int.* **53**, 1704–1710 (2004).
 43. Zhang, C., Yuan, X., Wu, L., Han, Y. & Sheng, J. Study on morphology of electrospun poly(vinyl alcohol) mats. *Eur. Polym. J.* **41**, 423–432 (2005).
 44. Yördem, O. S., Papila, M. & Menciloğlu, Y. Z. Effects of electrospinning parameters on polyacrylonitrile nanofiber diameter: An investigation by response surface methodology. *Mater. Des.* **29**, 34–44 (2008).
 45. Xu, C. Y., Inai, R., Kotaki, M. & Ramakrishna, S. Aligned biodegradable nanofibrous structure: A potential scaffold for blood vessel engineering. *Biomaterials* **25**, 877–886 (2004).
 46. Wang, X. *et al.* Formation of water-resistant hyaluronic acid nanofibers by blowing-assisted electro-spinning and non-toxic post treatments. *Polymer (Guildf)*. **46**, 4853–4867 (2005).
 47. Li, D. *et al.* Electrospinning Nanofibers as Uniaxially Aligned Arrays and Layer-by-Layer Stacked Films. *Adv. Mater.* **16**, 361–366 (2004).
 48. Ki, C. S. *et al.* Electrospun three-dimensional silk fibroin nanofibrous scaffold. *J. Appl. Polym. Sci.* **106**, 3922–3928 (2007).
 49. Alfaro De Prá, M. A., Ribeiro-do-Valle, R. M., Maraschin, M. & Veleirinho, B. Effect of collector design on the morphological properties of polycaprolactone electrospun fibers. *Mater. Lett.* **193**, 154–157 (2017).
 50. Mit-uppatham, C., Nithitanakul, M. & Supaphol, P. Ultratime electrospun polyamide-6 fibers: Effect of solution conditions on morphology and average fiber diameter RID C-4353-2008. *Macromol. Chem. Phys.* **205**, 2327–2338 (2004).
 51. Casper, C. L., Stephens, J. S., Tassi, N. G., Chase, D. B. & Rabolt, J. F. Controlling surface morphology of electrospun polystyrene fibers: Effect of humidity and molecular weight in the electrospinning process. *Macromolecules* **37**, 573–578 (2004).
 52. Bock, N., Woodruff, M. A., Hutmacher, D. W. & Dargaville, T. R. Electrospinning, a reproducible method for production of polymeric microspheres for biomedical applications. *Polymers (Basel)*. **3**, 131–149 (2011).
 53. Zong, X. *et al.* Structure and process relationship of electrospun bioabsorbable

- nanofiber membranes. *Polymer (Guildf)*. **43**, 4403–4412 (2002).
54. Songsurang, K., Praphairaksit, N., Siraleartmukul, K. & Muangsin, N. Electro spray fabrication of doxorubicin-chitosan-tripolyphosphate nanoparticles for delivery of doxorubicin. *Arch. Pharm. Res.* **34**, 583–592 (2011).
 55. Jafari-Nodoushan, M., Barzin, J. & Mobedi, H. Size and morphology controlling of PLGA microparticles produced by electro hydrodynamic atomization. *Polym. Adv. Technol.* **26**, 502–513 (2015).
 56. Park, C. H. *et al.* Preparation of Polymer/Drug Nano- and Micro-Particles by Electro spraying. *Macromol. Symp.* **249–250**, 116–119 (2007).
 57. Gao, Y. *et al.* Morphology control of electro sprayed core–shell particles via collection media variation. *Mater. Lett.* **146**, 59–64 (2015).
 58. Burger, C., Hsiao, B. S. & Chu, B. Nanofibrous Materials and Their Applications. *Annu. Rev. Mater. Res.* **36**, 333–368 (2006).
 59. Meng, F., Jiang, Y., Sun, Z., Yin, Y. & Li, Y. Electrohydrodynamic liquid atomization of biodegradable polymer microparticles: Effect of electrohydrodynamic liquid atomization variables on microparticles. *J. Appl. Polym. Sci.* **113**, 526–534 (2009).
 60. Khajavi, R. & Abbasipour, M. Electrospinning as a versatile method for fabricating coreshell, hollow and porous nanofibers. *Sci. Iran.* **19**, 2029–2034 (2012).
 61. Yarin, A. L. Coaxial electrospinning and emulsion electrospinning of core-shell fibers. *Polymers for Advanced Technologies* **22**, 310–317 (2011).
 62. Chang, M.-W., Stride, E. & Edirisinghe, M. Controlling the thickness of hollow polymeric microspheres prepared by electrohydrodynamic atomization. *J. R. Soc. Interface* **7 Suppl 4**, S451–S460 (2010).
 63. Li, D. & Xia, Y. Direct fabrication of composite and ceramic hollow nanofibers by electrospinning. *Nano Lett.* **4**, 933–938 (2004).
 64. Persano, L., Camposeo, A., Tekmen, C. & Pisignano, D. Industrial upscaling of electrospinning and applications of polymer nanofibers: A review. *Macromol. Mater. Eng.* **298**, 504–520 (2013).
 65. Yao, S. *et al.* Drug-nanoencapsulated PLGA microspheres prepared by emulsion electro spray with controlled release behavior. *Regen. Biomater.* **3**, 1–9 (2016).
 66. Jirsák, O. & Dao, T. Production, properties and end-uses of nanofibres. *Nanotechnol. Constr.* **3** 1–5 (2009). doi:10.1007/978-3-642-00980-8_11
 67. Huang, Z.-M., Zhang, Y.-Z., Kotaki, M. & Ramakrishna, S. A review on polymer nanofibers by electrospinning and their applications in nanocomposites. *Compos. Sci. Technol.* **63**, 2223–2253 (2003).
 68. Mohammadzadehmoghadam, S., Dong, Y. & Jeffery Davies, I. Recent progress in electrospun nanofibers: Reinforcement effect and mechanical performance. *J. Polym. Sci. Part B Polym. Phys.* **53**, 1171–1212 (2015).
 69. Gibson, P., Schreuder-Gibson, H. & Rivin, D. Transport properties of porous membranes based on electrospun nanofibers. *Colloids Surfaces A Physicochem. Eng. Asp.* **187–188**, 469–481 (2001).

70. Graham, K. *et al.* Polymeric Nanofibers in Air Filtration Applications. *Fifteenth Annu. Tech. Conf. Expo Am. Filtr. Sep. Soc.* 9–12 (2002).
71. Graham, S. ‘Smart’ Silicon Dust Could Help Screen for Chemical Weapons - Scientific American. *SCIENTIFIC AMERICAN* (2002).
72. Gibson, P. W., Schreuder-Gibson, H. L. & Rivin, D. Electrospun fiber mats: Transport properties. *AIChE J.* **45**, 190–195 (1999).
73. Smith, D. & Reneker, D. Insoluble nanofibers of linear poly(ethylenimine) and uses therefor. (2001).
74. Norris, I. D., Shaker, M. M., Ko, F. K. & MacDiarmid, A. G. Electrostatic fabrication of ultrafine conducting fibers: Polyaniline/polyethylene oxide blends. *Synth. Met.* **114**, 109–114 (2000).
75. Senecal, K., Samuelson, L., Sennett, M. & Schreuder-Gibson, H. Conductive (electrical, ionic and photoelectric) membrane articles, and method for producing same. 3 (2001).
76. Senecal, K. J. *et al.* Photoelectric Response from Nanofibrous Membranes. *MRS Proc.* **708**, 1–5 (2001).
77. Haider, A., Haider, S. & Kang, I. K. A comprehensive review summarizing the effect of electrospinning parameters and potential applications of nanofibers in biomedical and biotechnology. *Arab. J. Chem.* (2015). doi:10.1016/j.arabjc.2015.11.015
78. Chew, S., Wen, Y., Dzenis, Y. & Leong, K. The Role of Electrospinning in the Emerging Field of Nanomedicine. *Curr. Pharm. Des.* **12**, 4751–4770 (2006).
79. Rogina, A. Electrospinning process: Versatile preparation method for biodegradable and natural polymers and biocomposite systems applied in tissue engineering and drug delivery. *Appl. Surf. Sci.* **296**, 221–230 (2014).
80. Ventre, M., Natale, C. F., Rianna, C. & Netti, P. A. Topographic cell instructive patterns to control cell adhesion, polarization and migration. *J. R. Soc. Interface* **11**, 20140687–20140687 (2014).
81. Whited, B. M. & Rylander, M. N. The influence of electrospun scaffold topography on endothelial cell morphology, alignment, and adhesion in response to fluid flow. *Biotechnol. Bioeng.* **111**, 184–195 (2014).
82. Cao, H., McHugh, K., Chew, S. Y. & Anderson, J. M. The topographical effect of electrospun nanofibrous scaffolds on the in vivo and in vitro foreign body reaction. *J. Biomed. Mater. Res. A* **93**, 1151–1159 (2010).
83. Chou, S. F., Carson, D. & Woodrow, K. A. Current strategies for sustaining drug release from electrospun nanofibers. *J. Control. Release* **220**, 584–591 (2015).
84. Son, Y. J., Kim, W. J. & Yoo, H. S. Therapeutic applications of electrospun nanofibers for drug delivery systems. *Arch. Pharm. Res.* **37**, 69–78 (2013).
85. Tibbitt, M. W., Rodell, C. B., Burdick, J. A. & Anseth, K. S. Progress in material design for biomedical applications. *Proc. Natl. Acad. Sci. U. S. A.* **112**, 14444–51 (2015).
86. Lendlein, A. Polymers in biomedicine. *Macromol. Biosci.* **10**, 993–997 (2010).

87. Maitz, M. F. Applications of synthetic polymers in clinical medicine. *Biosurface and Biotribology* **1**, 161–176 (2015).
88. Nair, L. S. & Laurencin, C. T. *Biodegradable polymers as biomaterials. Progress in Polymer Science (Oxford)* **32**, 762–798 (Pergamon, 2007).
89. Vert, M. Degradable and bioresorbable polymers in surgery and in pharmacology: beliefs and facts. *J. Mater. Sci. Mater. Med.* **20**, 437–446 (2009).
90. Seo, S.-J., Mahapatra, C., Singh, R. K., Knowles, J. C. & Kim, H.-W. Strategies for osteochondral repair: Focus on scaffolds. *J. Tissue Eng.* **5**, 204173141454185 (2014).
91. Gombotz, W. R. & Pettit, D. K. Biodegradable Polymers for Protein and Peptide Drug Delivery. *Bioconjug. Chem.* **6**, 332–351 (1995).
92. Kapoor, D. N. *et al.* PLGA: a unique polymer for drug delivery. *Ther Deliv* **6**, 41–58 (2015).
93. Maurus, P. B. & Kaeding, C. C. Bioabsorbable implant material review. *Operative Techniques in Sports Medicine* **12**, 158–160 (2004).
94. Li, Q. *et al.* Biodegradable and photocrosslinkable polyphosphoester hydrogel. *Biomaterials* **27**, 1027–1034 (2006).
95. Zhao, Z., Wang, J., Mao, H. Q. & Leong, K. W. Polyphosphoesters in drug and gene delivery. *Advanced Drug Delivery Reviews* **55**, 483–499 (2003).
96. Zhang, Z., Kuijer, R., Bulstra, S. K., Grijpma, D. W. & Feijen, J. The in vivo and in vitro degradation behavior of poly(trimethylene carbonate). *Biomaterials* **27**, 1741–1748 (2006).
97. Banerjee, A., Chatterjee, K. & Madras, G. Enzymatic degradation of polymers: a brief review. *Mater. Sci. Technol.* **30**, 567–573 (2014).
98. El-Sherbiny, I. & Yacoub, M. Hydrogel scaffolds for tissue engineering: Progress and challenges. *Glob. Cardiol. Sci. Pract.* **2013**, 316–42 (2013).
99. Ueda, H. & Tabata, Y. Polyhydroxyalkanoate derivatives in current clinical applications and trials. *Advanced Drug Delivery Reviews* **55**, 501–518 (2003).
100. Vauthier, C., Dubernet, C., Fattal, E., Pinto-Alphandary, H. & Couvreur, P. Poly(alkylcyanoacrylates) as biodegradable materials for biomedical applications. *Adv. Drug Deliv. Rev.* **55**, 519–548 (2003).
101. Barkan, Y. *et al.* Comparative evaluation of polycyanoacrylates. *Acta Biomater.* **48**, 390–400 (2017).
102. Khadka, D. B. & Haynie, D. T. Protein- and peptide-based electrospun nanofibers in medical biomaterials. *Nanomedicine: Nanotechnology, Biology, and Medicine* **8**, 1242–1262 (2012).
103. Ulery, B. D., Nair, L. S. & Laurencin, C. T. Biomedical Applications of Biodegradable Polymers. *J. Polym. Sci. B. Polym. Phys.* **49**, 832–864 (2011).
104. Tamada, Y. & Ikada, Y. Cell adhesion to plasma-treated polymer surfaces. *Polymer (Guildf)*. **34**, 2208–2212 (1993).
105. Mazia, D., Schatten, G. & Sale, W. Adhesion of cells to surfaces coated with

- polylysine. Applications to electron microscopy. *J. Cell Biol.* **66**, 198–200 (1975).
106. Wu, M.-H. Simple poly(dimethylsiloxane) surface modification to control cell adhesion. *Surf. Interface Anal.* **41**, 11–16 (2009).
 107. Huang, J. & Ding, J. Nanostructured interfaces with RGD arrays to control cell–matrix interaction. *Soft Matter* **6**, 3395 (2010).
 108. Kim, T. G. & Park, T. G. Biomimicking Extracellular Matrix: Cell Adhesive RGD Peptide Modified Electrospun Poly(D,L-lactic-co-glycolic acid) Nanofiber Mesh. *Tissue Eng.* **12**, 221–233 (2006).
 109. Li, M., Mondrinos, M. J., Chen, X. & Lelkes, P. I. Electrospun blends of natural and synthetic polymers as scaffolds for tissue engineering. *Conf. Proc. ... Annu. Int. Conf. IEEE Eng. Med. Biol. Soc. IEEE Eng. Med. Biol. Soc. Annu. Conf.* **6**, 5858–61 (2005).
 110. Keane, T. J. & Badylak, S. F. Biomaterials for tissue engineering applications. *Semin. Pediatr. Surg.* **23**, 112–118 (2014).
 111. Tsurkan, M. V., Levental, K. R., Freudenberg, U. & Werner, C. Enzymatically degradable heparin-polyethylene glycol gels with controlled mechanical properties. *Chem. Commun.* **46**, 1141–1143 (2010).
 112. Fonseca, K. B., Bidarra, S. J., Oliveira, M. J., Granja, P. L. & Barrias, C. C. Molecularly designed alginate hydrogels susceptible to local proteolysis as three-dimensional cellular microenvironments. *Acta Biomater.* **7**, 1674–1682 (2011).
 113. Ma, P. X. Biomimetic materials for tissue engineering. *Adv. Drug Deliv. Rev.* **60**, 184–198 (2008).
 114. Mele, E. Electrospinning of natural polymers for advanced wound care: towards responsive and adaptive dressings. *J. Mater. Chem. B* **4**, 4801–4812 (2016).
 115. Weigel, P. H., Hascall, V. C. & Tammi, M. Hyaluronan synthases. *Journal of Biological Chemistry* **272**, 13997–14000 (1997).
 116. Wang, X., Ding, B. & Li, B. Biomimetic electrospun nanofibrous structures for tissue engineering. *Mater. Today* **16**, 229–241 (2013).
 117. Al-Assaf, S., Navaratnam, S., Parsons, B. J. & Phillips, G. O. Chain scission of hyaluronan by peroxyntirite. *Arch. Biochem. Biophys.* **411**, 73–82 (2003).
 118. Kogan, G., Šoltés, L., Stern, R., Schiller, J. & Mendichi, R. Hyaluronic Acid: Its Function and Degradation in in vivo Systems. *Stud. Nat. Prod. Chem.* **34**, 789–882 (2008).
 119. Patterson, J. *et al.* Hyaluronic acid hydrogels with controlled degradation properties for oriented bone regeneration. *Biomaterials* **31**, 6772–6781 (2010).
 120. Olsen, D. *et al.* Recombinant collagen and gelatin for drug delivery. *Advanced Drug Delivery Reviews* **55**, 1547–1567 (2003).
 121. Mithieux, S. M., Rasko, J. E. J. & Weiss, A. S. Synthetic elastin hydrogels derived from massive elastic assemblies of self-organized human protein monomers. *Biomaterials* **25**, 4921–4927 (2004).
 122. Rnjak-Kovacina, J. *et al.* Electrospun synthetic human elastin:collagen composite

- scaffolds for dermal tissue engineering. *Acta Biomater.* **8**, 3714–3722 (2012).
123. Sell, S. A. *et al.* Cross-linking methods of electrospun fibrinogen scaffolds for tissue engineering applications. *Biomed. Mater.* **3**, 045001 (2008).
 124. Wnek, G. E., Carr, M. E., Simpson, D. G. & Bowlin, G. L. Electrospinning of nanofiber fibrinogen structures. *Nano Lett.* **3**, 213–216 (2003).
 125. Jayakumar, R., Prabakaran, M., Nair, S. V. & Tamura, H. Novel chitin and chitosan nanofibers in biomedical applications. *Biotechnol. Adv.* **28**, 142–150 (2010).
 126. Li, D.-H., Liu, L.-M., Tian, K.-L., Liu, J.-C. & Fan, X.-Q. Synthesis, biodegradability and cytotoxicity of water-soluble isobutylchitosan. *Carbohydr. Polym.* **67**, 40–45 (2007).
 127. Tashiro, T. Antibacterial and Bacterium Adsorbing Macromolecules. *Macromol. Mater. Eng.* **286**, 63–87 (2001).
 128. Martinac, A., Filipović-Grčić, J., Voinovich, D., Perissutti, B. & Franceschinis, E. Development and bioadhesive properties of chitosan-ethylcellulose microspheres for nasal delivery. *Int. J. Pharm.* **291**, 69–77 (2005).
 129. Francis Suh, J.-K. & Matthew, H. W. . Application of chitosan-based polysaccharide biomaterials in cartilage tissue engineering: a review. *Biomaterials* **21**, 2589–2598 (2000).
 130. Geng, X., Kwon, O. H. & Jang, J. Electrospinning of chitosan dissolved in concentrated acetic acid solution. *Biomaterials* **26**, 5427–5432 (2005).
 131. Ohkawa, K., Cha, D., Kim, H., Nishida, A. & Yamamoto, H. Electrospinning of chitosan. *Macromol. Rapid Commun.* **25**, 1600–1605 (2004).
 132. Min, B. M. *et al.* Chitin and chitosan nanofibers: Electrospinning of chitin and deacetylation of chitin nanofibers. *Polymer (Guildf)*. **45**, 7137–7142 (2004).
 133. Khan, F. & Ahmad, S. R. Polysaccharides and Their Derivatives for Versatile Tissue Engineering Application. *Macromol. Biosci.* **13**, 395–421 (2013).
 134. Kundu, S. *Silk biomaterials for tissue engineering and regenerative medicine.* (Woodhead Publishing, 2014).
 135. Vepari, C. & Kaplan, D. L. Silk as a Biomaterial. *Prog. Polym. Sci.* **32**, 991–1007 (2007).
 136. Rockwood, D. N. *et al.* Materials fabrication from Bombyx mori silk fibroin. *Nat. Protoc.* **6**, 1612–1631 (2011).
 137. Jin, H.-J., Fridrikh, S. V., Rutledge, G. C. & Kaplan, D. L. Electrospinning Bombyx mori Silk with Poly(ethylene oxide). *Biomacromolecules* **3**, 1233–1239 (2002).
 138. Chen, J.-P., Chen, S.-H. & Lai, G.-J. Preparation and characterization of biomimetic silk fibroin/chitosan composite nanofibers by electrospinning for osteoblasts culture. *Nanoscale Res. Lett.* **7**, 170 (2012).
 139. Cappello, J. & McGrath, K. P. in 311–327 (1993). doi:10.1021/bk-1994-0544.ch026
 140. Brandenberger, H., Nüssli, D., Piëch, V. & Widmer, F. Monodisperse particle production: A method to prevent drop coalescence using electrostatic forces. *J.*

- Electrostat.* **45**, 227–238 (1999).
141. Gomez, A., Bingham, D., Juan, L. d. & Tang, K. Production of protein nanoparticles by electrospray drying. *J. Aerosol Sci.* **29**, 561–574 (1998).
 142. Xie, J. & Wang, C.-H. Encapsulation of proteins in biodegradable polymeric microparticles using electrospray in the Taylor cone-jet mode. *Biotechnol. Bioeng.* **97**, 1278–1290 (2007).
 143. Chen, R. R. & Mooney, D. J. Polymeric growth factor delivery strategies for tissue engineering. *Pharm. Res.* **20**, 1103–12 (2003).
 144. Zhu, G., Mallery, S. R. & Schwendeman, S. P. Stabilization of proteins encapsulated in injectable poly (lactide- co-glycolide). *Nat. Biotechnol.* **18**, 52–57 (2000).
 145. Ding, L., Lee, T. & Wang, C.-H. Fabrication of monodispersed Taxol-loaded particles using electrohydrodynamic atomization. *J. Control. Release* **102**, 395–413 (2005).
 146. Hong, Y., Li, Y., Yin, Y., Li, D. & Zou, G. Electrohydrodynamic atomization of quasi-monodisperse drug-loaded spherical/wrinkled microparticles. *J. Aerosol Sci.* **39**, 525–536 (2008).
 147. Ranganath, S. H., Kee, I., Krantz, W. B., Chow, P. K.-H. & Wang, C.-H. Hydrogel Matrix Entrapping PLGA-Paclitaxel Microspheres: Drug Delivery with Near Zero-Order Release and Implantability Advantages for Malignant Brain Tumour Chemotherapy. *Pharm. Res.* **26**, 2101–2114 (2009).
 148. Kumar Narahariseti, P. *et al.* In vivo performance of implantable biodegradable preparations delivering Paclitaxel and Etanidazole for the treatment of glioma. *Biomaterials* **28**, 886–894 (2007).
 149. Xie, J., Marijnissen, J. C. M. & Wang, C. H. Microparticles developed by electrohydrodynamic atomization for the local delivery of anticancer drug to treat C6 glioma in vitro. *Biomaterials* **27**, 3321–3332 (2006).
 150. Nie, H., Dong, Z., Arifin, D. Y., Hu, Y. & Wang, C.-H. Core/shell microspheres via coaxial electrohydrodynamic atomization for sequential and parallel release of drugs. *J. Biomed. Mater. Res. Part A* **95A**, 709–716 (2010).
 151. Nie, H., Fu, Y. & Wang, C.-H. Paclitaxel and suramin-loaded core/shell microspheres in the treatment of brain tumors. *Biomaterials* **31**, 8732–8740 (2010).
 152. Freiberg, S. & Zhu, X. X. Polymer microspheres for controlled drug release. *Int. J. Pharm.* **282**, 1–18 (2004).
 153. Wu, Y. *et al.* Electrospayed core-shell microspheres for protein delivery. *Chem. Commun.* **46**, 4743 (2010).
 154. Li, C., Yu, D.-G., Williams, G. R. & Wang, Z.-H. Fast-Dissolving Core-Shell Composite Microparticles of Quercetin Fabricated Using a Coaxial Electrospray Process. *PLoS One* **9**, e92106 (2014).
 155. Yu, D.-G. *et al.* Polymer-based nanoparticulate solid dispersions prepared by a modified electrospraying process. *J. Biomed. Sci. Eng.* **04**, 741–749 (2011).
 156. Yu, D.-G. *et al.* Solid lipid nanoparticles self-assembled from electrospayed polymer-based microparticles. *J. Mater. Chem.* **21**, 15957 (2011).

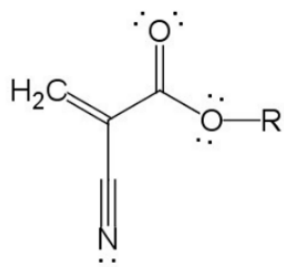
157. Yu, D.-G., Yang, J.-H., Wang, X. & Tian, F. Liposomes self-assembled from electrosprayed composite microparticles. *Nanotechnology* **23**, 105606 (2012).
158. Wang, Y. *et al.* Fabrication of core-shell micro/nanoparticles for programmable dual drug release by emulsion electrospraying. *J. Nanoparticle Res.* **15**, 1726 (2013).
159. Wu, Y., MacKay, J. A., R. McDaniel, J., Chilkoti, A. & Clark, R. L. Fabrication of Elastin-Like Polypeptide Nanoparticles for Drug Delivery by Electrospraying. *Biomacromolecules* **10**, 19–24 (2009).
160. Arya, N., Chakraborty, S., Dube, N. & Katti, D. S. Electrospraying: A facile technique for synthesis of chitosan-based micro/nanospheres for drug delivery applications. *J. Biomed. Mater. Res. Part B Appl. Biomater.* **88B**, 17–31 (2009).
161. Kim, S.-Y. *et al.* Size Control of Chitosan Capsules Containing Insulin for Oral Drug Delivery via a Combined Process of Ionic Gelation with Electrohydrodynamic Atomization. *Ind. Eng. Chem. Res.* **50**, 13762–13770 (2011).
162. Xu, Y. & Hanna, M. A. Electrosprayed bovine serum albumin-loaded tripolyphosphate cross-linked chitosan capsules: Synthesis and characterization. *J. Microencapsul.* **24**, 143–151 (2007).
163. Suksamran, T. *et al.* Biodegradable alginate microparticles developed by electrohydrodynamic spraying techniques for oral delivery of protein. *J. Microencapsul.* **26**, 563–570 (2009).
164. Suksamran, T. *et al.* Methylated N-(4-N,N-dimethylaminocinnamyl) chitosan-coated electrospray OVA-loaded microparticles for oral vaccination. *Int. J. Pharm.* **448**, 19–27 (2013).
165. Watanabe, H., Matsuyama, T. & Yamamoto, H. Preparation of immobilized enzyme gel particles using an electrostatic atomization technique. *Biochem. Eng. J.* **8**, 171–174 (2001).
166. Park, H. *et al.* Fabrication of cross-linked alginate beads using electrospraying for adenovirus delivery. *Int. J. Pharm.* **427**, 417–425 (2012).
167. Xie, J. & Wang, C.-H. Electrospray in the dripping mode for cell microencapsulation. *J. Colloid Interface Sci.* **312**, 247–255 (2007).

Chapter 2

Electrospinning of ECA to fabricate aligned surfaces to control cells adhesion

2.1 Cyanoacrylate adhesives

Alkyl-2-cyanoacrylates (ACAs) were discovered in the 1949 by Ardis¹ and their adhesives properties were described in the 1959 by Coover². They are made up of cyanoacrylic acid and a side chain group –R which can be a methyl, ethyl, butyl or octyl (Figure 2.1)³⁻⁵. Generally, ACAs are in liquid solution and are characterized by low viscosity⁶. Since ACAs monomers are highly reactive, they result poorly handleable, because they can start to polymerize rapidly at room temperature in presence of moisture or basic compounds (Figure 2.2)^{2,6,7}. However, thanks to their fast polymerization, ACAs have shown to be hemostatic, stopping blood leakage. Moreover, they were also able to inhibit the growth of bacteria⁸⁻¹⁴.



<i>R</i> group	Name
	Methyl-2-CA
	Ethyl-2-CA
	Butyl-2-CA
	Octyl-2-CA

Figure 2.1 Structure of the cyanoacrylates adhesives

ACAs polymers showed several properties – mechanical, viscoelastic, thermal, degradation and biocompatibility – which change relatively to the ACA monomer and in particular to the respective side chains (Table 2.1)^{15–19}. Long side chain polymers present higher flexibility; contrarily, short side chain polymers have high strength bond^{14,16}; setting rate is slower for long side chain polymers respect to the short side chain ones. Slow polymerization rate implicates less heat production during the setting^{16,20}. Finally, ACA polymers with longer side chain need more time to be degraded¹⁵.

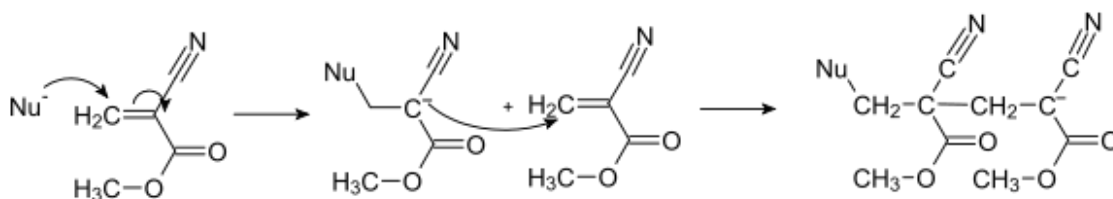


Figure 2.2 Anionic polymerization of the MCA. The mechanism of polymerization is the same also for the other cyanoacrylate monomers.

The degradation of ACA polymers *in vivo* occurs through two mechanisms: enzymatic degradation and hydrolysis degradation (Figure 2.3). Esterases of the serum, lysosomes and the pancreatic juice, induce the formation of the alkoxyalcohol and the poly-cyanoacrylic acid^{6,21,22}. Both are water soluble, so they are eliminated through kidneys⁶.

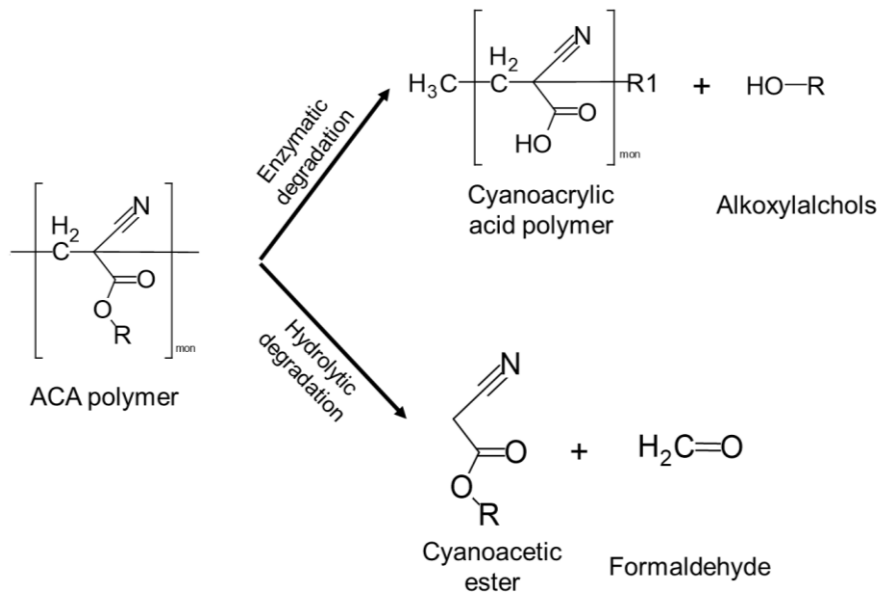


Figure 2.3 *In vivo* degradation of the ACA polymers can occur through enzymatic degradation, resulting in poly-cyanoacrylic acid and alkoxyalcohol, and via hydrolytic degradation, releasing cyanoacetic ester and formaldehyde. For group R see Figure 1.1.

Another mechanism, which degrades the ACA polymers, is hydrolytic degradation through the inverse Knoevenagel reaction, which results in releasing formaldehyde and cyanoacetic ester^{6,15,23}. The inverse Knoevenagel reaction rate also depends on the length of the side chain, resulting faster for short side chain ACA polymers, while slower for longer side chain ones¹⁵. This means that the release of formaldehyde, due to the polymer degradation, is related to respective side chains^{6,15}. In fact, its release was seen to be higher for MCA and ECA¹⁵. Therefore, considering that the formaldehyde is toxic for tissue, its release negatively characterizes the safety and biocompatibility of the ACAs. Hence, the relation between the degradation rate and biocompatibility: ACAs with shorter chain are more tissue toxic respect to the ones with longer chain. However, hydrolytic degradation leads to the 5% of degradation in 24h in water and at physiological pH, and it is slower than the enzymatic degradation, which is predominant *in vivo*^{6,23}.

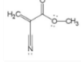






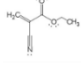
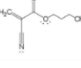
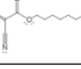
ACAs polymers	Flexibility	Strength bond	Polymerization rate	Heat production	Degradation rate	Biocompatibility
MCA 	Increase 	Increase 	Increase 	Increase 	Increase 	Increase 
ECA 						
BCA 						
OCA 						

Table 2.1 Dependence of the ACAs polymers properties on the side chain length.

2.1.1 Usage of the cyanoacrylate as biomedical adhesives

Since the 1966, ACAs polymers were used in clinical therapies as agents for bone fixation or wound closure and as surgery glue^{6,7,14,24,25}. The first to be used was the methyl-2-cyanoacrylate (MCA) and it was applied on wound or surgery incisions because it was more accepted and less painful than suturing²⁵⁻²⁸. Years later, the other ACAs were used instead of the MCA because it is subjected to rapid degradation *in vivo*, inducing tissue toxicity and inflammation. In fact, ACAs with longer side chain have shown less complication upon their application²⁶. Octyl-2-cyanoacrylate (OCA) and butyl-2-cyanoacrylate (BCA) are mostly used as medical glue for wound care. They can form a water resistant thin coating on wound site, thanks to the polymerization induced by water and proteins. The thin film keeps together the wound edges, allowing movement thanks to its flexibility. Moreover, they form a barrier against bacteria, preventing infections^{14,29}. Ethyl-2-cyanoacrylate (ECA) is less used as wound care tool because it results in a brittle film which can present prematurely fractures and the risk is to leave exposed the wound¹⁴. It has more internal usages: it has been applied in bone fixation and nerve repair. In fact, despite its toxicity, ECA is preferred for this usage because of its higher strength bond and its faster degradation respect to BCA and OCA, which

reduce its permanence *in vivo*. In bone fixation, ECA has shown to ameliorate the stability of a bone autograft compared to screw-using method and to induce less inflammation than OCA and BCA^{24,30,31}. This is because their slower degradation rate causes a prolonged permanence of the polymers, inducing inflammation. In nerve repair, ECA was put in contact with transected nerve, causing no toxicity during nerve regeneration³²⁻³⁴.

2.1.2 Poly-ECA coatings through the electrospinning

Despite the good ability in fixation and good results, when was used internally to the organism, the development of new strategies of application of ECA in biomedical field was limited by its poor handleability, due to its high reactivity in presence of weak bases, such as water. Such limit was surpassed in a recent work in which ECA was stabilized with DMSO, resulting in a gel, which was used to produce fibers through the electrospinning³⁵. Fibers were melted such to create coatings on surfaces. The coatings showed to have a particular roughness derived from the disposition of the fibers previously electrospun. Such coatings had properties exploitable in self-cleaning surfaces and protective covering. In addition, they also have been shown good biocompatibility, confirming the *in vivo* results of ECA polymers.

2.2 Organization of skeletal muscle tissue

Skeletal muscle tissue is responsible of the voluntary movements in living organism. This tissue is constituted by multiple fascicles of muscular fibers, which in turn are formed by the myotubes. Such tubular structures are generated from fusions of myoblasts upon their differentiation (Figure 2.4). This process, in fact, induces the fusion of plasmatic membrane of the myoblasts, such to acquire a long cylindrical and multinucleated structures, inducing the formation of myotubes. Myotubes are characterized by the presence of myofibrils in their cytoplasm (or sarcoplasm), formed by myosin (thick filaments) and actin (thin filaments).

They are arranged in repeated units, called sarcomeres, that are aligned along the axis of the myotube (Figure 2.4)³⁶.

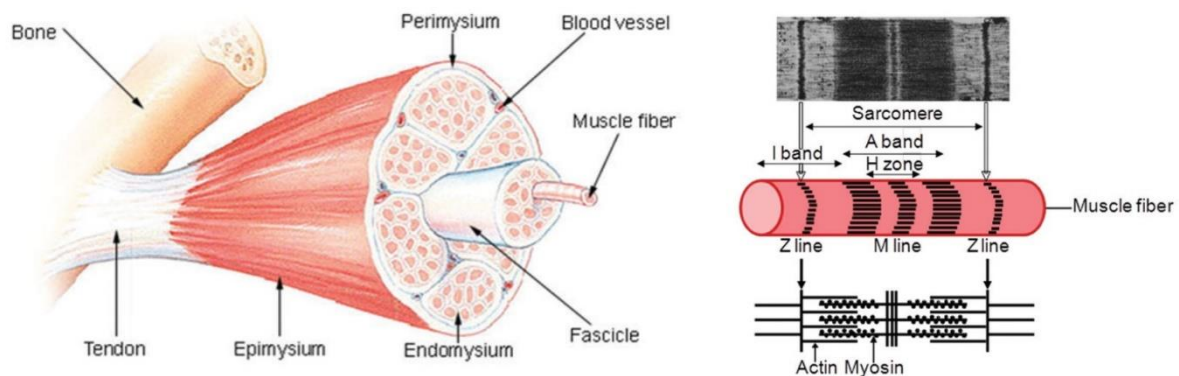


Figure 2.4 On the left, the structure of muscle tissue constituted of muscular fascicle, which in turn are formed by myotubes. On the right, schematic that shows the sarcomere organization^{37,38}.

The sarcomere is delimited by two Z bands, at which the actin filaments are anchored. Myosin instead, is attached at the M line, placed in the middle of the sarcomere. The filaments of actin and the myosin are overlapped in the A band of the sarcomere. In this band, during the contraction, the myosin pulls toward the M line the actin filaments, decreasing the length of the sarcomere, inducing the contraction of the muscle³⁶.

The contractile mechanism involved other components. The nervous stimuli which allow the contraction, is linked to the endoplasmic reticulum (or sarcoplasmic reticulum), in which calcium ions are stored. The release of calcium from this cell compartment is required for muscle contraction. Nervous stimuli can be propagated across the whole myotubular structure, through the T tubules. Finally, when the muscle is in relaxed state. The interaction between actin and myosin is prevented by the troponin and tropomyosin proteins.

2.2.1 Strategies for skeletal muscle regeneration

The clinical approach for the regeneration of the skeletal muscle consists of an *ex vivo* strategy. The cells are harvested from the patients or a donor, in order to be cultivated, such to

produce a functional tissue *in vitro*, which are implanted in the injury site³⁶. More advanced approaches have been tried to be developed by using of 3D scaffold with gel of collagen^{39,40}. This strategy, however have limited capacity to produce large tissue *in vitro*⁴⁰. Implementation of such scaffold lead to the fabrication of vascularized muscle tissue by using embryonic fibroblasts, myoblasts and endothelial cell^{41,42}. Despite good results, clinal therapy requires large constructs with axial vascularization. In addition, the use of embryonic cells can be object of ethical issues⁴³.

Currently, the use of the materials associated to micro and nanofabrication methods has opened possibilities to design new strategies for the musculoskeletal tissue regeneration^{36,44}. An essential point, in engineering of muscle skeletal tissue, is to induce a pre-alignment of myoblasts, such to reproduce the native condition. In this way, the muscle fibers formation can be increased⁴⁵. Alignment of cells *in vitro* can be achieved by controlling the topographical cues. In fact, they can affect the cells shape, disposition, size and cellular response. Concerning the skeletal muscle cells, aligned topography affect positively the formation of oriented patterns of cells, suitable for the formation of the myotubes. Photolithography, soft lithography and electrospinning was used to fabricate controlled topography. However, electrospinning is a technique characterized by very simple operability, low cost and flexibility, because a wide range of properties can be used to obtain fibers. In addition, depending on the collector used, different topography can be obtained.

2.3 Fabrication of aligned ECA coating for myoblast cells alignment.

The improvement in ECA handleability leads to the possibility to produce coating, through the thermal treatment of the electrospun fibers. Upon their melting, fibers leave their

micrometric topography on the surfaces. Herein, this protocol was exploited to produce coating with a specific topography. By using a rotating collector, highly aligned poly-ECA fibers were obtained. Successively, the thermal treatment was used such to create an oriented topography on glass surface. Finally, skeletal myoblast cells were used to demonstrate that the oriented topography was able to drive their disposition on the ECA coating.

2.4. Experimental section

2.4.1 PECA electrospinning

According to the protocol proposed in Mele *et al.*³⁵, equal volumes of ECA and DMSO were mixed in the same glass vial, forming a gel-like phase, which was dilute in acetone to concentration of 4% v/v and stirred overnight. The solutions were electrospun with a syringe pump with a flow rate of 4 mL h⁻¹ and a voltage ranged from 8kV to 10kV. Random fibers were collected on an aluminum foil placed at 15 cm far from the needle, while aligned fibers were collected on a rotating collector placed at the same distance (Figure 2.5). Different speeds of the rotating collector (1000, 3000 and 5000rpm) were used in order to have the highest alignment degree of the fibers. All the fibers were fabricated at 25°C at constant relative humidity. Then, both random and aligned fibers were put on glass cover slip and fixed on it thermally with 150°C for 20 seconds, obtaining a transparent hydrophobic coating.

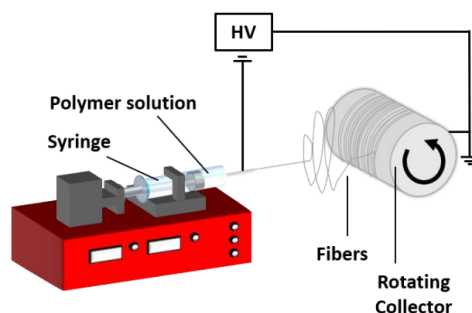


Figure 2.5 Schematic of the electrospinning set-up used to fabricate PECA aligned fibers

2.4.2 Fibers characterization

Random and aligned PECA fibers and PECA-coated glass obtained from the melting of random and aligned fibers were sputtered with gold forming a 10-nm thick film on them and were observed at SEM, working in high-vacuum with an acceleration voltage of 15kV. The size of the fibers was obtained analyzing the SEM images through the Fiji software. The alignment degree was calculated through the Fiji software plug-in Directionality, by using local gradient orientation analysis.

2.4.3 Cells viability

In a preliminary study, 3T3 fibroblast cells were used to assess the biocompatibility of the fibers before and after the melting process. Each side of non-melted and melted fibers were treated with UV light for 20 minutes. Before the seeding, non-melted fibers were fixed at the bottom of the wells with a PDMS ring, since they float in aqueous solutions. Fibroblasts were seeded with Dulbecco's modified Eagle's medium (DMEM), 10% fetal bovine serum (FBS), 100 IU/mL penicillin, 100 µg/mL streptomycin and 2 mM L-glutamine, incubated at 37°C and 5% CO₂ saturated humidity atmosphere. The medium was changed every 2 days. They were seeded on non-melted and melted fibers with a density of 1500 cells/cm². Wells without fibers were the control. The viability was acquired after 24h of seeding with the MTT (3-(4,5-

Dimethylthiazol-2-yl)-2,5-Diphenyltetrazolium Bromide) assay. After 24h, the medium was replaced with PBS containing 0.2mg/ml of MTT, incubating the cells for 4 hours. Successively, the PBS was removed, and isopropanol was added in order to dissolve the formazan salts. The absorbance of each well was acquired with a multiwell plate reader at 595 nm. The viability from each sample was normalized on the control.

Once understood the bioavailability of the PECA-coated glass, C2C12 mouse myoblasts were seeded at a density of 10000 cells/cm² on them. Bare glass coverslips were considered as control substrates. C2C12 were cultured with DMEM, 10% FBS, 100 IU/mL penicillin, 100 µg/mL streptomycin and 2 mM L-glutamine. Normal culture conditions (37°C and 5% CO₂ saturated humidity atmosphere) were applied, and culture medium was changed every 3 days. Biocompatibility of the substrates was evaluated through WST-1 assay (2-(4-iodophenyl)-3-(4-nitrophenyl)-5-(2,4-disulfophenyl)-2 H-tetrazolium monosodium salt). The assay was performed at 1, 3 and 5 days from cell seeding by incubating cultures with a 1:11 dilution of WST-1 reagent in proliferative medium for 2 h. Absorbance of the supernatants was read at 450 nm with a multiwell plate reader. The viability from each sample was normalized on the control.

2.4.4 Optical and confocal microscope analysis

C2C12 seeded for 24 hours on glass and PECA-coated glass, random and aligned, were stained with Coomassie blue in order to observe them at the optical microscope. Cells were washed twice with PBS and fixed with 4% paraformaldehyde (PFA) in PBS per 20 minutes at 4°C. Successively, cells were washed in PBS two times and then incubated with 0.02% Coomassie brilliant blue R-250 in methanol: acetic acid: water, 46.5:7:46.5 (v/v/v) for 3 minutes⁴⁶. The cells were rinsed several times in water to remove the excess of Coomassie blue. Then the cells were observed with the optical microscope directly in the multiwell plate.

Cell interactions with the substrates were investigated on proliferating cultures at 24h from seeding by immunocytochemistry staining of vinculin, which is a protein involved in focal adhesions. The samples were first fixed in 4% PFA in PBS for 20 minutes, and then incubated with 1 mg/mL sodium borohydride in PBS for 10 minutes to reduce unspecific fluorescence and auto-fluorescence. Cell membranes were permeabilized with 0.1% Triton X-100 in PBS for 15 minutes. Antibody unspecific binding sites were saturated with 10% goat serum in PBS for 1 h, and, subsequently, primary antibodies against vinculin (murine IgG anti-vinculin antibody, 1:50 diluted in 10% goat serum) was added. After 30 minutes of incubation at 37 °C, the samples were rinsed with 10% goat serum. Then, secondary green fluorescent antibody (anti-mouse diluted 1:50 in 10% goat serum for murine IgG anti-vinculin antibody) was added. Secondary antibody was supplied with 100 μM TRITC-phalloidin for F-actin staining, and 1 μM DAPI for nucleus counterstaining. After 30 minutes of incubation at 25 °C, the samples were rinsed with 0.45 M NaCl in PBS for 1 minute to remove weakly bound antibodies and observed with a confocal laser scanning microscope.

2.4.5 Statistical methods

The fibers size analysis was performed on three samples for each fibrous sample, obtained with different rotation rate. The average of size measurements ($n = 100$) was obtained along the respective standard errors. Alignment degree was obtained analyzing 10 SEM images through the Fiji software Directionality. The biological assays were performed twice. The level of significance was $p \leq 0.05$.

2.5 Results and discussion

2.5.1 Fibers characterization

PECA-DMSO solution was electrospun using a static and rotating collector. In Figure 4 are showed the fibers obtained by changing the speed rotation of the collecting surface. All the fibers present a beads-free morphology, but the surface of the fibers was irregular due to the relative humidity, able to affect their surface⁴⁷. When a static collector was used, the PECA fibers were obtained without a set orientation, resulting in an alignment degree of 45%, and their average size was $2.1 \pm 0.4 \mu\text{m}$. With the rotating collector at 1000 rpm, the fibers started to have a partial orientation, which had a degree of the 53% and the average size was $1.7 \pm 0.3 \mu\text{m}$. Increasing the speed at 3000 rpm, the fibers reached the degree of orientation of 85% and the size was measured to be $1.6 \pm 0.3 \mu\text{m}$.

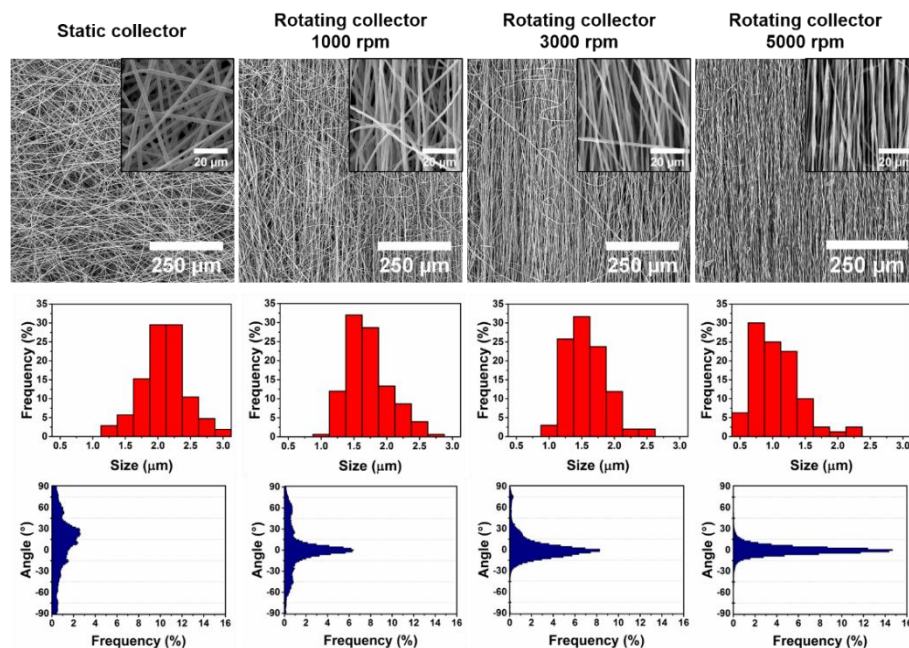


Figure 2.6 On the top. SEM images of the fibers obtained with a static collector and at different collecting speed, 1000, 3000 and 5000 rpm. In the inset, SEM images of the respective fibers at higher magnification. In the middle. Size distribution of the fibers obtained with static collector and at different collecting speed, 1000, 3000 and 5000 rpm. On the bottom. Distribution of the orientation fibers for each fibrous sample.

Finally, at a speed rotation of 5000 rpm, the orientation degree was 86% and the size was $1.2 \pm 0.4 \mu\text{m}$. The results suggested that increasing the rotation speed of the collector, the alignment degree of the fibers increases, while the size decreases, due to the stretching forces induced by the rotating collector. The trends are in according to other works in which rotating collectors were used^{48,49}.

For samples fabricated at 3000 and 5000 rpm, the orientation degree was quite similar, respectively 85% and 86%. However, the samples obtained at collecting speed of 5000 rpm, showed thinner fibers and higher number of fibers aligned, as reported in the relative orientation distribution graph in Figure 2.6. Therefore, for the next experiments, the fibers electrospun and collected at 5000 rpm were used.

2.5.2 Evaluation of coating biocompatibility and cell morphology

To obtain the coating with the oriented topography, fibers collected at 5000 rpm were put on a glass coverslip and were subjected to the melting process at 150°C for 20 seconds. The process induces their partial fusion, as reported in Mele *et al.*³⁵. Due to this, the fibers left a coating on the glass, which kept the topography of the fibers previously electrospun, as it is shown in Figure 2.7.

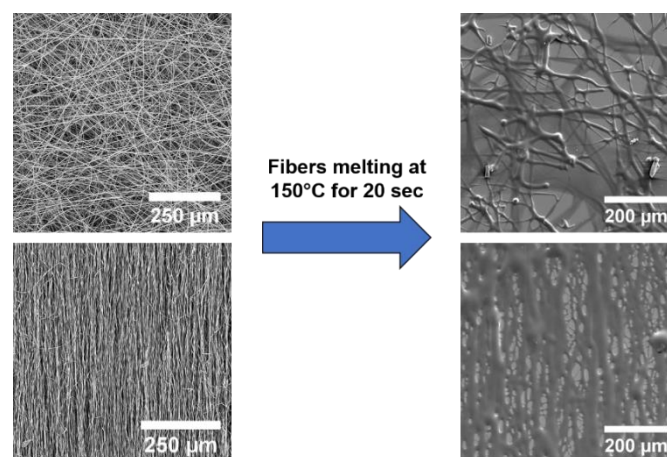


Figure 2.7 Fibers melting process at 150°C for 20 sec. On the right, how the fibers appear before the treatment, while on the right how they appear after the melting.

Not-melted and melted fibers were used as substrates for seeding 3T3 fibroblast cells, in order to investigate their biocompatibility (Figure 2.8). After 24 hours, cells seeded on not-melted fibers, both random and aligned, have shown low viability. Contrary, cells seeded on the melted fibers, presented higher viability. Those cells, which adhered on the aligned oriented PECA coating, showed a viability comparable with the control. While, cells seeded on the randomly oriented PECA coating, showed lower viability respect to the aligned fibers and the control. The low viability of cells on not-melted fibers could be due to the presence of solvent. Therefore, the melting process allowed the evaporation of the residual solvent, making more suitable PECA to be used as substrate for cells. In addition, 3T3 cells have shown higher viability on melted aligned substrate than the melted random one.

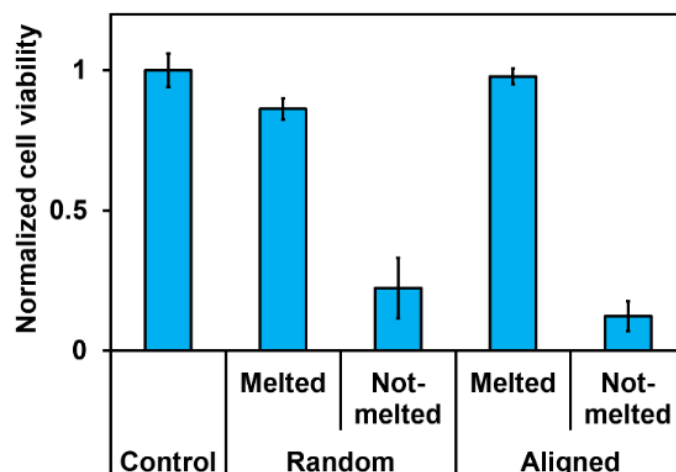


Figure 2.8 Viability of 3T3 cells seeded on glass (control), melted and not melted fibers, oriented both aligned and random, after 24h

This result is in accord with the already existing literature. In fact, as reported in previous works, aligned topography has particular cues that trig specific responses in several kinds of cells, such as migration, viability and differentiation⁵⁰⁻⁵². The most responsive cells are those which belonged to that kind of tissue which have a structural anisotropy which is related to its function⁵⁰. Nervous tissues, cardiac and skeletal muscle tissue, tendons and blood vessels

present an oriented ECMs which allow the tissue to have an orientation, which is believed to be necessary for cells function in vivo⁵³. Therefore, oriented substrates able to mimic features of the native ECMs could facilitate the growth of specialized cells of this kind of tissues^{54,55}.

Murine myoblasts C2C12 are immortalized and undifferentiated cells. They can be differentiated in skeletal muscle cells in presence of the right molecular stimuli³⁵. After the differentiation, skeletal muscle cells start to fuse their membrane and creating aligned polynucleate cells. Here, C2C12 cells were seeded on PECA-coated glass, both random and aligned. After 24h, the cells adhered on the PECA substrates, acquiring an elongated morphology and an aligned disposition when are attached on the oriented PECA coating.

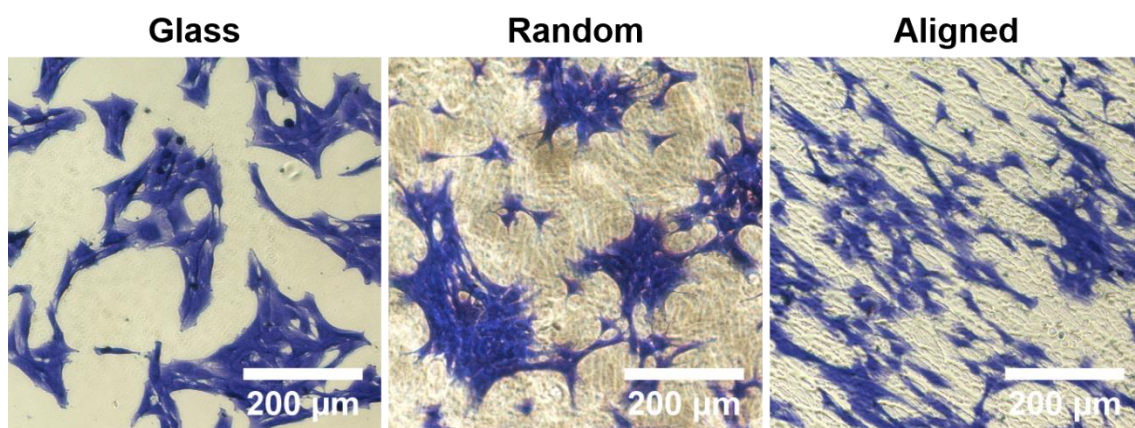


Figure 2.9 C2C12 myoblast cells fixed and stained with Coomassie brilliant blue R-250 on glass, randomly oriented PECA coating and aligned oriented PECA coating after 24h.

In Figure 2.9, this particular cell disposition can be observed along the presence of the PECA coating. Furthermore, C2C12 were also observed by using confocal microscope, in order to analyze their morphology and adhesion on the PECA coating. Cell morphology was similar when the cells were seeded on glass and random PECA coating. On the other hand, when they were seeded on the aligned fibers, cells acquired an elongated morphology, which was reflected in the F-actin disposition and consequently in their cytoskeleton.

With the aim to evaluate the correct adhesion of C2C12 cells on the PECA coatings and a possible rearrangement of the actin filament, confocal microscope images were acquired for cells seeded on all the samples (Figure 2.10). Vinculin, a protein present at the focal adhesion of the cells, was observed to be at the edges of each cell, following their shape. Therefore, its expression suggested a well adhesion of the cells on the substrate. Moreover, for cells plated on aligned PECA coating, the vinculin is more expressed such to allow a better adhesion of C2C12 on the PECA substrate. Actin the cells seeded on aligned PECA, was rearranged such to allow the cell to acquire an elongated morphology, suggesting that the cells was able to sense the topography of the coatings.

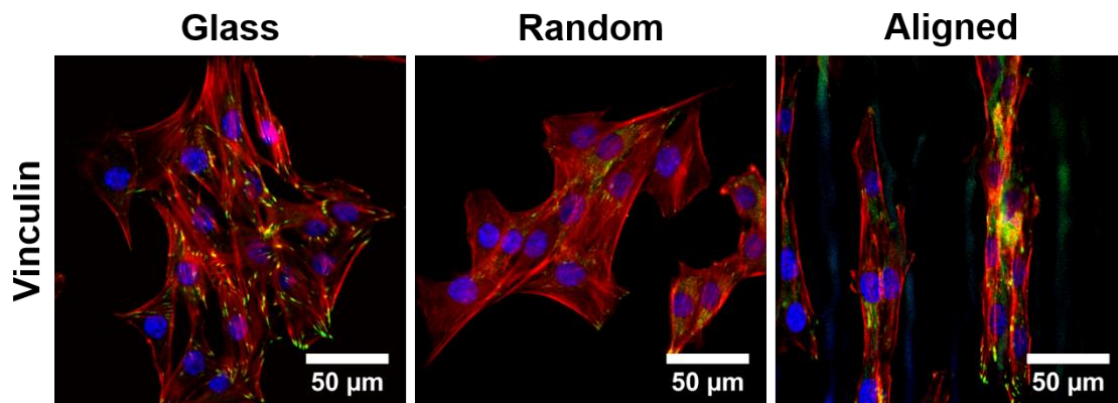


Figure 2.10 Confocal microscope images of C2C12 after 24h on glass, random and aligned PECA coating. In blue the nuclei stained with the DAPI; in red the F-actin stained with the phalloidin-TRITC; in green the vinculin in the focal adhesions.

Finally, C2C12 cells were kept in culture for 5 days, in order to investigate their viability when they are attached on the PECA coatings. In Figure 2.11, C2C12 viability on glass, random and aligned PECA coating, up to five days is shown. After 1 and 3 days of culture, cells seeded on the PECA-coated glass had the same viability, but lower than the viability of cells seeded on glass ($p < 0.05$). However, after 5 days, the cells attached on aligned PECA coating, showed higher viability respect to the random PECA coating and comparable viability respect to the control ($p > 0.05$). These results suggest that the PECA coating is not

toxic for the C2C12 myoblasts, and they can grow similarly to the control after five days. Nevertheless, aligned PECA fibers, after 5 days was able to induce more viability ($p < 0.05$), maybe due to a higher number of cells connected among themselves, disposed in an oriented way. In fact, previous works showed that when this kind of cells are cultured in a way which mimic the in vivo condition, they seem to increase their viability^{56,57}.

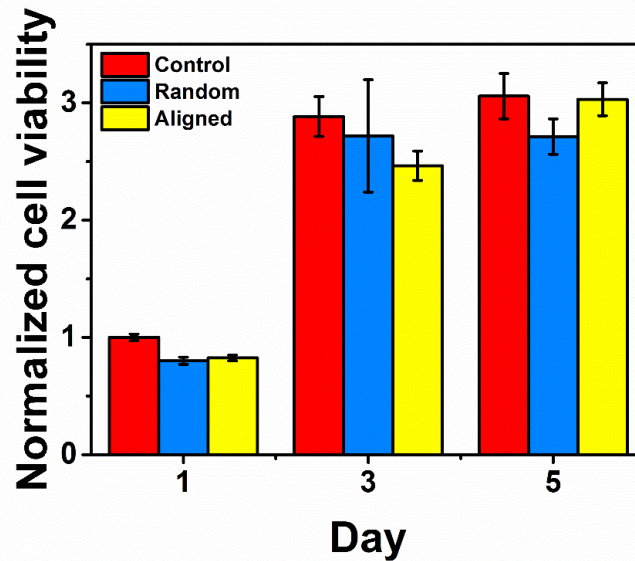


Figure 2.11 Viability of C2C12 myoblasts on glass, random and aligned PECA coating up to 5 days.

2.6 Conclusions

ECA is one of the monomer of the cyanoacrylates adhesives which is generally used as fixative agents in medical practice, especially for internal application on bone and nerve regeneration^{24,30-34}. Despite the release of formaldehyde is relatively high, ECA degradation rate is fast enough to allow its removal in short time, allowing the regeneration of the tissue^{15,24}. Although the interesting properties showed by ECA, its development, as material for biomedical application, is limited by its high reactivity in presence of weak bases⁶. Recently, a novel protocol was developed in order to stabilize ECA solution such to produce fibers through the electrospinning³⁵. Fibers were used to produce coating which kept the roughness of the fibers previously electrospun.

In this work, PECA fibers were obtained through the electrospinning and the process was optimized such to produce aligned fibers with high alignment degree. Aligned electrospinning fibers were used to produce a PECA coated surface, though a melting process, which kept the topography of the electrospun fibers³⁵. The coating resulted biocompatible and not toxic. Moreover, the oriented topography, left by the aligned fibers, was able to induce the aligned disposition of myoblasts C2C12 on the PECA substrate. They also showed an elongated morphology, a reorganized cytoskeleton structure and more focal adhesions. Altogether, the results showed that PECA aligned fibers can be used as a substrate for cell growth, especially for cell belonged to tissue with anisotropic structure.

2.7 Bibliography

1. Ardis, A. E. Preparation of monomeric alkyl alpha-cyano-acrylates. US 2,467,927 (1947).
2. Quinn, J. V. *Tissue Adhesives in Clinical Medicine*. (BC Decker, Inc, 2005). doi:10.1017/CBO9781107415324.004
3. Weber, S. C. & Chapman, M. W. Adhesives in orthopaedic surgery. A review of the literature and in vitro bonding strengths of bone-bonding agents. *Clin. Orthop. Relat. Res.* **191**, 249–261 (1984).
4. Shermak, M. A. *et al.* Fixation of the craniofacial skeleton with butyl-2-cyanoacrylate and its effects on histotoxicity and healing. *Plastic and reconstructive surgery* **102**, 309–18 (1998).
5. Toriumi, D. M., Raslan, W. F., Friedman, M. & Tardy, M. E. Histotoxicity of cyanoacrylate tissue adhesives. A comparative study. *Arch. Otolaryngol. Head. Neck Surg.* **116**, 546–550 (1990).
6. Vauthier, C., Dubernet, C., Fattal, E., Pinto-Alphandary, H. & Couvreur, P. Poly(alkylcyanoacrylates) as biodegradable materials for biomedical applications. *Adv. Drug Deliv. Rev.* **55**, 519–548 (2003).
7. Leonard, F., Kulkarni, R. K., Brandes, G., Nelson, J. & Cameron, J. J. Synthesis and degradation of poly (alkyl alpha-cyanoacrylates). *J. Appl. Polym. Sci.* **10**, 259–272 (1966).
8. Greer, R. O. Studies concerning the histotoxicity of isobutyl-2-cyanoacrylate tissue adhesive when employed as an oral hemostat. *Oral Surgery, Oral Med. Oral Pathol.* **40**, 659–669 (1975).
9. Chandra, R. K., Handorf, C., West, M., Kruger, E. A. & Jackson, S. Histologic effects of autologous platelet gel in skin flap healing. *Arch. Facial Plast. Surg.* **9**, 260–263 (2007).
10. Pérez, M., Fernández, I., Márquez, D. & Guerra Bretaña, R. M. Use of N-butyl-2-cyanoacrylate in oral surgery: Biological and clinical evaluation. *Artif. Organs* **24**, 241–243 (2000).
11. Harper, M. C. Viscous isoamyl 2-cyanoacrylate as an osseous adhesive in the repair of osteochondral osteotomies in rabbits. *J. Orthop. Res.* **6**, 287–292 (1988).
12. Bhaskar, S. N., Jacoway, J. R., Margetis, P. M., Leonard, F. & Pani, K. C. Oral tissue response to chemical adhesives (cyanoacrylates). *Oral Surgery, Oral Med. Oral Pathol.* **22**, 394–404 (1966).
13. de Almeida Manzano, R. P., Naufal, S. C., Hida, R. Y., Guarnieri, L. O. & Nishiwaki-Dantas, M. C. Antibacterial analysis in vitro of ethyl-cyanoacrylate against ocular pathogens. *Cornea* **25**, 350–351 (2006).

14. Singer, A. J., Quinn, J. V., Clark, R. E. & Hollander, J. E. Closure of lacerations and incisions with octylcyanoacrylate: A multicenter randomized controlled trial. *Surgery* **131**, 270–276 (2002).
15. Barkan, Y. *et al.* Comparative evaluation of polycyanoacrylates. *Acta Biomater.* **48**, 390–400 (2017).
16. Mizrahi, B. *et al.* Elasticity and safety of alkoxyethyl cyanoacrylate tissue adhesives. *Acta Biomater.* **7**, 3150–3157 (2011).
17. Cheung, K. H., Guthrie, J., Otterburn, M. S. & Rooney, J. M. The dynamic mechanical properties of poly(alkyl 2-cyanoacrylates). *Die Makromol. Chemie* **188**, 3041–3046 (1987).
18. Tseng, Y. C., Hyon, S. H. & Ikada, Y. Modification of synthesis and investigation of properties for 2-cyanoacrylates. *Biomaterials* **11**, 73–79 (1990).
19. Kulkarni, R. K., Porter, H. J. & Leonard, F. Glass transition temperatures of poly(alkyl α -cyanoacrylates). *J. Appl. Polym. Sci.* **17**, 3509–3514 (1973).
20. Pascual, G. *et al.* Cytotoxicity of Cyanoacrylate-Based Tissue Adhesives and Short-Term Preclinical In Vivo Biocompatibility in Abdominal Hernia Repair. *PLoS One* **11**, e0157920 (2016).
21. Müller, R. H., Lherm, C., Herbert, J. & Couvreur, P. In vitro model for the degradation of alkylcyanoacrylate nanoparticles. *Biomaterials* **11**, 590–595 (1990).
22. Scherer, D., Robinson, J. R. & Kreuter, J. Influence of enzymes on the stability of polybutylcyanoacrylate nanoparticles. *Int. J. Pharm.* **101**, 165–168 (1994).
23. Vezin, W. R. & Florence, A. T. In vitro heterogeneous degradation of poly(n-alkyl alpha-cyanoacrylates). *J. Biomed. Mater. Res.* **14**, 93–106 (1980).
24. Saska, S. *et al.* Fixation of autogenous bone grafts with ethyl-cyanoacrylate glue or titanium screws in the calvaria of rabbits. *Int. J. Oral Maxillofac. Surg.* **38**, 180–186 (2009).
25. Reece, T. B., Maxey, T. S. & Kron, I. L. A prospectus on tissue adhesives. *Am. J. Surg.* **182**, S40–S44 (2001).
26. Marcovich, R., Williams, A. L., Rubin, M. A. & Wolf, J. S. Comparison of 2-octyl cyanoacrylate adhesive, fibrin glue, and suturing for wound closure in the porcine urinary tract. *Urology* **57**, 806–810 (2001).
27. Hallock, G. G. Expanded applications for octyl-2-cyanoacrylate as a tissue adhesive. *Ann. Plast. Surg.* **46**, 185–9 (2001).
28. King, M. E. & Kinney, A. Y. Tissue adhesives: A new method of wound repair. *Nurse Pract.* **24**, 66–75 (1999).
29. Burns, D. T., Brown, J. K., Dinsmore, A. & Harvey, K. K. Base-activated latent

- fingerprints fumed with a cyanoacrylate monomer. A quantitative study using Fourier-transform infra-red spectroscopy. *Anal. Chim. Acta* **362**, 171–176 (1998).
30. Esteves, J. C., Monteiro, J. M., Aranega, A. M., Betoni Junior, W. & Sonoda, C. K. Utilization of Ethyl Cyanoacrylate and 2-Octyl Cyanoacrylate Adhesives for Autogenous Bone Graft Fixation: Histomorphometric Study in Rats. *J. Oral Implantol.* **40**, 411–417 (2014).
 31. Nemoto, H. *et al.* Orbital Floor Reconstruction With Ethyl-2-Cyanoacrylate. *Ann. Plast. Surg.* **74**, 195–198 (2015).
 32. Landegren, T., Risling, M., Hammarberg, H. & Persson, J. K. E. Selectivity in the reinnervation of the lateral gastrocnemius muscle after nerve repair with ethyl cyanoacrylate in the rat. *Front. Neurol.* **APR**, 1–9 (2011).
 33. Merolli, A., Marceddu, S., Rocchi, L. & Catalano, F. In vivo study of ethyl-2-cyanoacrylate applied in direct contact with nerves regenerating in a novel nerve-guide. *J. Mater. Sci. Mater. Med.* **21**, 1979–1987 (2010).
 34. Rickett, T. *et al.* Ethyl-cyanoacrylate is acutely nontoxic and provides sufficient bond strength for anastomosis of peripheral nerves. *J. Biomed. Mater. Res. A* **90**, 750–4 (2009).
 35. Mele, E. *et al.* Zwitterionic Nanofibers of Super-Glue for Transparent and Biocompatible Multi-Purpose Coatings. *Sci. Rep.* **5**, 1–13 (2015).
 36. Ostrovidov, S. *et al.* Skeletal Muscle Tissue Engineering: Methods to Form Skeletal Myotubes and Their Applications. *Tissue Eng. Part B Rev.* **20**, 403–436 (2014).
 37. Sosa, H., Popp, D., Ouyang, G. & Huxley, H. E. Ultrastructure of skeletal muscle fibers studied by a plunge quick freezing method: myofilament lengths. *Biophys. J.* **67**, 283–292 (1994).
 38. training.seer.cancer.gov. SEER Training:Structure of Skeletal Muscle. (2015). Available at: <https://training.seer.cancer.gov/anatomy/muscular/structure.html>.
 39. Strohman, R. C. *et al.* Myogenesis and histogenesis of skeletal muscle on flexible membranes in vitro. *In Vitro Cell. Dev. Biol.* **26**, 201–8 (1990).
 40. Dennis, R. G., Kosnik, P. E., Gilbert, M. E. & Faulkner, J. A. Excitability and contractility of skeletal muscle engineered from primary cultures and cell lines. *Am. J. Physiol. Cell Physiol.* **280**, C288-95 (2001).
 41. Lesman, A., Gepstein, L. & Levenberg, S. Vascularization shaping the heart. *Ann. N. Y. Acad. Sci.* **1188**, 46–51 (2010).
 42. Levenberg, S. *et al.* Engineering vascularized skeletal muscle tissue. *Nat. Biotechnol.* **23**, 879–884 (2005).
 43. Klumpp, D., Horch, R. E., Kneser, U. & Beier, J. P. Engineering skeletal muscle tissue - new perspectives in vitro and in vivo. *J. Cell. Mol. Med.* **14**, 2622–2629 (2010).

44. Khademhosseini, A., Langer, R., Borenstein, J. & Vacanti, J. P. Microscale technologies for tissue engineering and biology. *Proc. Natl. Acad. Sci.* **103**, 2480–2487 (2006).
45. Lam, M. T., Huang, Y.-C., Birla, R. K. & Takayama, S. Microfeature guided skeletal muscle tissue engineering for highly organized 3-dimensional free-standing constructs. *Biomaterials* **30**, 1150–1155 (2009).
46. Mochizuki, Y. & Furukawa, K. Application of Coomassie brilliant blue staining to cultured hepatocytes. *Cell Biol. Int. Rep.* **11**, 367–371 (1987).
47. Casper, C. L., Stephens, J. S., Tassi, N. G., Chase, D. B. & Rabolt, J. F. Controlling surface morphology of electrospun polystyrene fibers: Effect of humidity and molecular weight in the electrospinning process. *Macromolecules* **37**, 573–578 (2004).
48. Kiselev, P. & Rosell-Llompart, J. Highly aligned electrospun nanofibers by elimination of the whipping motion. *J. Appl. Polym. Sci.* **125**, 2433–2441 (2012).
49. Alfaro De Prá, M. A., Ribeiro-do-Valle, R. M., Maraschin, M. & Veleirinho, B. Effect of collector design on the morphological properties of polycaprolactone electrospun fibers. *Mater. Lett.* **193**, 154–157 (2017).
50. Wang, X., Ding, B. & Li, B. Biomimetic electrospun nanofibrous structures for tissue engineering. *Mater. Today* **16**, 229–241 (2013).
51. Saino, E. *et al.* Effect of electrospun fiber diameter and alignment on macrophage activation and secretion of proinflammatory cytokines and chemokines. *Biomacromolecules* **12**, 1900–1911 (2011).
52. Lee, S., Tong, X., Han, L. H., Behn, A. & Yang, F. Winner of the Young Investigator Award of the Society for Biomaterials (USA) for 2016, 10th World Biomaterials Congress, May 17-22, 2016, Montreal QC, Canada: Aligned microribbon-like hydrogels for guiding three-dimensional smooth muscle tissue regeneration. *J. Biomed. Mater. Res. - Part A* **104**, 1064–1071 (2016).
53. Liu, W., Thomopoulos, S. & Xia, Y. Electrospun nanofibers for regenerative medicine. *Adv. Healthc. Mater.* **1**, 10–25 (2012).
54. Kim, T. G., Shin, H. & Lim, D. W. Biomimetic scaffolds for tissue engineering. *Adv. Funct. Mater.* **22**, 2446–2468 (2012).
55. Yang, F., Murugan, R., Wang, S. & Ramakrishna, S. Electrospinning of nano/micro scale poly(l-lactic acid) aligned fibers and their potential in neural tissue engineering. *Biomaterials* **26**, 2603–2610 (2005).
56. Chen, M. C., Sun, Y. C. & Chen, Y. H. Electrically conductive nanofibers with highly oriented structures and their potential application in skeletal muscle tissue engineering. *Acta Biomater.* **9**, 5562–5572 (2013).
57. Wang, D. *et al.* Tissue-specific mechanical and geometrical control of cell viability and

actin cytoskeleton alignment. *Sci. Rep.* **4**, 6160 (2014).

Chapter 3

Electrospun silk fibroin fibers for human platelets lysate release

3.1 Silk fibroin

Silk fibroin is a structural protein that constitutes the cocoons of the *Bombyx mori*. In the yarns of the cocoons, fibroin resulted to be coated by the sericin, which is a gum-like protein (Figure 3.1)¹. The fibroin is the major component of the cocoons (72-81%), while the remaining part is sericin (19-28%)^{1,2}. Fibroin in the cocoons is made up by a heavy chain (H) with a molecular weight of 325kDa and a light chain (L) of 25kDa³, which are linked by a disulfide bond at the C-terminus of the H-chain, forming the H-L complex⁴. Thanks to the glycoprotein P25 (25kDa), six H-L complexes are assembled non-covalently in the silk fibroin polymer⁴. The amino acids composition of the fibroin protein is mainly characterized by glycine (Gly = 43%), alanine (Ala = 30%) and serine (Ser = 12%)⁵. More precisely, the H

chain consists of repeated hexapeptide Gly-Ala-Gly-Ala-Gly-Ser and the dipeptide Gly-Ala/Ser/Tyr, which self-assemble in hydrophobic antiparallel β -sheets during the silk worms spinning⁴.

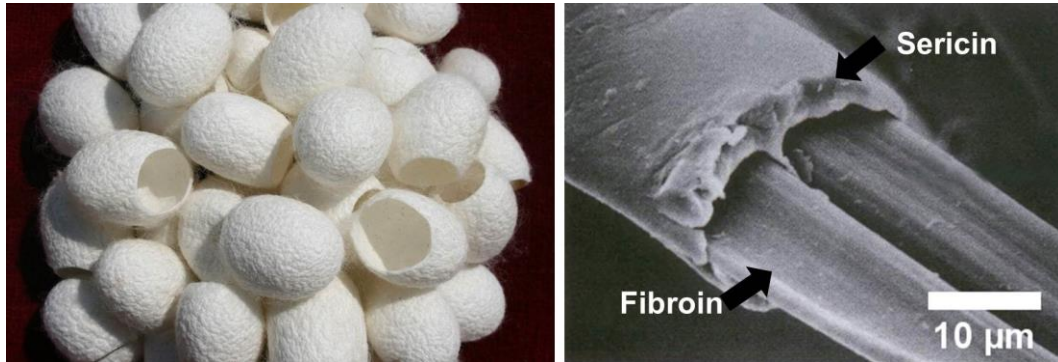


Figure 3.1 Images show silkworms' cocoons on the left, while on the right SEM micrograph of a cocoons yarn structure, in which fibroin and sericin are highlighted.

Contrary to the H chain, L chain has not repetition in its primary structure and contains principally valine, isoleucine and leucine and acidic amino acids⁶, which make it more hydrophilic⁴. Due to its composition and structure, fibroin protein results hydrophobic⁷, and characterized by a semi-crystalline structure containing two phases: one highly ordered crystalline, formed by the hydrophobic antiparallel β -sheets, which is alternated with a less organized phase (Figure 3.2). In particular, the crystalline phase remarkably influences the physical and chemical properties of the fibroin, such as its strength, toughness, refractive index, water solubility and degradation^{8,9}. The amorphous part contributes to the flexibility and elasticity of the fibroin^{10,11}.

3.2 Silk fibroin as biomaterial

Silk fibroin was generally used for its high strength, as woven and as a suture material in medicine^{8,12}. More recently, silk fibroin has become attractive as a material for biomedical application thanks to its proved biocompatibility and low immunogenicity¹². The use of fibroin as biomaterials was also possible thanks to the development of protocols which permit

its extraction from the cocoons of silkworms. The extraction of fibroin from the cocoons is a process known as regeneration and it results in an aqueous solution. Regeneration allows to have fibroin alone without sericin, which has showed to induce immunological response, both *in vitro* and *in vivo*^{3,13}. Water soluble regenerated silk fibroin (RSF) has the advantage to be more processable, such to be used to fabricate films, hydrogels, sponges, nanoparticles and fibers^{3,8,12,14–17}. Moreover, problem related to use of solvent can be avoided¹².

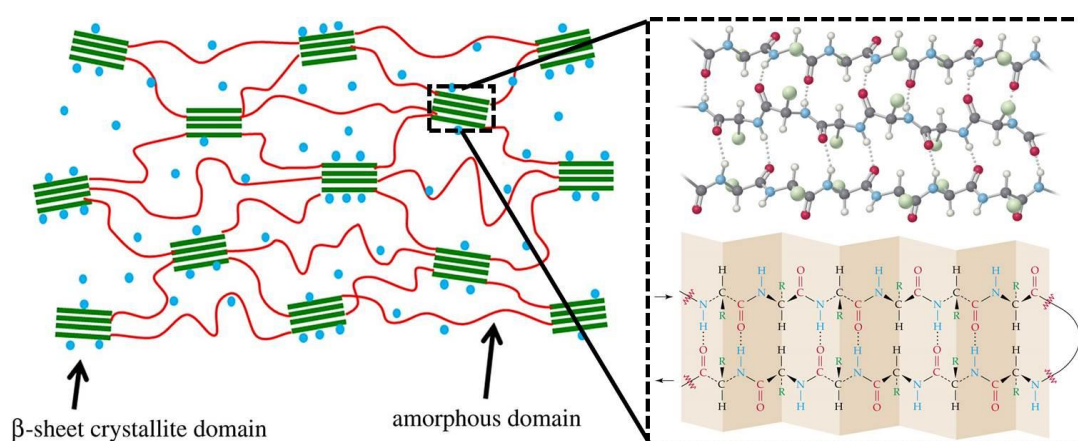


Figure 3.2 Schematic that show the secondary structure of the silk fibroin. The hydrophobic peptide of the aminoacidic sequence self-assemble, such to form antiparallel β -sheets, which are alternated with amorphous domain¹⁸. The β -sheets content characterizes physical and chemical properties of the fibroin matrix. Figure is from Cheng et al., 2014¹⁸.

RSF self-assembles from the water solution such to acquire structures which native silk fibroin showed as well: an amorphous state (called silk I) presenting α -helices, and a crystalline state (called silk II) with high β -sheets content^{5,8,19,20}. In addition, only RSF can self-assembles in a third helical structure (silk III), which can be formed at the interface air/water²¹.

As for native fibroin, the β -sheets structures, characterizing silk II, affect several of its physical and chemical properties, such as degradation rate, hydrophobicity and hydrophilicity, transparency, mechanical strength, porosity, oxygen permeability, and thermal stability¹. Particularly interesting is the water stability provided by the β -sheet secondary structure:

while silk I is soluble in water; highly crystalline silk II does not dissolve in pure water⁹. The transition of the RSF from silk I to silk II is possible by modulating the hydration state of the fibroin^{9,21–24}. In fact, water allows the movement of protein chains with the consequent formation of the β -sheets^{9,25,26}. Therefore, the transition can be achieved through aqueous based process, but organic solvent can be used as well^{9,27–30}. However, the use of water vapor is preferred because is slower, more controlled and it allows to obtain different crystallinity degrees by varying the treatment duration. In addition, being a milder process, water vapor annealing can be applied even when sensitive molecules or cellular organelles are embedded in fibroin matrices^{9,31–34}.

RSF can be degraded by protease or via hydrolysis catalyzed by enzyme, resulting in amino acids which are resorbed by the organism. The enzymatic degradation starts from amorphous fibroin and then involves silk I and ultimately silk II structures³⁵. Furthermore, *in vitro* enzymatic degradation assays performed on fibroin fibrous scaffolds, have shown a slower degradation rate when the scaffold presented high crystallinity^{36,37}. *In vivo* studies confirmed the longer permanence of highly crystalline silk fibroin implants³⁸. The control on the degradation is especially interesting in drug delivery applications, since controlling the rate of degradation enables the prolonged and sustained delivery of active factors during the entire course of the therapy. *In vitro* investigations with highly crystalline silk fibroin matrices showed a slower release compared to the amorphous silk^{39–43}. The ability of the silk fibroin in controlling the release was found also *in vivo* using chemotherapeutic agents. They were released in a sustained way and this kept their concentration under the toxic threshold^{34,44}. So, such controlled delivery can keep the overall drug concentration low within the patient's body, reducing the frequency of the treatment administration⁴⁵.

Within the context of the biomedicine, the sustained release of growth factors from biodegradable polymeric matrices showed accelerated and improved wound healing and great

potential for more complete cells differentiation in tissue engineering⁴⁶⁻⁴⁸. Also, for chronic wounds, keeping low the concentration of growth factors and for longer time, can help their healing^{49,50}.

3.3 Platelet-derived proteins

Platelets are anucleate circulating cells and are involved in coagulation processes. Platelets are generated in the bone marrow by megakaryocytes, which release them, entering in the bloodstream⁵¹. Their task is to bind rapidly damaged blood vessels, such to aggregate and induce clot formation. Platelets are activated by the coagulation cascades which trig them to release proteins and factors, which play a crucial role in migration of mesenchymal, epithelial and endothelial cells, especially during wound healing process⁵². Therefore, upon activation, platelets can release platelet-derived growth factor (PDGF), vascular endothelial growth factor (VEGF), epidermal growth factor (EGF), fibroblast growth factor (FGF), transforming growth factor- β (TGF- β), heparin binding EGF-like growth factor (HB-EGF), matrix metalloproteinases (MMP) and interleukin 8 (IL-8)⁵².

PDGF is active during the first phase of the wound healing. It can induce proliferation of epithelial cells and recruit at the wound site white blood cells, to prevent infection and remove dead cells, and fibroblasts, able to depose matrix⁵³. low levels of PDGF have been found in chronic wound caused by diabetes⁵². FGF promote the activation of fibroblast, and endothelial cell proliferation, migration and differentiation. In combination with VEGF, FGF can induce angiogenesis⁵⁴. TGF- β is a potent attractant molecule toward white blood cells and fibroblast⁵². EGF and HB-EGF induce the proliferation of the epithelial cells and fibroblasts⁵³. Finally, IL-8 is a cytokine involved in formation of new skin tissue and new blood vessels. IL-8 rules the inflammation phase during the wound healing. Therefore, it can intervene in

unbalanced inflammatory situation restoring the normal course of the healing process and can have antibacterial role⁵⁵.

To exploit these important activities of the platelet-derived factors, platelets rich plasma (PRP) was obtained upon isolation of the platelets from human blood⁵⁶. Autologous PRP demonstrated to be able to help the regeneration and recovery of normal conditions, in case of chronic wound as well as several damaged tissues, such as bone⁵⁷, skin⁵⁸, peripheral nerve⁵⁹, and cardiac muscle⁶⁰. Three-dimensional gel was also produced with PRP, upon addition of fibrinogen, fibronectin, thrombin, calcium gluconate and clotting agents. PRP gel can be applied at the wound site, releasing efficiently the functional platelets-derived factors⁶¹. Clinical trials have investigated the potential of platelet derived systems (PRP and PRP-gel) in tissue regeneration on human. Some trials showed ameliorated conditions and improved healing, while others did not show improvements^{62,63}. A limit of using PRP is related to its extraction⁵². PRP is obtained from the blood of single donor. However, platelets concentration can change from each individual. Therefore, to reduce interindividual variability, a new protocol for isolating the platelets proteins uses different blood samples, which derive from more than one donor^{64,65}. The process results in extraction of the platelet-derived proteins, by lyophilizing the PRP⁶⁵. Lyophilization causes the lysis of the platelets, allowing the release of the platelet proteins. Allogeneic human-derived platelets lysate (hPL) is obtained as a lyophilized powder and it is highly enriched with platelets-derived proteins. *In vitro* experiments showed that hPL supports every stage of the wound healing, favoring cells growth and angiogenesis, and stimulating the recruitment of white blood cells, also thanks to its sustained release^{55,66,67}, while *in vivo* hPL was observed to support bone regeneration and the recovery of non-healing wounds^{68,69}. Consequently, gels fabricated from allogeneic hPL, demonstrated their effectiveness on the wound closure on a mice model⁵².

Despite these promising results, on-the-spot preparation, difficult handling, storage at low temperature to preserve the activity of the factors are some of the technical and practical limitations that still hinder the hPL usage as therapeutic tool^{70,71}. Therefore, there is a need of designing a device that could conjugate the sustained release of the allogenic hPL with an easier handling on a wound, while keeping the hPL factors well-preserved. This would allow a more effective use of the hPL molecules in the wound care management.

3.4 Fabrication of electrospun silk fibroin fibers encapsulating hPL⁷²

To overcome the limits in its usage, in this work, hPL was electrospun with silk fibroin in order to produce fibers able to encapsulate it. Such system was used to control the hPL releasing rate by tuning the degradability of silk fibroin. Moreover, protective effect on sensitive molecules typical of the fibroin was also exploited in order to preserve the activity of hPL proteins⁷³⁻⁷⁶.

Generally, to electrospin silk fibroin, PEO is added because it adjusts the viscosity of the regenerate silk fibroin, as reported in previous works⁷⁷⁻⁸⁰. The use of electrospun fibers grants materials with high porosity and high surface area, which are characteristics provided by the micro and nanofibers. Therefore, electrospun materials allow efficient gas exchange, to absorb wound exudate as well as support cell proliferation and migration. All the above-mentioned features successfully mimic the natural extracellular matrix, thus improving and sustaining the healing process of the wounds⁸¹⁻⁸⁴.

Herein, silk fibroin fibers were fabricated along the hPL, resulting in high proteins loading. The characterization of the kinetic release showed the effective control on the protein release through the manipulation of fibroin crystallinity. The protein release assessment was carried out with an *in vitro* test that was developed to simulate *in vivo* degradation conditions. Therefore, different crystalline mats were subjected to degradation and the release of albumin

from them was traced^{85,86}. Once released from silk fibroin fibers, hPL has shown to retain its ability to induce and sustain the viability of primary adult human dermal fibroblasts (HDFa) *in vitro*. Finally, the possibility to use silk fibroin for the preservation of hPL biological activity was proved even after thermal stress at 60 °C, demonstrating the improvement of the shelf-life of hPL, granted by the fibroin matrix. Our construct can be proposed as a valid, easy-to-fabricate and durable alternative to the PRP gel in the wound care management.

3.5 Experimental section

3.5.1 Fibroin regeneration

Fibroin was extracted from *Bombyx mori* cocoons according to the protocol previously described by Rockwood *et al.* (Figure 3.3)¹². Firstly, the cocoons were cut and boiled for 30 minutes in a water solution of 0.023M of Na₂CO₃; subsequently, the fibers were washed with MilliQ (Ohms) water and dried. Degummed fibroin was solubilized in an aqueous solution of 9.3 M of lithium bromide at 60°C for 4 hours and dialyzed in a tube with a MWCO of 3,500 kDa for 3 days against MilliQ water. Finally, regenerated fibroin was centrifuged twice at 9000 rpm, for 20 minutes at 4°C. To quantify the fibroin concentration, 1 mL of regenerated fibroin solution was left to dry under an aspirating hood. Then, the dried film was weighted, obtaining the concentration of silk fibroin in the solution. The concentration was found to be in a range between 60 and 80 mg/mL.

3.5.2 Fibers fabrication and water vapor treatment

To produce the fibers, fibroin 60 mg/mL solution was used. To facilitate the electrospinning process and fabricate the fibers, PEO powder 25% w/w_{silk} was added to a 60 mg/ml aqueous solution of fibroin and stirred overnight⁷⁷.

Once a homogeneous solution was obtained, FITC-albumin powder was added such to obtain a concentration of 2% w/w_{silk}. To add hPL, solutions of it 7% and 14% w/w_{silk} were added to not diluted silk fibroin solution. Therefore, hPL solutions need to have an enough volume to dilute the silk fibroin solution at 60mg/mL. The final concentration of the hPL in the electrospun fibers were 5% and 10% w/w respectively. The fibers were electrospun at 20°C in a controlled humidity environment (30% - 40% relative humidity) with a syringe pump (NE-1000, New Era Pump Systems, Inc.) equipped with a blunt 19G needle, at a flow rate of 1 mLh⁻¹ (Figure S1A). An aluminum, grounded collector was placed at 20cm from the needle, while a voltage of 18 kV was applied (EH40R2.5, Glassman High Voltage, Inc.). In the case of the hPL loaded fibers, the following parameters were considered: a flow rate of 1.2 mLh⁻¹, a needle - collector distance of 30 cm, and a voltage of 23 kV. These parameters were considered in order to have a continuous electrospinning process and to avoid having wet fibers on the collector.

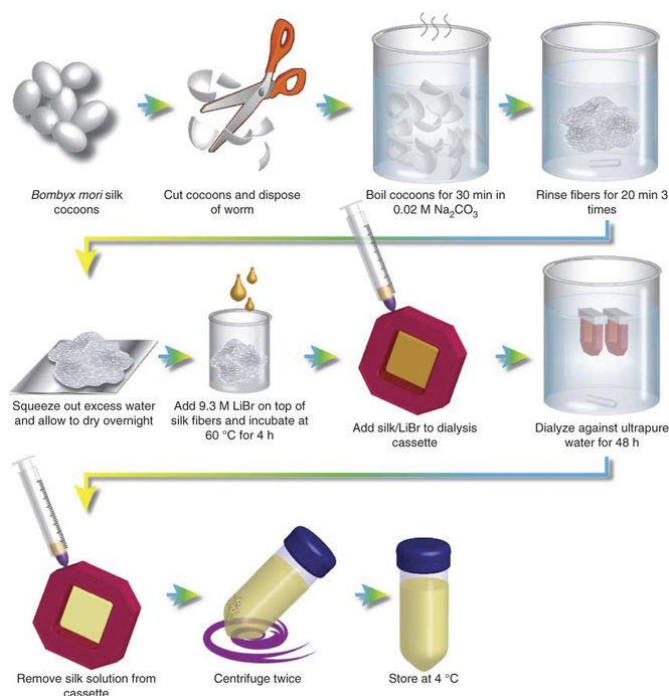


Figure 3.3 Regeneration protocol for silk fibroin from cocoons, optimized by Rockwood et al.¹². The regeneration can permit the extraction of silk fibroin, such to have it in aqueous solution. Figure is from article of Rockwood et al., 2011.

The crystallinity degree of the silk fibroin fibrous mats was increased via water vapor annealing. The treatment was performed in a vacuum oven (VO500EA, MLS, Italy) at 40°C and 85-90% of relative humidity. Different treatment times were used for the different crystallization reported (Figure S1B), ranging from 10 minutes to 6 hours.

3.5.3 Fibers Characterization

- **Morphology**

Fiber morphology was characterized by scanning electron microscopy (SEM) using a JEOL JSM-6490LA microscope, in high vacuum with an acceleration voltage of 15kV. The samples were previously coated with a 10-nm-thick gold layer with a Cressington 208HR high resolution sputter coater (Cressington scientific instrument Ltd, U.K.). Size analysis was performed with ImageJ software. To evaluate the encapsulation of the FITC-albumin molecules, confocal imaging was performed with a laser scanning confocal microscope (Nikon A1R).

- **Fibroin crystallinity characterization**

Characterization of the fiber crystallinity was performed by Fourier transform infrared spectroscopy (FTIR). Samples were measured in Attenuated Total Reflectance (ATR) mode using MIRacle ATR accessory (PIKE Technologies) coupled to a Fourier Transform Infrared (FTIR) spectrometer (Equinox 70 FT-IR, Bruker). All the spectra were acquired in a spectral range from 4000 to 600 cm^{-1} , with a scanning resolution of 4 cm^{-1} , accumulating 64 scans.

The deconvolution of the fibroin amide I peak was performed as reported previously by Guzman-Puyol *et al.* and Hu *et al.*^{87,88}. The software was PeakFit 4.11⁸⁷ and the wavenumber positions of the different components were deduced by calculation of the second-order derivative⁸⁷. The fitting of the different contributions was performed using Gaussian-shaped

peaks, using a fixed width for each considered peak. The crystallinity content was obtained from the ratio between the areas of the β -sheets peaks and the total area of the amide I peak

3.5.4 Drug release assessment

- **Evaluation of the albumin presence in hPL through SDS-page**

To evaluate the presence of albumin in hPL, SDS-page electrophoresis was performed. SDS-PAGE, 12% w/v polyacrylamide separating gel and 4% w/v polyacrylamide stacking gel were used to resolve proteins at 120V for 90 minutes. A wide-range molecular weight (15–250 kDa) marker was run along with the proteins. hPL and of bovine serum albumin standard (BSA) were reduced with 50mM dithiothreitol (DTT) and heated at 75°C for 10 minutes. Different concentrations of hPL proteins were loaded on the gel (15 μ g, 7.5 μ g and 3.75 μ g). For BSA, 15 μ g was loaded. The gel was colored with Coomassie Brilliant Blue 0.1% in a mixture of methanol:acetic acid:water 40:10:50 v/v.

- **Characterization of the FITC-albumin release from silk fibroin fibers**

Electrospun silk fibroin unloaded (SF), loaded with FITC-albumin (SF-alb), loaded with hPL (SF-hPL), and loaded both with FITC-albumin and hPL (SF-alb-hPL) fibers, were weighted and placed in a 24 well-plate with 1 mL of PBS 0.04M at pH 7.4 and with 6.25 mU of protease XIV in 0.04M PBS pH 7.4 at 37°C and gently stirred on a tilting plate for 5 months. At given time points, the total volume was taken out and substituted with fresh medium. The amount of FITC-albumin was determined by correlating the absorbance at 495 nm with a calibration curve measured by using the same media, after subtraction of a blank spectra obtained by measuring the SF and SF-hPL samples. The measurements were carried out using a UV-visible spectrophotometer (Cary 6000i-Varian) from 450 nm to 550 nm.

To characterize the effect of the enzymatic degradation on the samples, three SF-alb-hPL mats having different crystallinity (22%, 35% and 45%) were incubated at 37°C for 1 month,

either with PBS or in the presence of PBS containing the enzyme (6.25U/mg_{fibers}). The medium was completely replaced every day. Subsequently, the mats were washed with MilliQ water for 10 minutes five times, in order to remove traces of salt and enzyme. After the final timepoint, the samples were rinsed, dried and imaged by SEM.

3.5.5 Evaluation of the hPL biological activity released from the fibers.

- **Biological activity of the released hPL**

Primary human dermal fibroblasts from an adult donor (HDFa) were seeded in Medium 106, containing 2% v/v of fetal bovine serum, 1 µg/mL of hydrocortisone, 10 ng/mL human epidermal growth factor, 3 ng/mL of basic fibroblast growth factor, and 10 µg/mL of heparin. The cells were split every 7 days and seeded at a density of 4500 cells/cm². Medium was changed every day.

To assess the retained activity of the released hPL, 20 mg of SF and SF-hPL fibers, at 24% of crystallinity, were incubated, after sterilization with UV treatment for 20 minutes for each side, in 4 mL of serum-free culture medium for 24h at 37°C. The low crystallinity of the mats permits the dissolution of the matrix and the complete release of all the factors in 24h hours. The concentration of hPL released in serum-free culture medium, was of 250 µg/mL, which was the minimum concentration able to increase the viability of the HDFa, as observed in a previous experiment (Figure S8). Twenty-four hours before the treatment, cells were seeded with a density of 4500 cells/cm² in complete culture medium. The day after, some cells were used to assess the viability before the treatment with the samples. This reading was labeled time point zero. The rest were washed with PBS and incubated according to the following conditions: SF extract, SF-hPL extracts, culture media containing the same hPL amount released from the SF-hPL, and serum-free culture media and complete culture media as controls. Cells viability was evaluated with WST-1 assay, by adding the reagent directly in

culture medium with a 1:11 v/v ratio. The assay was performed after 1, 3, and 5 days of treatment, acquiring the absorbance at 450 nm, through a multiwell plate reader (instrument) and normalizing all the outcome signals with respect to the absorbance value at the zero-time point.

- **Improvement of hPL shelf-life**

With the aim of mimicking a degradation process, an oven treatment at 60 °C, such to induce a thermal stress, was performed on SF and SF-hPL samples and on aliquots of plain and hPL-containing serum-free culture medium. The electrospun mats were cut to be 20 mg in mass, containing 1 mg of hPL each and were dissolved, after the oven treatment and 20 minutes of UV sterilization cycle for each side, in 4 ml of serum free culture media for 24 h at 37 °C, to release the encapsulated hPL and prepare the extract for the following cell experiments. All the electrospun samples were 24% crystalline, so they fully dissolved during the 24 hours incubation. For the control samples, lyophilized hPL was dissolved in the serum-free medium in order to have the same concentration of the electrospun samples (250 µg/ml). Three treatment time points were investigated: 24 hours, 48 hours and 72 hours. HDFa cells were seeded onto 96-well plates at a density of 4500 cells/cm² and let attached overnight. The next morning, cells were treated with the prepared extracts from the thermally treated samples above listed. WST-1 viability assay was performed after 5 days, acquiring the absorbance at 450 nm and normalizing all the outcome signals with respect to the absorbance value of the negative control. The residual activity of the hPL was calculated from the ratio of the cell viability observed in the case of the thermally treated mats and the cell viability in the case of the untreated samples.

- **Cells morphology**

To evaluate the morphology of the cells directly seeded onto the fibrous mats, electrospun silk fibroin fibers were collected on 14 mm coverslips and treated with water vapor, as previously

explained. After UV sterilization for 20 minutes, HDFa were seeded on SF and SF-hPL matrices and observed under the confocal microscope after 1, 3 and 5 days of growth. Cells were washed twice with PBS, fixed with PFA 4% for 10 minutes, and treated with Triton X-100 0.1% in PBS for additional 10 minutes. Afterwards, the samples were incubated with a blocking solution of 1% BSA in PBS for 20 minutes and then stained with Alexa Fluor™ 488 Phalloidin (diluted 1:40 in 1% BSA) for 20 minutes. All the steps were performed at room temperature. Finally, the cells were mounted on glass slide with ProLong™ Diamond Antifade Mountant containing DAPI for nuclear staining and stored at 4°C.

3.5.6 Statistical methods

The fibers size analysis was performed on three samples for each fibrous formulation (SF, SF-alb, SF-hPL and SF-alb-hPL) before and after the water vapor annealing. The average of size measurements ($n = 400$) was obtained along the respective standard errors.

Three samples of each fibrous sample and each condition (not treated, treated for 10 minutes and treated for 6 hours with water vapor) were used for FITR analysis, acquiring 5 spectra from each of them, which were averaged to obtain the final spectrum for the deconvolution. The same samples (three for each crystallinity degree and three for each fibers type) were used to investigate the release. The average of the release from the triplicates was obtained with the respective standard errors. For cell viability assays, the statistics were performed through the analysis of variance (ANOVA), followed by post-hoc Bonferroni correction. The cell viability tests were repeated 3 times for each fibrous sample. The average with the standard error was obtained. A value of $p \leq 0.05$ was considered statistically significant.

3.6. Results and discussions

3.6.1 Fibers characterization

Silk fibroin was electrospun from aqueous solution, upon the addition of PEO, as reported in previous works^{77,79,80}. Silk fibroin fibers were obtained unloaded (SF), loaded with FITC-albumin (SF-Alb), hPL (SF-hPL) and with both (SF-Alb-hPL) (Figure 3.4 and 3.5). All the fibrous samples showed smooth and beads-free morphology. Their average diameter was measured to be 370 ± 3 nm, 330 ± 2 nm, 360 ± 3 nm, and 480 ± 2 nm, respectively. After the water vapor treatment was performed, no statistically significant changes in the average diameter was observed, with dimensions of 400 ± 4 nm, 370 ± 3 nm, 480 ± 4 nm, and 530 ± 8 nm, respectively.

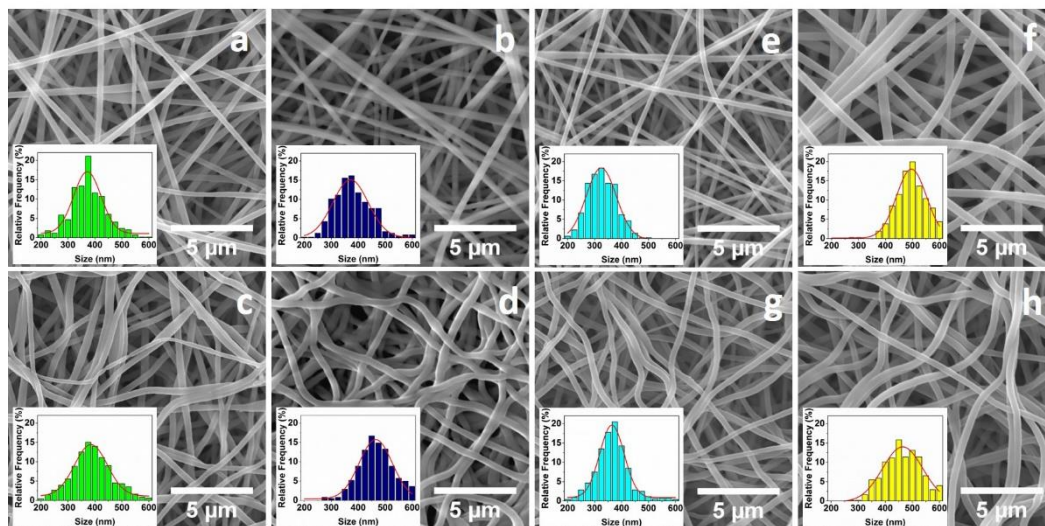


Figure 3.4 SEM images of SF (a and c), SF-hPL (b and d), SF-Alb (e and g) and SF-Alb-hPL (f and h) fibers mats obtained by electrospinning. The fiber morphology is characterized before (up images) and after (down images) the water vapor treatment. The insets show the corresponding size distributions.

Size and the morphology of fibers did not significantly change upon the addition of the FITC-albumin or hPL. The amount of hPL loaded in the fiber was 5% (w/w). By increasing the concentration of hPL, the electrospinning process was less continuous, and fibers were obtained with beads (figure 3.5). After the water vapor treatment, all the fibrous samples

showed a flattened morphology, which is proper of the fibroin fibers post-treatment, which does not lead to relevant changes at the fibrous surface (Figure 3.4 e-h).

Since the complexity of the hPL composition, their detection can result difficult to investigate. To make easier these procedures, albumin conjugated with FITC was used as a protein tracer. Albumin was chosen because it is one of the protein of the hPL, as shown in SDS-page in Figure 3.6 and confirmed in literature^{85,86}.

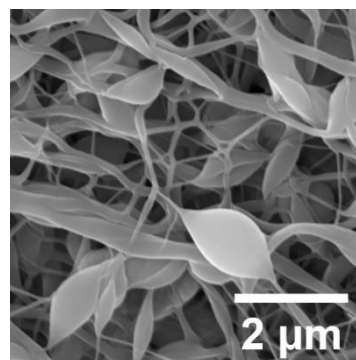


Figure 3.5 SEM image of SF-hPL mat when 10% (w/w) was used. Fibers resulted with beads

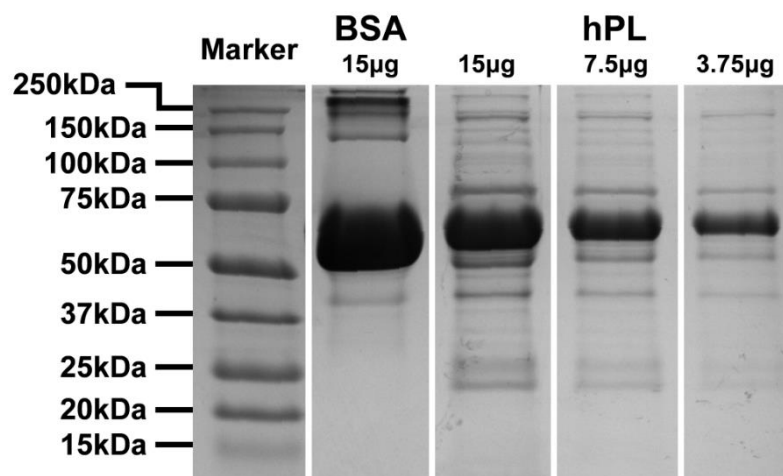


Figure 3.6 SDS-page of a BSA standard and hPL at different concentration.

The evaluation of the FITC-albumin encapsulation was performed by acquiring FITC fluorescence from the fibers with a confocal microscope. For samples encapsulating FITC-albumin (SF-alb and SF-alb-hPL), the fibers resulted fluorescent, suggesting its correct encapsulation. Moreover, FITC fluorescence was homogeneously distributed along the fibers.

No differences were observed when the hPL was added to the system (Figure 3.7). Contrarily, fibers without FITC-albumin (SF and SF-hPL) did not show fluorescence (Figure 3.8).

These outcomes suggested the efficient encapsulation of the hPL as well as its homogenous distribution in electrospun fibers. In addition, the confirmation of the hPL encapsulation was obtained from the *in vitro* test below in the test.

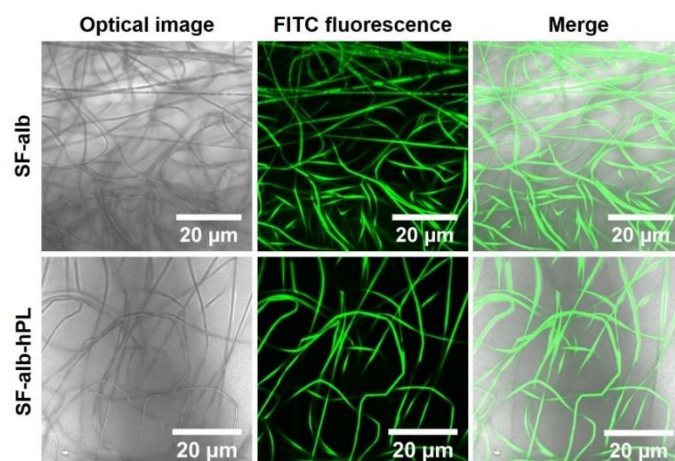


Figure 3.7 Confocal microscope images of SF-alb (a, b and c), and SF-alb-hPL (d, e and f).

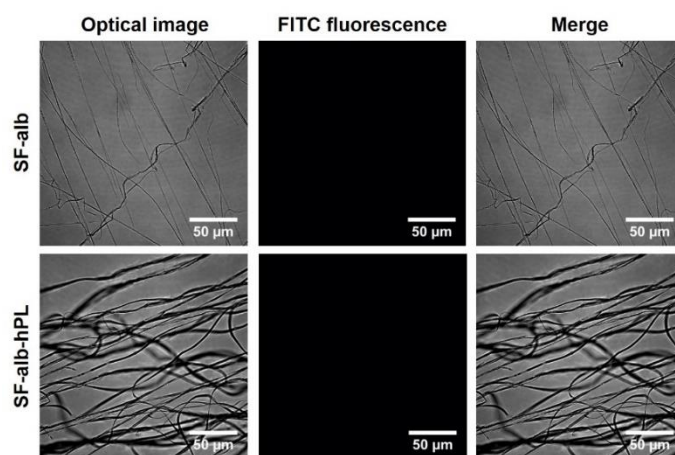


Figure 3.8 Confocal microscope images of the silk fibroin fibers, SF (a, b, c) and SF-hPL (d, e, f).

Since is related to fibroin degradation, the manipulation of the silk fibroin crystallinity can result useful in tailoring the release kinetics from the electrospun samples. The control of the crystallinity was performed through treatment at different time with water vapor. The

characterization of such modification, induced by water vapor annealing, was carried out on all the samples with FT-IR analysis.

Silk fibroin is characterized by a peak ranged from 1700 to 1600 cm^{-1} , called amide I, which corresponds to the sum of the vibrations due to the stretching of carbonyl group in the proteins backbone⁹. Depending on type of hydrogen bond, in which the carbonyl group is involved, secondary structure of the proteins (random coils, α -helices, β -sheets, turns) can be determined^{88,89}.

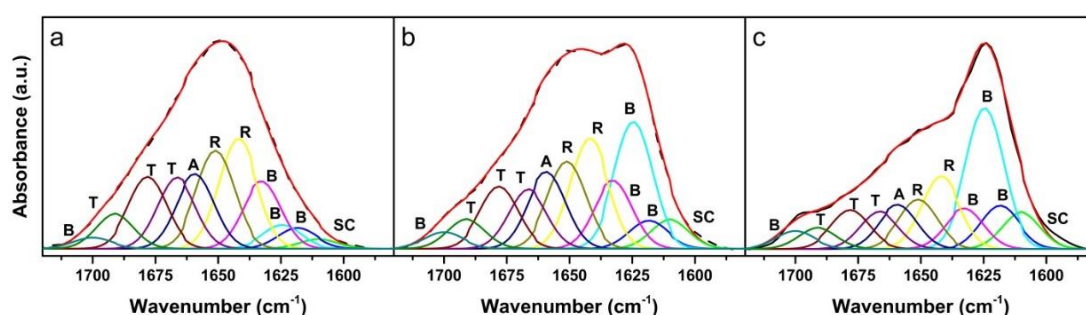


Figure 3.9 Deconvoluted FT-IR spectra of the amide I of three samples a, b and c respectively not treated, treated for 5 minutes and for 6 hours. In this case the crystallinity content for these sample are respectively 21%, 34% and 45%. SC = side chains; B = β -sheets; R = random coils; A = α -helices; T = turns.

This peak was found in all the fibrous samples. For not treated samples, the peak was at 1651 cm^{-1} . After the treatment with the water vapor, β -sheets increased and their contributes increased as well in the FT-IR spectra showing a change in the peak shape after 5 minutes with a shoulder at 1628 cm^{-1} , while a shift after 6 hours at 1624 cm^{-1} ^{88,89}. Since the crystallinity of silk fibroin is related to the β -sheets, deconvoluting the amide I peak was necessary to calculate the crystallinity degree of the fibroin for each sample treated at different time⁸⁸. Not treated electrospun fibers showed a β -sheets content ranged from 21% and 24% (Figure 3.9a). After 5 minutes of treatment, crystallinity reached a degree of 34-36%, while after 6 hours, 44-46% (Figure 3.9 b and c).

3.6.2 Evaluation of FITC-albumin release

Once optimized the water vapor treatment, such to have the control on the crystallinity manipulation, fibrous samples (SF, SF-alb, SF-hPL and SF-alb-hPL) with different crystallinity degree, were used to assess the release kinetic. The experiment intended to evaluate the release kinetic, mimicking the *in vivo* degradation conditions of fibroin. It was observed that high crystalline fibroin-based implants can remain in the body for 6 to 12 months^{38,90}. To have similar degradation rate in this experiment, protease XIV was used in a such concentration as induce a similar time of degradation.

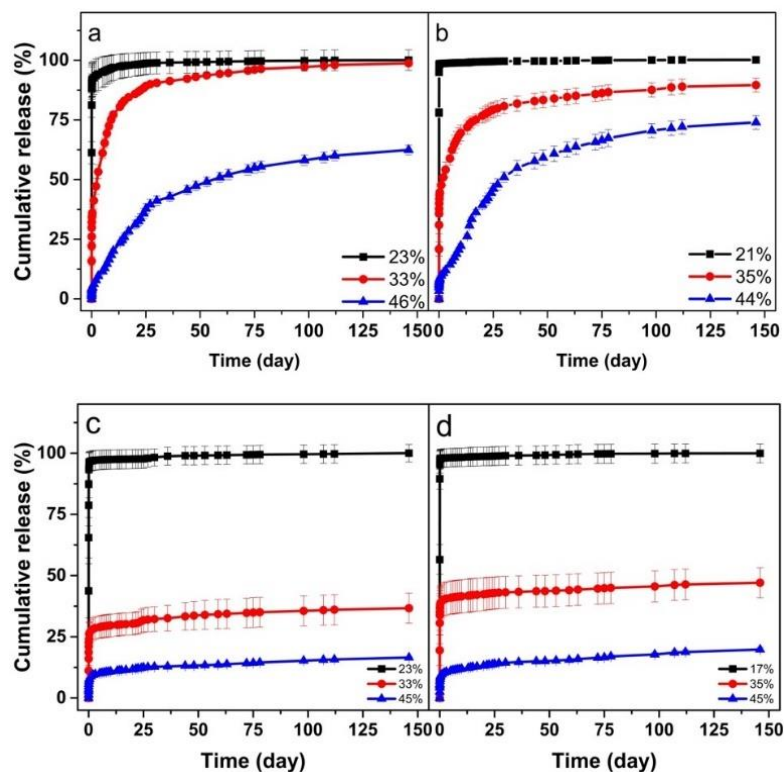


Figure 3.10 FITC-albumin released in presence of the protease XIV from electrospun mats with FITC-albumin, in a, and with FITC-albumin and hPL, in b. In c and d, FITC-albumin released in PBS buffer without the Protease XIV, from electrospun mats loaded respectively with FITC-albumin and loaded with both FITC-albumin and hPL. The percentages indicate the crystallinity of the electrospun mats used in the experiments.

Kinetic release evaluations were performed for a period of 5 months, through the quantification of the FITC-albumin released from the fibers in time. The results of the release

from fibrous samples (SF and SF-alb-hPL) with and without the enzymatic activity are reported in Figure 3.10. In all the cases, the fibers with the lowest crystallinity were totally dissolved within 1 hour and all the FITC-albumin was completely released, both with and without enzyme. In the samples with about 30% crystallinity, FITC-albumin showed an initial burst release in the first hour, reaching the $33\pm3\%$, $38\pm3\%$, of the loaded FITC-albumin. A net difference was observed for samples with higher crystallinity of about 45%, which only released $4\pm0.5\%$ and 6 ± 1 of the total loaded FITC-albumin. Similar amounts of FITC-albumin were observed to be released from both the fibrous samples without the enzyme (Figure 3.10 c and d; Table 3.1).

Samples	Crystallinity	Burst release 0-24 h	Sustained release 1-25 d	Sustained release 26-146 d
SF-Alb	23%	100%	-	
	33%	41%	90%	100%
	46%	6%	38%	62%
SF-Alb-hPL	21%	100%	-	-
	35%	48%	80%	90%
	44%	10%	46%	74%

Table 3.1 Summary of the release kinetics of FITC-albumin from SF-alb and SF-alb-hPL samples reported in Figure 3.8.

After the initial burst, which took 24h, the release continued with a slower rate for all the samples incubated with the enzyme. To give an idea, considering the released amount after 25 days, the SF-alb samples with 33% crystallinity showed a release of $90\pm1\%$, and samples with crystallinity of 46% released $38\pm2\%$ of the total (Figure 3.10a). Similarly (Figure 3.10b), the SF-Alb-hPL samples showed a release of $80\pm3\%$ for the mats with 35% of crystallinity and 46 ± 2 for the 44% crystalline mat after 25 days (Table 3.1). Contrarily, this second phase of the release was absent, in all the samples without the protease XIV. In fact, the release in

absence of the enzyme was stopped after the burst release. For them, a plateau in the release was observed instead of the slower sustained release (Figure 3.10 c and d).

These results showed how the release of FITC-albumin from the silk fibroin fibers was characterized from two different phases: the burst release and the degradation-dependent release. The burst release was due to the dissolution of the amorphous part of fibroin; the degradation-dependent phase was induced and ruled by the presence of the enzyme. The role of the enzymatic degradation is confirmed by the kinetic release obtained in absence of the protease XIV and by SEM images. In fact, Figure 3.11 showed the loss of the fibrous morphology in presence of the enzyme, confirming its degradation activity toward the fibrous mats. Furthermore, the loss of the fibers' morphology was higher when the crystallinity was low.

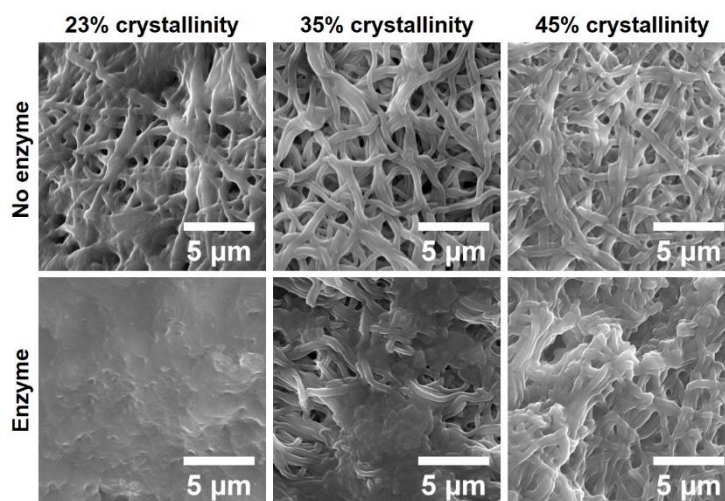


Figure 3.11 SEM images of SF-alb-hPL with different crystallinity. Micrographs a, b and c depict fiber morphology incubated in PBS for 1 month. Micrographs d, e and f, show the resulting morphology after incubation with protease XIV (6.25mU/mg_{fibers})

The release from silk fibroin matrices is related to its integrity. For this reason, dissolution or degradation of fibroin enables the release of molecules embedded in its matrix. As observed here, for very low crystallinity the dissolution of the amorphous content is faster and is the main pathway for degradation. For high crystallinity, the main pathway is the proteolytic

degradation that has shown to be dependent on the crystallinity degree of fibroin. Conversely, when the enzymatic degradation is absent, the degradation of fibroin only accounts for 4% of the mass^{15,90}.

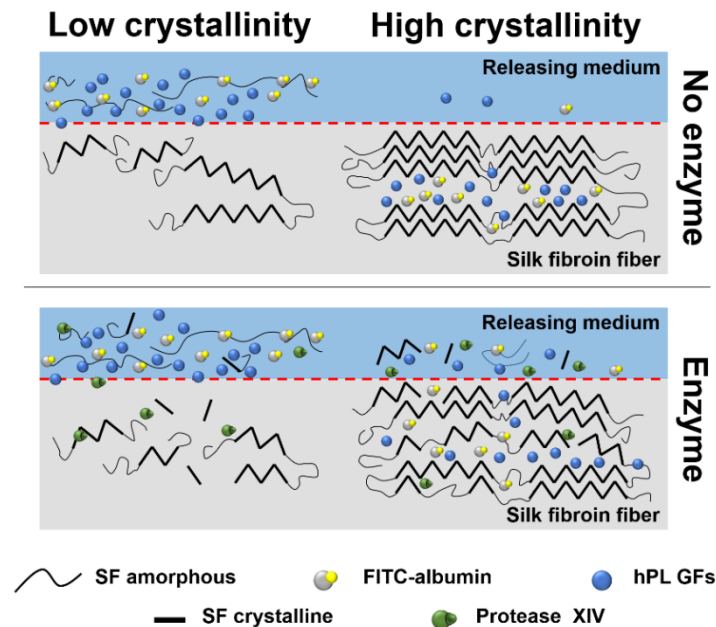


Figure 3.12 Proposed mechanism of controlled release from silk fibroin fibrous mats, considering the different silk fibroin crystallinity degree and the presence of the enzymatic activity. Low crystalline samples completely dissolved during the burst release, while the highly crystalline samples featured a reduced release due to the presence of the crystalline domains which impaired the diffusion of the FITC-albumin molecules. After the burst release, for the highly crystalline mats, when the enzyme degradation is not present, the molecules would remain entrapped in the fibroin matrix, whereas, by adding an enzyme, the degradation of the crystalline domain induces the release of the FITC-albumin and the other molecules embedded in it. Therefore, crystallinity also appeared to affect this second release step, since the silk fibroin crystalline domains constitute a physical barrier that limits the accessibility of the cleavage sites, leading to a slower degradation rate of the fibers during the release process. This leads to a crystallinity-dependent release.

In previous works by Hines and Kaplan^{39,40}, they hypothesized that the release of molecules from fibroin matrix can be distinguished in two phases: a first phase characterized by the diffusion of molecules throughout fibroin matrix, and a second phase driven by the degradation of the fibroin matrix. The model suggested by the authors are supported by the outcomes of this work. In particular, the results of this work showed that, beside the burst

release, the degradation-dependent release play a crucial role in releasing molecules from fibroin matrices. In fact, in absence of the enzymatic activity, the FITC-albumin would remain entrapped in the fibroin matrix. Whereas, addition of the enzyme induces the degradation of fibroin, enabling the release of FITC-albumin. Finally, both the diffusion and degradation dependent phase, have shown to be dependent on the crystallinity of fibroin matrix (Figure 3.12).

Beside the dependence of the releasing mechanism on fibroin matrix integrity and crystallinity, release kinetics are also affected by the molecular weight of the molecules embedded in the fibroin matrices^{39,92}. For high molecular weight molecules, the release from fibroin matrix, results slower. Conversely, for small molecular weight, the release is faster. In addition, it is worth to remember that, at physiological pH, fibroin results negatively charged. Therefore, release of charged molecules can be affected by the interaction that they can have with the fibroin. A previous work showed that negatively charged molecules was unexpectedly released slower than positive ones⁹². This was because the positive molecules can interact with the negatively charged fibroin, such to induce the formation of polyelectrolyte complexes, which were rapidly released⁹².

<i>hPL proteins</i>	<i>Molecular weight (kDa)</i>	<i>Isoelectric point</i>
Albumin (P02768)	66	4.7
pre-EGF (P01133)	133	5.5
PDGF-A/B (P04085; P01127)	27/27	9.5/9.3
VEGF (P15692)	27	9.2
TGF-β1 (P01137)	44	8.83

Table 3.2 *Molecular weight and predict isoelectric point for each principal protein of the hPL*

All the mechanisms above described, should undoubtedly affect the release of hPL proteins. However, the molecular weight effect as well as the ionic interaction, should be affect the

release of hPL proteins only in the burst phase, since the second phase is prevalently driven by the enzymatic degradation. In table 2 are reported the molecular weight and the predicted isoelectric point of the principal hPL proteins. Albumin results negatively charged at physiological pH. Therefore, at equal charge, only the molecular weight should affect the release. Thus, hPL negative proteins with higher molecular weight than albumin should have a slower kinetic; vice versa, negative proteins with lower molecular weight of albumin, would release faster.

For positive charged proteins, according to previous work⁹², the interaction with fibroin can result in formation of polyelectrolyte complexes, which result in fast release. Therefore, their release should be faster than albumin.

In any case, further study need to be performed in order to precisely investigate the kinetic release of the rest of the hPL proteins such to characterize the system.

3.6.3 Evaluation of the biological activity of the hPL released from the fibers.

- **Cell viability assay and cell morphology analysis**

Before the evaluation of the biological activity of the hPL released from the fibers, a dose-response experiment was performed, to understand the minimum concentration at which the hPL can induce an augmentation in cell viability. From this experiment a hPL concentration of 250 μ g/mL resulted enough to promote cell viability (data not shown).

To evaluate the activity of the hPL after the release from fibers, low crystalline SF and SF-hPL samples were incubated in the culture medium serum-free for 24h. The protease XIV was not used since the fibers were not crystallized, such to result in total dissolution of the mat. Figure 3.11 shows the viability of HDFa cells treated with medium with the fibers extracts. As control samples, cells were seeded FBS-free media (labeled as negative control), or in FBS-free media in which lyophilized hPL was dissolved with the same concentration (labeled

hPL), or in media with FBS (labeled FBS). The amount of hPL in the control was the same as the one released from SF-hPL fibers (250 $\mu\text{g}/\text{mL}$). The absorbance values of all the days were normalized on the absorbance values relative to the zero-time point.

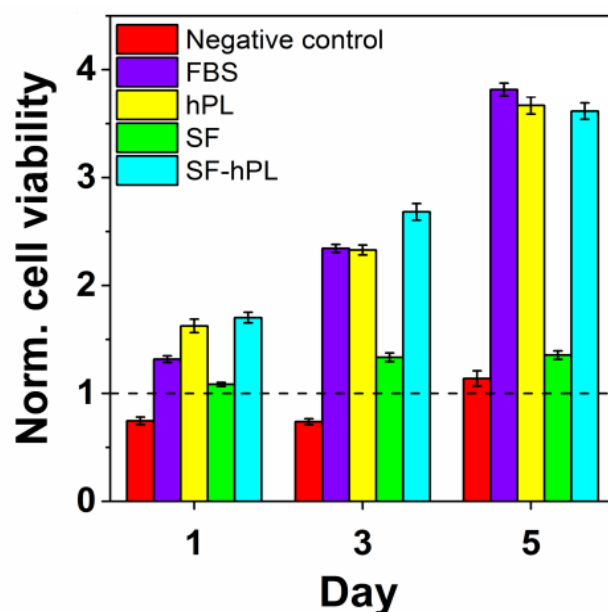


Figure 3.11 Viability of HDFa cells treated either with 250 $\mu\text{g}/\text{mL}$ of hPL or with the extracts of SF and SF-hPL fibers. The values were normalized with respect to the absorbance value of the cells before the treatments, which is showed as a dashed line in the graph.

After the first day of treatment, cells cultivated in media with hPL (hPL and SF-hPL) showed a significantly similar viability ($p>0.05$) and almost twice compared to the negative control ($p<0.0001$). This higher viability can be associated to the cell proliferation induced by the hPL, as reported before⁹³. These trends were confirmed after three and five days. Silk fibroin produce no effects on the cells viability, confirming that the increase of the cell viability is due the hPL released from the fibroin fibers. These results proved that the growth factors released from the SF-hPL were still active and that they could increase and sustain the cells viability of the HDFa cells for up to 5 days. Therefore, hPL activity was preserved during the fibers fabrication and treatment through the water vapor annealing.

To evaluate the role of the hPL in cell adhesion and morphology, HDFa were seeded on the SF and SF-hPL mats for 5 days. Intermediate crystalline fibrous mats were used to avoid their dissolution and allow the cells to attach. As control, the cells were seeded on coverslips with and without hPL. Figure 3.12 and 3.13 showed the cells attached respectively on glass and on the electrospun fibers after 1, 3 and 5 days. The cells cultivated with the hPL (hPL and SF-hPL) showed an elongated morphology, already after one day from the seeding, and was kept for all the 5 days. In absence of the hPL, cells acquired a rounded morphology, especially when are seeded on the unloaded SF. Therefore, results show that hPL was able to allow the cells to acquire elongated morphology. As shown by Barsotti *et al.*⁶⁷ and Anitua *et al.*⁹³, platelets-derived proteins induced similar changes on dermal fibroblast. This morphology was hypothesized to be associated to cell polarization, a complex process involved in cell migration and wound closure⁵⁵.

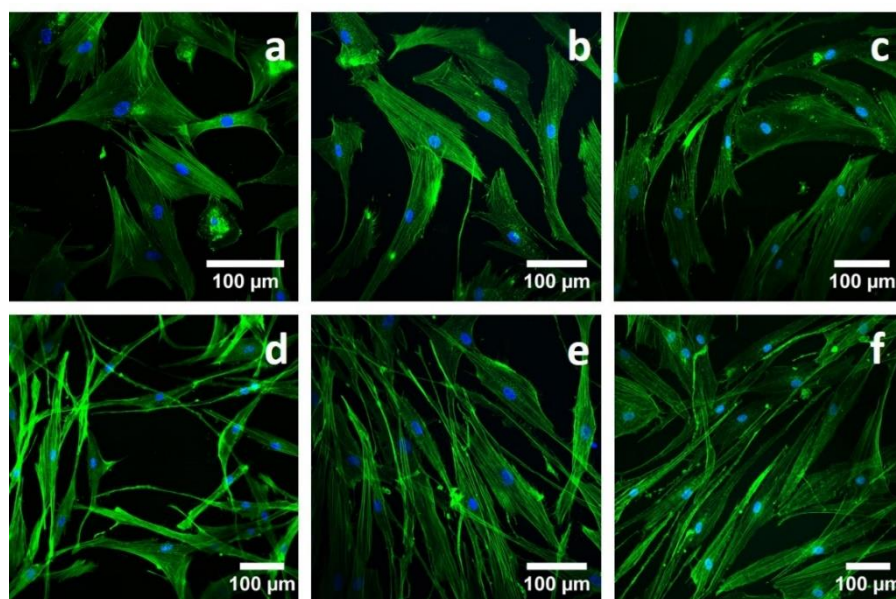


Figure 3.12 Confocal images depicting HDFa cells seeded on glass coverslips for (a) 1, (b) 3, and (c) 5 days; HDFa cells seeded on glass coverslips and treated with hPL-containing media for (d) 1, (e) 3, and (f) 5 days. F-actin is stained with the Alexa-fluor phalloidin (green), while nuclei are stained with DAPI (blue).

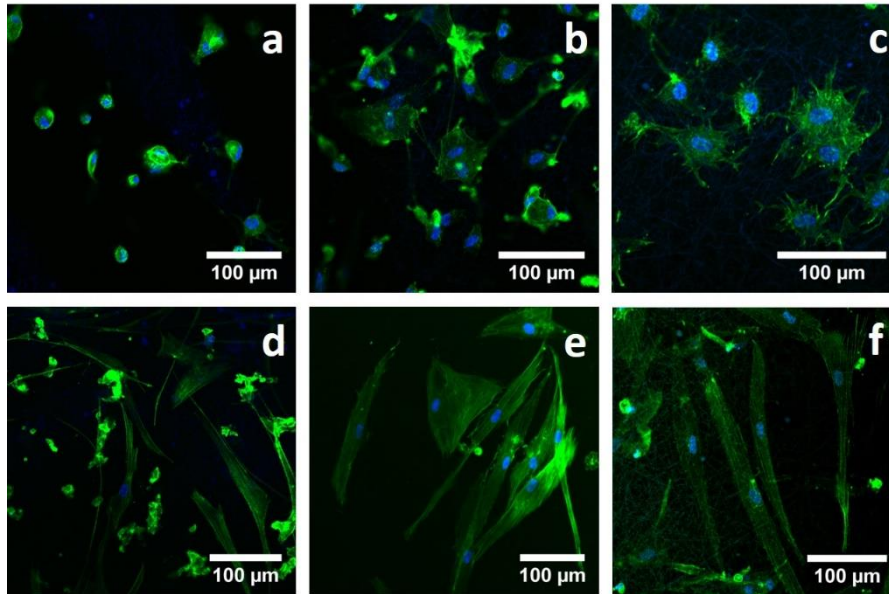


Figure 3.13 Confocal images depicting HDFa cells seeded on silk fibroin mats for (a) 1, (b) 3 and (c) 5 days; HDFa seeded on SF-hPL mats for (c) 1, (d) 3, (e) 5 days; F-actin is stained with the Alexa-fluor phalloidin (green), while nuclei are stained with DAPI (blue).

- **Evaluation of the preserving ability of silk fibroin toward the hPL**

To evaluate if the activity of hPL growth factors can be preserved upon the encapsulation in fibroin fibers, an accelerated stability test at 60°C was performed on the SF-hPL fibers and on the medium containing the hPL. In Figure 3,14, the residual activity of the hPL is shown. The activity of the hPL in solution was reduced at 60% after 1 day, while the reduction of the activity decreases to 40% after 2 and 3 days. On the other hand, the hPL released from the SF-hPL mats has shown no statistical difference ($p > 0.05$) with the non-treated sample, demonstrating the ability of silk to preserve the activity of growth factors of hPL.

The fabrication of a device able to encapsulate hPL and even preserve its activity, might be crucial for hPL usage. Preserving the activity of such pool of proteins for long time entails the fabrication of a device encapsulating hPL beforehand, which can be ready to use. In this way, the problems concerning the preparation and the handleability of the hPL gel are eliminated. Therefore, the usage of a fibrous patch instead a gel should improve its usage and increase the accessibility to also not-qualified personnel. Finally, since the fibroin was shown to be able in

preserving the hPL activity, procedures of storage can be simplified, avoiding the storage of hPL at very low temperature (-80°C), resulting in cost reduction.

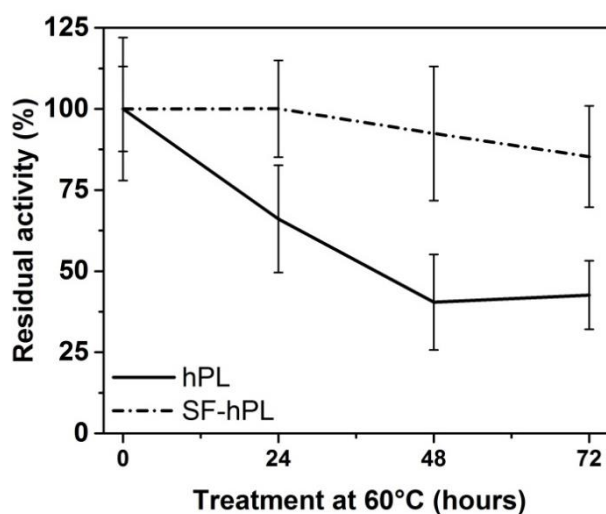


Figure 3.14 hPL activity of un-encapsulated hPL and hPL released from SF-hPL matrices after the accelerated stability test

3.7 Conclusions

In this work, the electrospinning process was optimized such to encapsulate hPL in silk fibroin fibers up to a concentration of 5% of the total mass of the fibers. The procedures of the crystallinity manipulation were fine controlled by the relative humidity and duration of treatment. Thanks to this, the fibers were obtained with different crystallinity degree, which resulted in a different release of FITC-albumin. By using a suitable releasing medium, which mimicked the degradation conditions of silk fibroin *in vivo*, the two-steps phases of the release from fibroin matrix were well distinguished: the rapid burst release and the slower degradation-dependent release. Both the phases were affected by the fibroin crystallinity increase, resulting in a slower pace.

hPL released from the fibers showed to be still active, promoting the cell viability of HDFa and inducing the cell to acquire a polarized morphology, which is typical of the migrating cells which are involved in wound healing^{55,67,70}. This demonstrated that hPL remained active

during the fabrication procedures. hPL kept its activity also after the accelerating test stability at 60°C, proving the protective activity of fibroin toward hPL, as already showed for other sensitive molecules and even for organelles^{9,31–33,41}. This suggests that hPL encapsulating in silk fibroin matrix has an extended shelf life, which could facilitate and improve the usage of hPL in clinical application, in which gel systems are currently used.

The development of such electrospun materials opened the possibility to an improving of the hPL application in wound care, which are currently stopped in using gel system. The use in medical procedures of an electrospun patch, like gauze materials, with such characteristics – possibility to pre-determine the release of the hPL proteins by controlling the fibroin crystallinity; possibility to prepare beforehand the patches, store them at room temperature, such to have a ready-to-use system – undoubtedly could facilitate the use of hPL. To this purpose, however, the system needs to be further characterized, in order to find the kinetic release of the other hPL components. But the potentialities of the device were clearly demonstrated.

3.8 Bibliography

1. Kundu, S. *Silk biomaterials for tissue engineering and regenerative medicine*. (Woodhead Publishing, 2014).
2. Lee, Y.-W. & Food and Agriculture Organization of the United Nations. *Silk reeling and testing manual*. (Food and Agriculture Organization of the United Nations, 1999).
3. Altman, G. H. *et al.* Silk-based biomaterials. *Biomaterials* **24**, 401–416 (2003).
4. Qi, Y. *et al.* A review of structure construction of silk fibroin biomaterials from single structures to multi-level structures. *International Journal of Molecular Sciences* **18**, (2017).
5. Zhou, C. Z. *et al.* Fine organization of Bombyx mori fibroin heavy chain gene. *Nucleic Acids Res.* **28**, 2413–9 (2000).
6. Shimura, K. Chemical composition and biosynthesis of silk proteins. *Experientia* **39**, 455–461 (1983).
7. Gamo, T., Inokuchi, T. & Laufer, H. Polypeptides of fibroin and sericin secreted from the different sections of the silk gland in Bombyx mori. *Insect Biochem.* **7**, 285–295 (1977).
8. Vepari, C. & Kaplan, D. L. Silk as a Biomaterial. *Prog. Polym. Sci.* **32**, 991–1007 (2007).
9. Hu, X. *et al.* Regulation of Silk Material Structure by Temperature-Controlled Water Vapor Annealing. *Biomacromolecules* **12**, 1686–1696 (2011).
10. Lotz, B. & Colonna Cesari, F. The chemical structure and the crystalline structures of Bombyx mori silk fibroin. *Biochimie* **61**, 205–14 (1979).
11. Ho, M. P., Wang, H. & Lau, K. T. Effect of degumming time on silkworm silk fibre for biodegradable polymer composites. *Appl. Surf. Sci.* **258**, 3948–3955 (2012).
12. Rockwood, D. N. *et al.* Materials fabrication from Bombyx mori silk fibroin. *Nat. Protoc.* **6**, 1612–1631 (2011).
13. Meinel, L. *et al.* The inflammatory responses to silk films in vitro and in vivo. *Biomaterials* **26**, 147–155 (2005).
14. Kundu, B., Rajkhowa, R., Kundu, S. C. & Wang, X. *Silk fibroin biomaterials for tissue regenerations*. *Advanced Drug Delivery Reviews* **65**, (2013).
15. Wenk, E., Merkle, H. P. & Meinel, L. Silk fibroin as a vehicle for drug delivery applications. *J. Control. Release Off. J. Control. Release Soc.* **150**, 128–141 (2011).
16. Mitropoulos, A. N. *et al.* Synthesis of Silk Fibroin Micro- and Submicron Spheres Using a Co-Flow Capillary Device. *Adv. Mater.* **26**, 1105–1110 (2014).

17. Seib, F. P., Jones, G. T., Rnjak-Kovacina, J., Lin, Y. & Kaplan, D. L. pH-Dependent Anticancer Drug Release from Silk Nanoparticles. *Adv. Healthc. Mater.* **2**, 1606–1611 (2013).
18. Cheng, Y. *et al.* On the strength of β -sheet crystallites of Bombyx mori silk fibroin. *J. R. Soc. Interface* **11**, 20140305 (2014).
19. Lu, Q. *et al.* Water-insoluble silk films with silk I structure. *Acta Biomater.* **6**, 1380–1387 (2010).
20. Jin, H.-J. & Kaplan, D. L. Mechanism of silk processing in insects and spiders. *Nature* **424**, 1057–1061 (2003).
21. Motta, A., Fambri, L. & Migliaresi, C. Regenerated silk fibroin films: Thermal and dynamic mechanical analysis. *Macromol. Chem. Phys.* **203**, 1658–1665 (2002).
22. Agarwal, N., Hoagland, D. A. & Farris, R. J. Effect of moisture absorption on the thermal properties of Bombyx mori silk fibroin films. *J. Appl. Polym. Sci.* **63**, 401–410 (1997).
23. Lawrence, B. D. *et al.* Effect of Hydration on Silk Film Material Properties. *Macromol. Biosci.* **10**, 393–403 (2010).
24. Sohn, S., Strey, H. H. & Gido, S. P. Phase Behavior and Hydration of Silk Fibroin. *Biomacromolecules* **5**, 751–757 (2004).
25. Hu, X., Kaplan, D. & Cebe, P. Dynamic Protein–Water Relationships during β -Sheet Formation. *Macromolecules* **41**, 3939–3948 (2008).
26. Hu, X., Kaplan, D. & Cebe, P. Effect of water on the thermal properties of silk fibroin. *Thermochim. Acta* **461**, 137–144 (2007).
27. Chen, X. *et al.* Conformation transition kinetics of regenerated Bombyx mori silk fibroin membrane monitored by time-resolved FTIR spectroscopy. *Biophys. Chem.* **89**, 25–34 (2001).
28. Mandal, B. B., Grinberg, A., Gil, E. S., Panilaitis, B. & Kaplan, D. L. High-strength silk protein scaffolds for bone repair. *Proc. Natl. Acad. Sci. U. S. A.* **109**, 7699–704 (2012).
29. Motta, A. *et al.* Silk Fibroin Processing and Thrombogenic Responses. *J. Biomater. Sci. Polym. Ed.* **20**, 1875–1897 (2009).
30. Floren, M. *et al.* Human mesenchymal stem cells cultured on silk hydrogels with variable stiffness and growth factor differentiate into mature smooth muscle cell phenotype. *Acta Biomater.* **31**, 156–166 (2016).
31. Mitropoulos, A. N. *et al.* Towards the fabrication of biohybrid silk fibroin materials: entrapment and preservation of chloroplast organelles in silk fibroin films. *RSC Adv.* **6**, 72366–72370 (2016).

32. Pritchard, E. M., Dennis, P. B., Omenetto, F., Naik, R. R. & Kaplan, D. L. Physical and Chemical Aspects of Stabilization of Compounds in Silk. *Biopolymers* **97**, 479–498 (2012).
33. Kluge, J. A. *et al.* Silk-based blood stabilization for diagnostics. *Proc. Natl. Acad. Sci.* **113**, 5892–5897 (2016).
34. Seib, F. P. & Kaplan, D. L. Doxorubicin-loaded silk films: Drug-silk interactions and in vivo performance in human orthotopic breast cancer. *Biomaterials* **33**, 8442–8450 (2012).
35. Numata, K., Cebe, P. & Kaplan, D. L. Mechanism of enzymatic degradation of beta-sheet crystals. *Biomaterials* **31**, 2926–2933 (2010).
36. Kim, J. H. *et al.* Preparation and in vivo degradation of controlled biodegradability of electrospun silk fibroin nanofiber mats. *J. Biomed. Mater. Res. A* **100**, 3287–3295 (2012).
37. Kim, U.-J., Park, J., Joo Kim, H., Wada, M. & Kaplan, D. L. Three-dimensional aqueous-derived biomaterial scaffolds from silk fibroin. *Biomaterials* **26**, 2775–2785 (2005).
38. Wang, Y. *et al.* In vivo degradation of three-dimensional silk fibroin scaffolds. *Biomaterials* **29**, 3415–3428 (2008).
39. Hines, D. J. & Kaplan, D. L. Mechanisms of Controlled Release from Silk Fibroin Films. *Biomacromolecules* **12**, 804–812 (2011).
40. Hines, D. J. & Kaplan, D. L. Characterization of Small Molecule Controlled Release From Silk Films. *Macromol. Chem. Phys.* **214**, 280–294 (2013).
41. Hofmann, S. *et al.* Silk fibroin as an organic polymer for controlled drug delivery. *J. Control. Release* **111**, 219–227 (2006).
42. Coburn, J. M., Na, E. & Kaplan, D. L. Modulation of vincristine and doxorubicin binding and release from silk films. *J. Control. Release* **220**, 229–238 (2015).
43. Wang, X. *et al.* Silk microspheres for encapsulation and controlled release. *J. Control. Release* **117**, 360–370 (2007).
44. Chiu, B. *et al.* Surgery combined with controlled-release doxorubicin silk films as a treatment strategy in an orthotopic neuroblastoma mouse model. *Br. J. Cancer* **111**, 708–715 (2014).
45. Boateng, J. S., Matthews, K. H., Stevens, H. N. E. & Eccleston, G. M. Wound Healing Dressings and Drug Delivery Systems: A Review. *J. Pharm. Sci.* **97**, 2892–2923 (2008).
46. Buckley, A., Davidson, J. M., Kamerath, C. D., Wolt, T. B. & Woodward, S. C. Sustained release of epidermal growth factor accelerates wound repair. *Proc. Natl. Acad. Sci. U. S. A.* **82**, 7340–4 (1985).

47. Sheridan, M. H., Shea, L. D., Peters, M. C. & Mooney, D. J. Bioabsorbable polymer scaffolds for tissue engineering capable of sustained growth factor delivery. *J. Control. Release* **64**, 91–102 (2000).
48. Putney, S. D. & Burke, P. A. Improving protein therapeutics with sustained-release formulations. *Nat. Biotechnol.* **16**, 153–157 (1998).
49. Bennett, N. T. & Schultz, G. S. Growth factors and wound healing: Part II. Role in normal and chronic wound healing. *Am. J. Surg.* **166**, 74–81 (1993).
50. Morimoto, N. *et al.* Novel Collagen/Gelatin Scaffold with Sustained Release of Basic Fibroblast Growth Factor: Clinical Trial for Chronic Skin Ulcers. *Tissue Eng. Part A* **19**, 1931–1940 (2013).
51. Yun, S.-H., Sim, E.-H., Goh, R.-Y., Park, J.-I. & Han, J.-Y. Platelet Activation: The Mechanisms and Potential Biomarkers. *Biomed Res. Int.* **2016**, 9060143 (2016).
52. Spanò, R. *et al.* Platelet-rich plasma-based bioactive membrane as a new advanced wound care tool. *J. Tissue Eng. Regen. Med.* n/a-n/a (2017). doi:10.1002/term.2357
53. Martin, P. Wound healing--aiming for perfect skin regeneration. *Science* **276**, 75–81 (1997).
54. Gurtner, G. C., Werner, S., Barrandon, Y. & Longaker, M. T. Wound repair and regeneration. *Nature* **453**, 314–321 (2008).
55. Backly, R. El *et al.* Platelet Lysate Induces In Vitro Wound Healing of Human Keratinocytes Associated with a Strong Proinflammatory Response. *Tissue Eng. Part A* **17**, 1787–1800 (2011).
56. Marx, R. E. *et al.* Platelet-rich plasma: Growth factor enhancement for bone grafts. *Oral Surg. Oral Med. Oral Pathol. Oral Radiol. Endod.* **85**, 638–46 (1998).
57. Alsousou, J., Thompson, M., Hulley, P., Noble, A. & Willett, K. The biology of platelet-rich plasma and its application in trauma and orthopaedic surgery: A REVIEW OF THE LITERATURE. *J. Bone Jt. Surg. - Br. Vol.* **91-B**, 987–996 (2009).
58. Martínez-Zapata, M. J. *et al.* Efficacy and safety of the use of autologous plasma rich in platelets for tissue regeneration: a systematic review. *Transfusion* **49**, 44–56 (2009).
59. Zheng, C. *et al.* Improved peripheral nerve regeneration using acellular nerve allografts loaded with platelet-rich plasma. *Tissue Eng. Part A* **20**, 3228–40 (2014).
60. Vu, T. D. *et al.* An autologous platelet-rich plasma hydrogel compound restores left ventricular structure, function and ameliorates adverse remodeling in a minimally invasive large animal myocardial restoration model: A translational approach. *Biomaterials* **45**, 27–35 (2015).
61. Nurden, A. T. Platelets, inflammation and tissue regeneration. *Thromb. Haemost.* **105**, S13–S33 (2011).

62. Driver, V. R., Hanft, J., Fylling, C. P., Berioux, J. M. & Autologel Diabetic Foot Ulcer Study Group. A prospective, randomized, controlled trial of autologous platelet-rich plasma gel for the treatment of diabetic foot ulcers. *Ostomy. Wound. Manage.* **52**, 68–70, 72, 74 passim (2006).
63. Mazzocca, A. D. *et al.* Platelet-Rich Plasma Differs According to Preparation Method and Human Variability. *J. Bone Jt. Surgery-American Vol.* **94**, 308–316 (2012).
64. Weibrich, G., Kleis, W. K. G., Hafner, G. & Hitzler, W. E. Growth factor levels in platelet-rich plasma and correlations with donor age, sex, and platelet count. *J. Cranio-Maxillofacial Surg.* **30**, 97–102 (2002).
65. Muraglia, A. *et al.* Combined platelet and plasma derivatives enhance proliferation of stem/progenitor cells maintaining their differentiation potential. *Cytotherapy* **17**, 1793–1806 (2015).
66. Yang, H. S. *et al.* Enhanced skin wound healing by a sustained release of growth factors contained in platelet-rich plasma. *Exp. Mol. Med.* **43**, 622–9 (2011).
67. Chiara Barsotti, M. *et al.* Effect of Platelet Lysate on Human Cells Involved in Different Phases of Wound Healing. *PLoS One* **8**, (2013).
68. El Backly, R. M. *et al.* A platelet-rich plasma-based membrane as a periosteal substitute with enhanced osteogenic and angiogenic properties: a new concept for bone repair. *Tissue Eng. Part A* **19**, 152–65 (2013).
69. Knighton, D. R., Ciresi, K. F., Fiegel, V. D., Austin, L. L. & Butler, E. L. Classification and treatment of chronic nonhealing wounds. Successful treatment with autologous platelet-derived wound healing factors (PDWHF). *Ann. Surg.* **204**, 322–30 (1986).
70. Anitua, E. *et al.* Effectiveness of autologous preparation rich in growth factors for the treatment of chronic cutaneous ulcers. *J. Biomed. Mater. Res. Part B Appl. Biomater.* **84B**, 415–421 (2008).
71. Fekete, N. *et al.* Platelet lysate from whole blood-derived pooled platelet concentrates and apheresis-derived platelet concentrates for the isolation and expansion of human bone marrow mesenchymal stromal cells: production process, content and identification of active comp. *Cytotherapy* **14**, 540–554 (2012).
72. Pignatelli, C. *et al.* Electrospun silk fibroin fibers for storage and controlled release of human platelet lysate. *Acta Biomater.* **73**, 365–376 (2018).
73. Putthanarat, S. *et al.* Nonlinear optical transmission of silk/green fluorescent protein (GFP) films. *Polymer (Guildf).* **45**, 8451–8457 (2004).
74. Kikuchi, J. *et al.* Spectroscopic investigation of tertiary fold of staphylococcal protein A to explore its engineering application. *Biomaterials* **20**, 647–654 (1999).
75. Lu, S. *et al.* Stabilization of Enzymes in Silk Films. *Biomacromolecules* **10**, 1032–1042

- (2009).
76. Wu, Y., Shen, Q. & Hu, S. Direct electrochemistry and electrocatalysis of heme-proteins in regenerated silk fibroin film. *Anal. Chim. Acta* **558**, 179–186 (2006).
 77. Jin, H.-J., Fridrikh, S. V., Rutledge, G. C. & Kaplan, D. L. Electrospinning Bombyx mori Silk with Poly(ethylene oxide). *Biomacromolecules* **3**, 1233–1239 (2002).
 78. Chutipakdeevong, J., Ruktanonchai, U. R. & Supaphol, P. Process optimization of electrospun silk fibroin fiber mat for accelerated wound healing. *J. Appl. Polym. Sci.* **130**, 3634–3644 (2013).
 79. Gil, E. S., Panilaitis, B., Bellas, E. & Kaplan, D. L. Functionalized Silk Biomaterials for Wound Healing. *Adv. Healthc. Mater.* **2**, 206–217 (2013).
 80. Schneider, A., Wang, X. Y., Kaplan, D. L., Garlick, J. A. & Egles, C. Biofunctionalized electrospun silk mats as a topical bioactive dressing for accelerated wound healing. *Acta Biomater.* **5**, 2570–2578 (2009).
 81. Zahedi, P., Rezaeian, I., Ranaei-Siadat, S.-O., Jafari, S.-H. & Supaphol, P. A review on wound dressings with an emphasis on electrospun nanofibrous polymeric bandages. *Polym. Adv. Technol.* **21**, 77–95 (2010).
 82. Abrigo, M., McArthur, S. L. & Kingshott, P. Electrospun nanofibers as dressings for chronic wound care: advances, challenges, and future prospects. *Macromol. Biosci.* **14**, 772–792 (2014).
 83. Hajiali, H. *et al.* Alginate–lavender nanofibers with antibacterial and anti-inflammatory activity to effectively promote burn healing. *J. Mater. Chem. B* **4**, 1686–1695 (2016).
 84. Romano, I. *et al.* Fumarate-loaded electrospun nanofibers with anti-inflammatory activity for fast recovery of mild skin burns. *Biomed. Mater.* **11**, 41001 (2016).
 85. Wolfe, P. *et al.* The Creation of Electrospun Nanofibers from Platelet Rich Plasma. *J Tissue Sci Eng* **24172**, 1072157–7552 (2011).
 86. Shanskii, Y. D. *et al.* Human platelet lysate as a promising growth-stimulating additive for culturing of stem cells and other cell types. *Bull. Exp. Biol. Med.* **156**, 146–151 (2013).
 87. Guzman-Puyol, S. *et al.* Low-Cost and Effective Fabrication of Biocompatible Nanofibers from Silk and Cellulose-Rich Materials. *ACS Biomater. Sci. Eng.* **2**, 526–534 (2016).
 88. Hu, X., Kaplan, D. & Cebe, P. Determining Beta-Sheet Crystallinity in Fibrous Proteins by Thermal Analysis and Infrared Spectroscopy. *Macromolecules* **39**, 6161–6170 (2006).
 89. Lawrence, B. D., Omenetto, F., Chui, K. & Kaplan, D. L. Processing methods to control silk fibroin film biomaterial features. *J. Mater. Sci.* **43**, 6967 (2008).

90. Zhou, J. *et al.* In vitro and in vivo degradation behavior of aqueous-derived electrospun silk fibroin scaffolds. *Polym. Degrad. Stab.* **95**, 1679–1685 (2010).
91. Seib, F. P. & Kaplan, D. L. Silk for drug delivery applications: Opportunities and challenges. *Isr. J. Chem.* **53**, 756–766 (2013).
92. Nultsch, K. & Germershaus, O. Silk fibroin degumming affects scaffold structure and release of macromolecular drugs. *Eur. J. Pharm. Sci.* **106**, 254–261 (2017).
93. Anitua, E., Pino, A. & Orive, G. Plasma rich in growth factors promotes dermal fibroblast proliferation, migration and biosynthetic activity. *J. Wound Care* **25**, 680–687 (2016).

Chapter 4

Polysaccharides-based formulation for oral delivery of curcumin

4.1. Curcumin

Curcumin is a molecule extracted from the dried powder of the rhizomes of the *Curcuma longa*. Generally, curcumin is soluble in organic solvents such as ethanol and vegetable oils. This makes difficult the preparation of liquid pharmaceutical formulations in order to use curcumin as biological active compounds¹⁻³. Curcumin has low solubility in acid and neutral aqueous solution, but it increases in alkaline pH, because of the hydrolysis of hydroxyl phenolic group⁴. In addition, curcumin can be found as isomers due to the keto-enolic equilibrium. The ketone form is predominant in acid pH, while the enol form is mainly present at neutral and basic pH⁵.

The stability of curcumin is dependent on the pH of the water or water/solvent solutions. In particular, it has a reasonable stability at pH 1-6 and it starts to degrade at pH>7. It was reported that at physiological pH, curcumin is subjected to almost total degradation (90%) after 30 minutes⁶. Curcumin is also sensitive to oxygen and light⁴.

Numerous investigations have been carried out to understand its biological activities and how such activities can be exploited in medical practices. *In vivo* and *in vitro* experiments have shown a role of the curcumin as antioxidant, anticancer, antiviral, antiarthritic, antiamyloid, and anti-inflammatory^{4,7,8}.

This broad range of action of curcumin derives from its ability to interact with factors in the human cells, which are involved in such mechanisms⁸. In particular, curcumin was observed to inhibit the activation of a nuclear factor kappa B (NF- κ B)⁹. This factor is involved in inflammation processes and, after its activation, it can induce acute and chronic inflammation. Furthermore, NF- κ B results active in some tumors, such as breast cancer, gastroenteric cancer, melanomas⁸. The activation of NF- κ B is dependent on the presence of pro-inflammatory stimuli. In details, in absence of pro-inflammatory stimuli, NF- κ B is bound to its inhibitor protein I κ B (inhibitor of κ B), which retains NF- κ B in the cytoplasm. When inflammatory stimuli reach the cells, I κ B is subjected to the phosphorylation, which induces its degradation. Successively, NF- κ B is free to enter the nucleus and to activate the transcription of proinflammatory and anti-apoptotic genes, such as interleukin 6 (IL-6), cyclooxygenase 2 (COX-2), metalloprotease (MMPs) and Bcl-2^{10,11}. Curcumin can prevent the phosphorylation of I κ B, and so to inhibit its degradation, keeping NF- κ B sequestered in the cytoplasm. In this way, NF- κ B is not able to enter the nucleus and to activate genes transcription. Furthermore, curcumin has shown to have other molecular targets, such as Src family protein tyrosine kinases (SFK) and c-JUN N-terminal kinase, and downregulation of nuclear factor- κ B (NF- κ B) p65, inhibitory subunit of NF- κ B (I κ B α), activator protein 1

(AP1), early growth response protein-1 (EGR1), epidermal growth factor receptor (EGFR), human epidermal growth factor receptor type-2 (HER2), insulin-like growth factors (IGF-1R), cyclooxygenase-2 (COX2), lipoxygenase (LOX), nitric oxide oxidase (NOS), tumor necrosis factor (TNF), matrix metalloproteinase (MMP)-2 and -9, urokinase-activated plasminogen activator (uPA), cyclin D and various chemokines¹²⁻¹⁵.

Curcumin activity was investigated in clinical trials in order to understand its effects in cancer therapy, chronic and acute inflammation and in central nervous system disease. Orally administrated curcumin (8g per day) has shown to induce the regression of pancreatic cancer, high-grade prostatic intraepithelial neoplasia (phase I) and multiple myeloma^{4,16-18}.

Curcumin in capsule was also administrated to patients with active rheumatoid arthritis or knee osteoarthritis and it showed to have a comparable therapeutic effect with non-steroidal antirheumatic drugs (NSAR), such as diclofenac and ibuprofen^{19,20}. Chronic administration of NSARs provoked serious side effects on stomach, resulting in gastritis or ulcer. Conversely, curcumin did not give any side effects, even after prolonged consumption²¹.

Finally, curcumin effects have been investigated in trials that regarded diseases of the central nervous system, such as the Alzheimer⁴.

Despite these good biological activities, such trials are only a part of the examples that have shown beneficial effects of curcumin. The rest of the clinical trials presented controversial outcomes, although the preclinical investigations showed results that proved the activity of curcumin. This discrepancy can be due to the low bioavailability of curcumin *in vivo*, derived from its low water solubility and high rate of metabolism. Thus, curcumin is subjected to a fast elimination from body²². Particularly, pharmacokinetics studies in rodents have shown that curcumin are poorly absorbed at the intestinal tract, after oral administration, and it is mostly lost with feces²³. In humans, the highest concentration of curcumin in plasma was 0.051 μ g/mL and it was reached after oral administration of 12 grams²⁴. Curcumin is also

processed by the enzyme of the phase I and II, which are in the small intestine and in the liver. They convert curcumin in more hydrophilic species, curcumin glucuronide and curcumin sulphate, inducing its elimination from the organism⁴.

4.2. Oral delivery systems for curcumin

Different strategies have been adopted to increase the bioavailability of curcumin: increasing the absorption at the intestinal tract or the inhibition of the metabolic clearance²³.

To increase the absorption of a molecule at the intestinal level, it should be considered that this process is a passive transport through the epithelium and follows the Fick's first law (Eq. 1).

$$\frac{dQ}{dt} = PA(Ca - Cb) \quad (1)$$

This equation states that the permeation rate (dQ/dt) of a molecule through a membrane is proportional to the exchange surface area of the apical side (A) and to the concentration of the molecule at the surface of the epithelium (Ca). The permeation rate also depends on the permeability coefficient of the molecule (P). Once the molecule is absorbed, it is introduced in the capillaries, which move away curcumin. Here in the basolateral side, the concentration of that molecule can be negligible ($Cb = 0$). In addition, only the soluble molecule can be absorbed, while the insoluble part is excreted with the feces.

Therefore, to increase the absorption of bioactive molecules, a good strategy is to have a high concentration of such compounds at intestinal tract. Consequently, an oral delivery system should necessarily solubilize and preserve their molecules in order to increase the number molecules available to be absorbed. More specifically, a delivery system should increase its bioaccessibility. This term refers to the fraction of the total amount of a substance that is potentially available for absorption. Bioaccessibility is therefore used to help predict bioavailability^{25,26}. In the case of the curcumin, by increasing its bioaccessibility, its

absorption increases as well. This was observed to saturate the metabolism of the phase I and II enzymes in the intestine and in the liver, leading to a prolonged half-life in the organism⁴. In fact, the inhibition of the metabolism of the enzymes of the phase I and II is another strategy that can be used for increasing the bioavailability of bioactive molecules. It can be inhibited by adjuvants that can be administrated with curcumin. For example, piperine, which is an alkaloid extracted from the black pepper or long pepper and responsible for their pungency, is an inhibitor of the hepatic and intestinal glucuronidation. The co-administration of piperine with curcumin, increases the absorption of the latter by 154% in rodents, and by 20-times in human respect to the control groups²⁷.

Several formulations were developed to increase bioaccessibility of curcumin and, consequently, its bioavailability. The use of emulsions, phospholipids complexes, liposomes and polymeric micelles have been widely used for encapsulating curcumin²⁸. Currently, since curcumin is not considered a real drug, but a nutraceutical molecule, the trend is to encapsulate it in an excipient food-based systems²⁸⁻³².

4.2.1. Functional, medical and excipient food

The research of the pharmaceutical and food industries has converged in the development of formulation able to prevent or treat human ailments. In particular, pharmaceutical industry is trying to produce drug formulations for the treatment of chronic and acute inflammations, because nonsteroidal anti-inflammatory drugs (NSAIDs) are mostly hydrophobic. On the other hand, food industry intends to design food-based approaches in order to ameliorate the human health through the diet³². Practically, there is a common interest in developing food-based formulations capable to increase the bioavailability of drugs and nutraceuticals, characterized by low water solubility. Thus, different types of food can be individuated: functional food, medical food and excipient food³².

Functional food derives from generally recognized as safe (GRAS) food ingredients and it can contain one or more food-grade bioactive compounds. For example, milk with vitamin D, yogurts with probiotic or cereals with ω -3 fatty acids, vitamins and minerals³².

Medical food consists of traditional food type (such as beverage, yogurt or confectionary) with pharmaceutical-grade bioactive molecules (drugs). Medical food can be also produces as nutritional fluid that is used to feed patients through a tube. This kind of food is administrated under medical supervision. Different preparations have been designed to manage or treat several diseases, such as Alzheimer's, diarrhea, depression, diabetes, and osteoporosis³².

Excipient food is usually used to increase the bioavailability of bioactive molecules. Generally, an excipient has not biological activity. However, it can increase the effects of the drug, when it is included in pharmaceutical formulations³³⁻³⁶. Pharmaceutical industry uses different excipients, such as lipids, surfactants, surfactants, synthetic polymers, carbohydrates, proteins, cosolvents, and salts. Similarly, an excipient food is not bioactive, but it increases the effects of nutraceutical or drugs dispersed in it. Excipient food can be very different. For instance, an excipient food can be an oil or yogurt that can help the solubilization of bioactive compounds in salads, vegetables or fruits. Previous studies have shown that a suitable dressing for a salad can increase the absorption of their carotenoids³⁷. In this case the excipient food is the oil that solubilizes the carotenoids.

4.2.2. Excipient food-base systems

As mentioned above, the limit of curcumin is its bioavailability, derived from its low solubility and high metabolism rate. This limitation can be overcome by encapsulating curcumin within an excipient-based system. This kind of formulation consist of excipient food that can help the chemical and biochemical stabilization of curcumin, increasing its bioaccessibility²⁸. Lipids, carbohydrates and proteins can be used to design such systems^{32,38-}

⁴⁶. Lipids forming micelles are able to solubilize lipophilic drugs or nutraceuticals. In fact, at intestinal tract, excipient lipids can form micelles that can solubilize the compounds and, depending on their dimensions, they can be absorbed *via* the portal vein or *via* the lymphatic route^{38,39}. Carbohydrates are abundant in food ingredients. They can be divided in digestible and not digestible, depending on their inclination to be degraded enzymatically in the gastrointestinal tract³². Starch, cellulose, pectin, alginate, chitosan and carrageenan are used as excipient food. Some of them, like pectin and alginate, can control the release of the active molecules at intestinal tract, since they are pH responsive⁴⁰⁻⁴². Pectin is also subjected to enzymatic degradation thanks to pectinase synthesized by the intestinal flora^{40,43}. Food proteins can be also used as excipient food. Proteins administrated with bioactive molecules, sensitive to the oxidation, like ω -3 fatty acids or carotenoids, can inhibit the degradation and increase absorption of these molecules⁴⁴. Lactoferrin has negative effects on the absorption of β -carotene, or casein and whey protein can alter negatively the permeability of bioactive molecules, acting on the tight junction of the intestinal epithelium^{45,46}. Finally, surfactant, minerals and chelating agents are also used as excipient food for improving the bioaccessibility of the bioactive agents³².

4.3. Polysaccharides-based system for improving curcumin bioaccessibility

Herein, to increase the bioaccessibility of curcumin water-based formulations were designed. To produce a formulation for the oral release, low-methoxy pectin (LMP), cornstarch (CS) and alginate (Alg) were used to produce particle formulations, by using the electrospray process and a calcium chloride water bath. CS and Alg were used as dispersing agents for solubilizing curcumin. In previous work, soluble starch has shown to increase the solubility of curcumin in water solutions. Then, curcumin released from this formulation, has shown to keep its antioxidant properties⁴⁷. Alginate solutions were noticed to have a dispersing effect

toward curcumin⁴⁸. LMP was used to encapsulate the CS/curcumin or Alg/curcumin solution. In fact, thanks to the presence of carboxylic groups in its structure, which can crosslink with Ca^{2+} , the releasing system can be rapidly prepared through an electrospray set-up that collects the sprayed drops in a water bath with calcium chloride. This procedure allows the crosslinking of LMP with the Ca^{2+} and the entrapment of the solutions polysaccharides containing curcumin. However, when Alg was included in the formulation, it participates to the gelation process along the LMP. As it will discuss below, it can change the release kinetic of curcumin. LMP was also used for its capability to be stable at acid pH. At low pH, LMP shrinks its structure, because of the protonation of the carboxylic group⁴⁹. This ability of LMP was widely exploited for releasing drugs at intestinal tract. In fact, since its resistance at acid pH and the absence of enzyme in the gastric juice able to degrade it, LMP can easily arrive in the gut. Here, the carboxylic groups acquire negative charges. This process induces the repulsions of the LMP chains and the loss of the particles structure. In addition, at the intestinal tract, pectinase, synthesized by the bacterial flora, can degrade LMP. Both mechanisms allow the release of drug loaded within LMP-based formulations preferentially in the gut^{50,51}.

Finally, Electrospray fabrication was used to obtain particles with high loading capacity. In this way, a very high number of curcumin molecules can reach the gut and be available for the absorption.

4.4. Experimental section

4.4.1. Analysis of the interaction CS/curcumin and Alg/curcumin

Curcumin was solubilized in ethanol with a concentration of 2mg/mL and then the same amount (5 μM) was added in water solutions with different concentration of CS, from 0 to 2.5mg/mL and Alg, from 0 to 2.5mg/mL. Curcumin was added in CS and Alg solutions

previously warmed in the microwave. Warming these solutions, CS and Alg chains were opened and hydrated. Then, since the solutions were pre-heated, the ethanol, in which curcumin was dissolved, evaporated⁴⁷. The solutions were used to investigate the fluorescence of curcumin in each solution with different concentration of CS and Alg, by using a spectrofluorometer exciting at 430 nm and acquiring the emission in a range from 470 to 700 nm.

4.4.2 Particles preparation

To prepare the particles, curcumin was dissolved in ethanol 2mg/mL and was added in a CS solution 20 mg/mL, such to have a concentration of 200µg/mL. The same amount of curcumin was added to the Alg solution 20 mg/mL. Both CS and Alg solutions were previously warmed in the microwave, as previously described. The solutions were added to an LMP solution 8% (w/v) or 4% (w/v), in order to obtain four different solutions: LMP 4%/CS 1%, LMP 2%/CS 1%, LMP 4%/Alg 1% and LMP 2%/CS 1% (the percentages are w/v). Curcumin loaded in all the solutions was 1% respect to CS or Alg. All the solutions were stirred for 15min and then they were electrosprayed through a vertical set-up, with a voltage of 30kV. At the collector, an aluminum container with 100mL of a stirred 5% calcium chloride solution was placed. The distance from the flat needle (21G) was 15 cm. After the electrospray, the particles were centrifuged three times with MilliQ water at 5000rpm for 10min, in order to remove unbound materials. The washed particles were dried by a freeze-dryer. The particles were pre-frozen by dipping in liquid nitrogen before placing in the freeze-dryer in which water was evaporated under 0.03 mbar and -49 °C. The dried particles were used for the characterizations. At the end, the following formulations were obtained: (A) LMP:CS:curc 80/19.8/0.2, (B) LMP:CS:curc 66/32.7/0.3, (C) LMP:Alg:curc 80/19.8/0.2, (D) LMP:Alg:curc 66/32.7/0.3. The respective controls are listed in Table 4.1.

Sample	Formulation
A	LMP:CS:curc 66/32.7/0.3
B	LMP:CS:curc 80/19.8/0.2
C	LMP:Alg:curc 66/32.7/0.3
D	LMP:Alg:curc 80/19.8/0.2
E	LMP:curc 99.5/0.5
F	LMP:curc 99.7/0.3
G	Alg:curc 99/1
A1	LMP:CS 66/33
B1	LMP:CS 80/20
C1	LMP:Alg 66/33
D1	LMP:Alg 80/20
E1	LMP 100-2
F1	LMP 100-4
G1	Alg 100

Table 4.1 Here the list of the formulations produced and their materials ratio.

Part of the particles from the formulations C, D, E, F and G were treated with acid vapors at room temperature for 12h hours⁵². The acid environment was obtained by filling a chamber with a 1M HCl solution and closing it after placing the particles.

4.4.3 Particles characterization

- **Morphology**

Particles morphology was characterized by scanning electron microscopy (SEM) in high vacuum with an acceleration voltage of 15kV. The samples were previously coated with a 7-nm-thick gold layer with a high-resolution sputter coater. Size analysis was performed with ImageJ software. Cross sections of the particles were obtained by infiltrating the particles with epoxy Spurr (SPI-Chem) resin. Once the resin has hardened for 48h in oven at 65°C, the blocks were cut with an ultra-microtome, until the particles were reached, and a cross section obtained. The cross sections were coated with a 7-nm-thick gold layer with a high-resolution sputter coater and observed with the SEM.

- **Encapsulation efficiency (EE) and loading capacity**

The loading capacity and EE of the different formulations were evaluated by inducing the release of curcumin in a mixture water:ethanol 1:9. The amount of curcumin was determined by correlating the absorbance at 430 nm with a calibration curve measured by using the same media. The loading capacity and the EE were calculated by equations (2) and (3):

$$\text{Loading capacity (\%)} = \frac{\text{curcumin encapsulated (mg)}}{\text{total weight of particles (mg)}} \times 100 \quad (2)$$

$$\text{EE (\%)} = \frac{\text{curcumin encapsulated (mg)}}{\text{curcumin loaded initially (mg)}} \times 100 \quad (3)$$

- **FT-IR analysis**

Particles were characterized by Fourier transform infrared spectroscopy (FTIR). Samples were measured in Attenuated Total Reflectance (ATR) mode using MIRacle ATR accessory coupled to a FTIR spectrometer. All the spectra were acquired in a spectral range from 4000 to 600 cm^{-1} , with a scanning resolution of 4 cm^{-1} , accumulating 64 scans.

4.4.4. Drug release study

Particles were weighted (20 mg) and placed in 5 mL of gastric simulated buffer (PBS 0.01 M, pH 2, pepsin 40U/mL)⁵³ at 37°C and gently stirred on a tilting plate for 2h. Successively, the particles were collected by centrifugation and put in 5 mL of intestinal simulated buffer (PBS 0.01 M, pH 7, pectinase 19U/mL, α -amylase 30U/mL)⁴³ at 37°C and gently stirred on a tilting plate for 8h. At given time points, 0.5 mL was taken out from each sample. The collected samples were centrifuged at 5000 rpm for 5 minutes at room temperature. The supernatants were measured at the spectrophotometer, while the pellets were put back in the solution with experiments, after addition of an equal volume of fresh medium. The amount of curcumin was

determined by correlating the absorbance at 430 nm with a calibration curve measured by using the same media. To the pellet, 0.5 mL of fresh medium was added and stirred. After stirring, it was put to the vials with the experiments.

4.4.5. Statistical methods

The size analysis was performed on three different batch for each sample. The average of size measurements (n = 200) was obtained along the respective standard deviations.

Three samples, from different batch, were used for FITR analysis, acquiring 3 spectra from each of them, which were averaged to obtain the final spectrum. The same samples were used to investigate the release. The average of the release from the triplicates was obtained with the respective standard deviations.

4.5. Results and discussion

4.5.1. Dispersion of curcumin in CS and Alg solutions

When an equal concentration of curcumin was added to CS or Alg solutions, its fluorescence increased, as increasing the concentration of the two polysaccharides. (Figure 5.1 and 5.2). In absence of the two polysaccharides, curcumin does not emit, because the fluorescence was quenched by the water⁵⁴. In addition, the emission peak had a blue shift, from 560 nm without the polysaccharides to 510nm with the highest CS concentration (Figure 5.1), while to 518 nm with the highest Alg concentration (Figure 5.2).

Generally, when curcumin is in aqueous solutions, its molecules tend to stack, inhibiting the fluorescence process. In hydrophobic surrounding, they are dispersed and can acquire the fluorescence ability. As previously showed, when curcumin interacts with the hydrophobic domains of casein micelles and bovine or human serum albumin, the fluorescence intensity of curcumin increases, by increasing the concentration of these dispersing agent⁵⁵⁻⁵⁷. In addition,

curcumin fluorescence can be also triggered by increasing the solution viscosity⁵⁸. Here, a similar mechanism can be supposed. CS and Alg solutions have a viscosity that solubilizes curcumin molecules. However, further studies need to be performed to understand better the interaction mechanism.

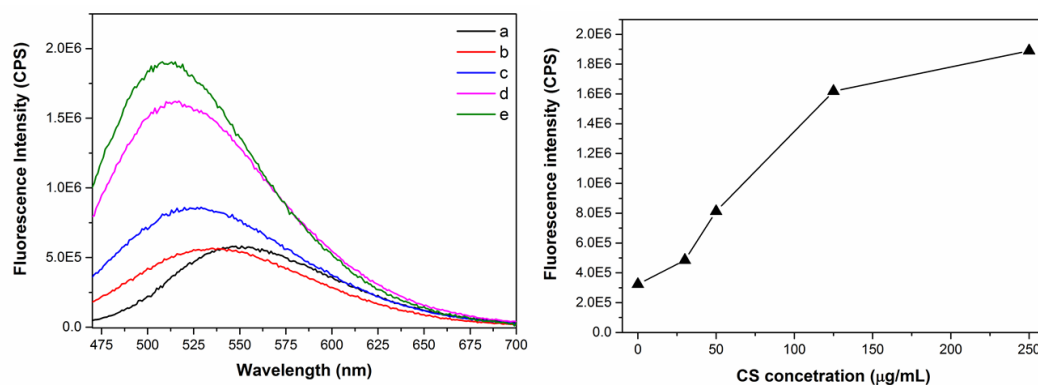


Figure 4.1 On the left, the emission spectra of curcumin (5 μM) with different concentration of CS (a = 0; b = 0.3 mg/mL; c = 0.6 mg/mL; d = 1.3 mg/mL; e = 2.5 mg/mL); on the right, the augmentation of the fluorescence intensity at 510 nm in relation to the CS concentration.

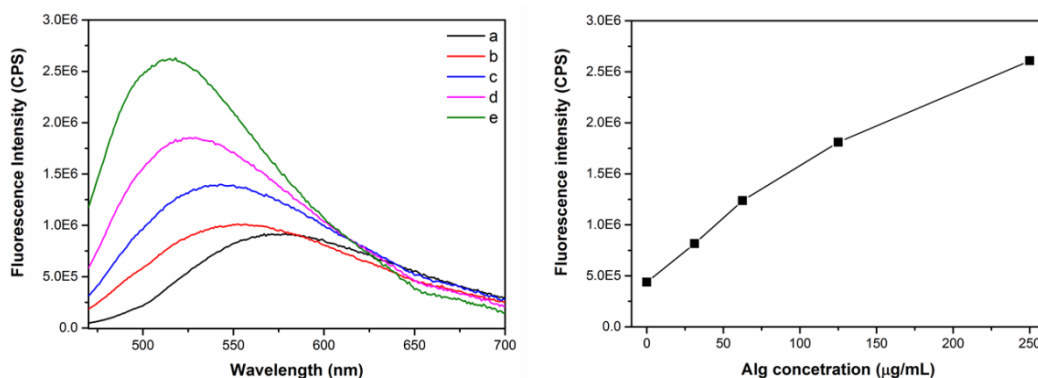


Figure 4.2 On the left, the emission spectra of curcumin (5 μM) with different concentration of Alg (a = 0; b = 0.3 mg/mL; c = 0.6 mg/mL; d = 1.3 mg/mL; e = 2.5 mg/mL); on the right, the augmentation of the fluorescence intensity at 510 nm in relation to the Alg concentration.

4.5.2. Particles characterization

Dried particles from all the samples showed rounded-like shape and wrinkled surface (Figure 5.3, 5.4, 5.5 and 5.6). Particles sizes are listed in Table 5.2. However, they were not statistically different among the formulations.

Sample	Size ($\mu\text{m} \pm \text{SD}$)
A	366 \pm 80
B	433 \pm 86
C	369 \pm 66
D	482 \pm 99
E	459 \pm 54
F	572 \pm 110
G	877 \pm 98
A1	402 \pm 82
B1	441 \pm 92
C1	477 \pm 131
D1	482 \pm 110
E1	472 \pm 85
F1	485 \pm 81
G1	927 \pm 87

. **Table 4.2** Average of the size for each formulation.

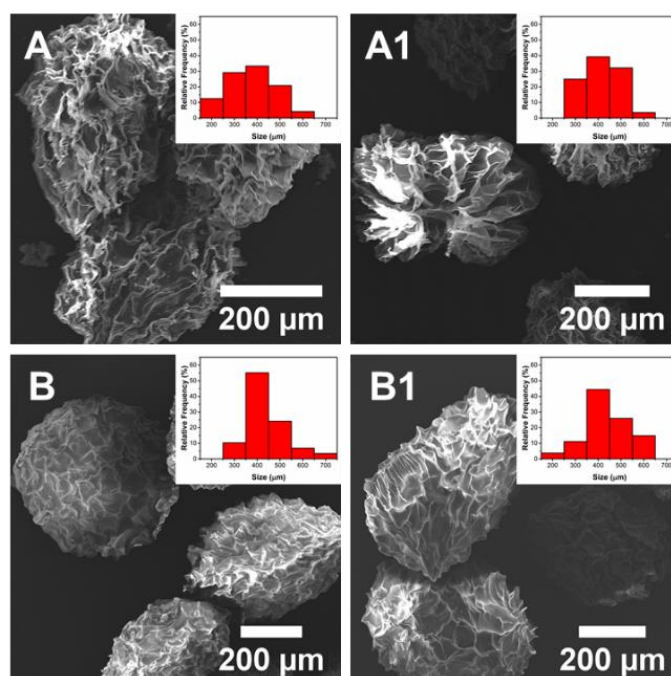


Figure 4.3 SEM images of the formulation LMP:CS A, B, A1 and B1 (see Table 5.1). In the inset, the size distribution for each sample.

Cross sections of the samples have shown that particles are characterized by internal porosity (Figure 5.7). All the samples presented a parallel porous disposition, which derived from the electrostatic stretching during the electrospray process. In cross sections of the particles A, B, A1 and B1 inclusions of materials were observed. They are relative to the presence of CS, which was embedded in the particles through the crosslinking of the LMP with the Ca^{2+} .

Contrarily, cross sections of the formulation C, D, C1 and D1 did not present such inclusions, because the Alg was crosslinked with the calcium chloride.

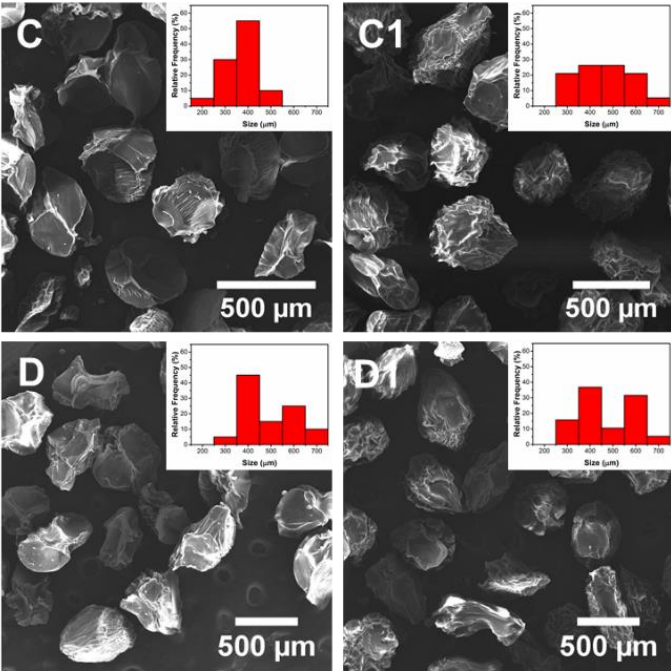


Figure 4.4 SEM images of the formulation LMP:Alg C, D, C1 and D1 (see Table 5.1). In the inset, the size distribution for each sample.

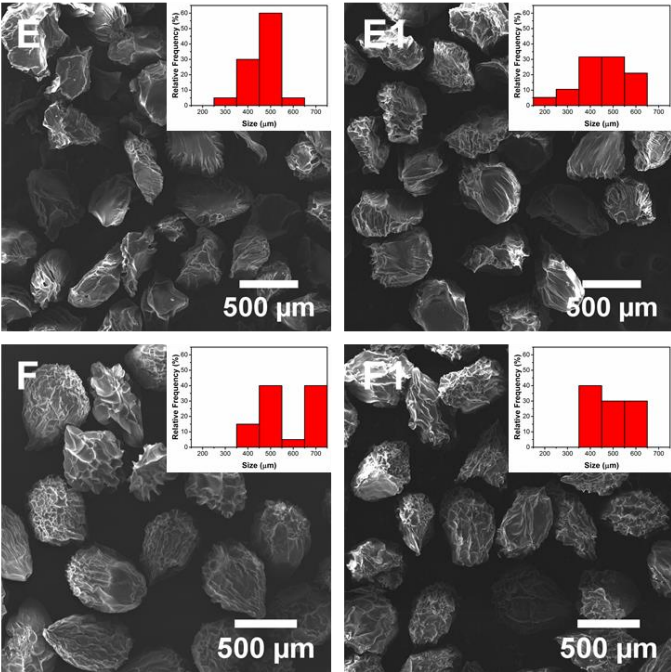


Figure 4.5 SEM images of the formulation encapsulating LMP E, F, E1 and F1 (see Table 5.1). In the inset, the size distribution for each sample.

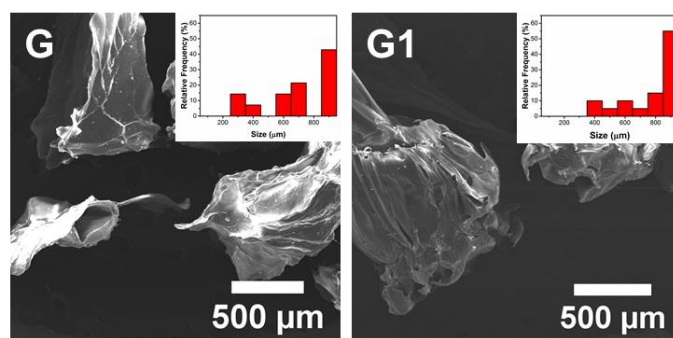


Figure 4.6 SEM images of the formulation Alg G and G1 (see Table 5.1). In the inset, the size distribution for each sample.

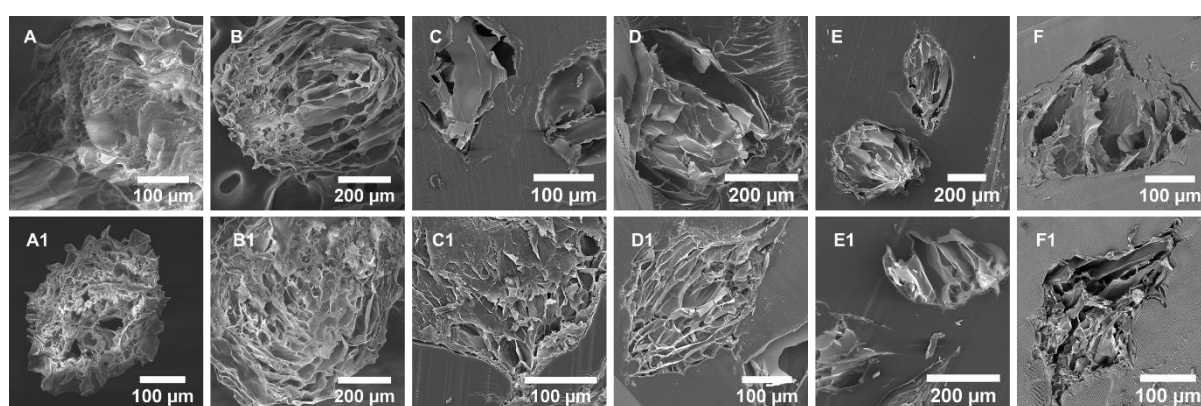


Figure 4.7 Cross sections of the dried particles from each sample.

4.5.3. Curcumin encapsulation

The results relative to the EE and loading capacity are reported in Table 5.3. Preparations A and B showed the lowest EE, respectively, $44\pm 1\%$ and $57\pm 1\%$. The formulations C, D, E and F have an EE respectively of $81\pm 2\%$, $89\pm 1\%$, $92\pm 4\%$ and $93\pm 3\%$. Particles of the formulation G had an EE of $75\pm 2\%$. The data suggested that the presence of CS affected negatively the EE. In addition, LMP resulted important for increasing the encapsulation efficiency. LMP contribute can be observed when the it is absent in the particles, like the G formulation, or when the its content is increased in the formulation. In fact, comparing the results of the A with B or C with D (in which LMP% in A and C < LMP% in B and D and C, see Table 5.1), EE was higher by 13% and 7% respectively. Finally, the loading capacity of curcumin was lower than 1% for all the formulations.

	A	B	C	D	E	F	G
EE (%)	44±0.65	57±1	81±2	89±1	92±4	93±3	75±2
Loading capacity (%)	0.18±0.03	0.15±0.03	0.3±0.02	0.2±0.01	0.28±0.03	0.22±0.03	0.21±0.01

Table 4.3 EE and loading capacity results obtained for each sample.

4.5.4. Curcumin release characterization

The aim of the study is to obtain a formulation able to preserve curcumin until the intestinal tract, where it will be absorbed. Therefore, it should reduce the release of curcumin in the gastric fluid in order to increase the bioaccessibility at intestinal tract.

To characterize the release of curcumin from each formulation, the experiment was performed in two different media, one simulating the gastric environment, the other the intestine environment. Then, the test was carried out for 10 hours. The results obtained from formulations A, B, C, D, E, F and G are reported in Figure 4.8 and summarized in Table 4.4. In gastric simulated medium, the release of curcumin from all the samples resulted slower than the release in intestinal simulated medium. This can be explained by the absence of the electrostatic repulsions among the LMP polymer chains. Since LMP has a pKa of 3.5, at pH below the carboxylic groups are protonated (-COOH)⁴¹. Therefore, the absence of coulomb repulsion induced the linear pectin molecules to interact to such an extent that they produce insoluble complexes limiting the release of curcumin⁵⁹. When the pH is increased, the carboxylic groups of LMP acquired negative charge, inducing the repulsions of the LMP chains and the loss of the particles structure, allowing a faster release of curcumin.

Analyzing the release of curcumin at acid pH, particles B and F were characterized by a kinetic slower respect to the other particles release kinetics. In fact, after 2h, B and F released respectively 36±2% and 35±1% of the total curcumin, while the other formulations A, C, D, E and G respectively 44±4%, 50±2%, 49±4%, 43±4% and 60±5%. This is because B and F were prepared by electrospraying a more concentrated LMP solution. Therefore, the structure

is more packed, and it impedes the release of curcumin. However, the formulation D, which has been also fabricated from higher concentrated LMP solution, showed a release similar to A, C and G. This suggested that the inclusion of alginate in the formulation induced a faster releasing rate of curcumin. As shown in previous work, LMP has shown to be more stable at acid pH when it is not bound to Alg⁴¹. In addition, hydrogels of LMP and Alg in a ratio 1:1 have shown to swell more than hydrogels made of Alg or LMP^{40,42}. Therefore, this could result in a faster diffusion of the curcumin, which could allow its release.

As the pH increases, the particles with CS (particles A, B, E and F,) were completely degraded and curcumin totally released after 6h. Contrarily, those with Alg (C, D and G) released about 85% of the total curcumin after 6h. The slower release of curcumin from LMP:Alg particles at higher pH is because the particles were not completely degraded. As shown in other works, crosslinked Alg and blend of crosslinked LMP:Alg, have shown a decrease of the releasing rate of molecules at neutral pH⁴².

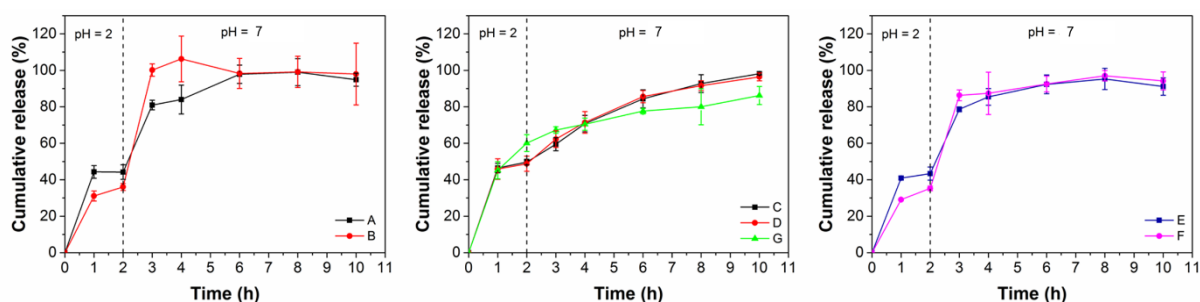


Figure 4.8 Release of curcumin from the particles formulation A, B (left), C, D, G (middle), E and F (right). The first 2h of the experiment were performed at pH = 2, while the next 8h at pH = 7. The two media were prepared as described in the experimental section.

Altogether, these data showed that the particles with CS were able to retain more curcumin at acid pH, minimizing the release of curcumin in the gastric simulated fluid, thanks to the capability of LMP to be stable at low pH. While, particles with Alg allowed a higher release of curcumin at acid pH, because the alginate participates to the releasing process, probably inducing the swelling of the particles^{40,41}. On the other hand, in the intestinal simulated fluid, LMP alone allowed a poor control on the release of curcumin, which was mostly released in 4

or 6h. Conversely, the inclusion of Alg has shown to support the sustained release of curcumin at neutral pH. Therefore, these outcomes suggested that the use of CS in the formulation did not give important advantages. In fact, besides low EE, CS allowed a poor control on the curcumin release at neutral pH. This can be a limit because sustaining the release of bioactive agents at intestinal level has shown to increase their bioaccessibility and bioavailability^{60,61}. Formulations C and D have shown to assure a control on the release of curcumin in the intestinal simulated fluid. However, they had an important loss of curcumin content in the gastric simulated medium.

Sample	Release after 2 hours (pH=2)	Release after 6 hours (pH=5,5)
A	44±4%	98±5%
B	36±2%	98±8%
C	50±2%	84±5%
D	49±4%	86±3%
E	43±4%	92±5%
F	35±1%	92±4%
G	60±5%	77±2%

Table 4.4 Summary of the release kinetics of curcumin from particle samples reported in Figure 4.8.

4.5.5. Acid vapors treatment

To overcome this limitation, a treatment with acid vapors was performed. The objective is to induce the protonation of the carboxylic groups both of LMP and Alg, such to minimize the electrostatic repulsion⁵². In this way the polysaccharides can interact, shrinking the particles structure, and reduce the curcumin release in gastric simulated medium.

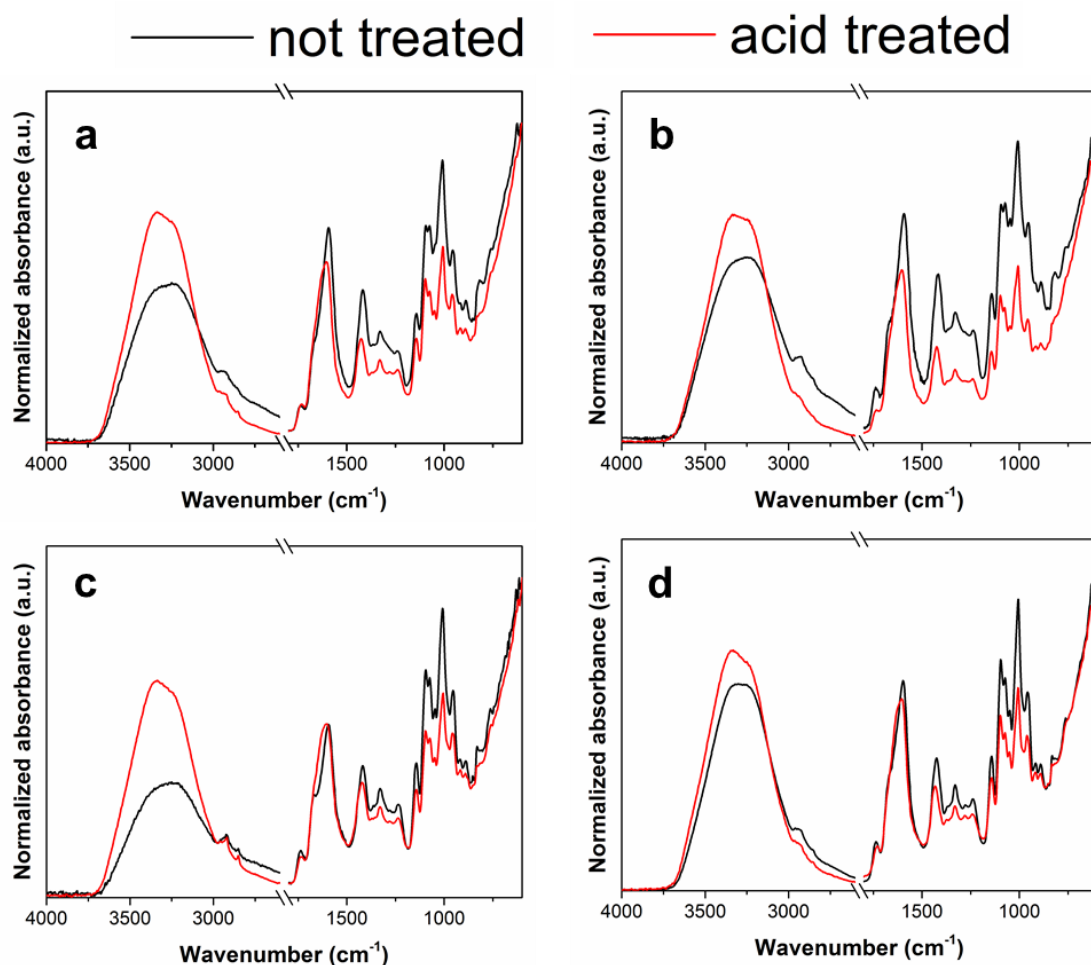


Figure 4.9 FT-IR spectra of the formulation C, D, E and F respectively in a, b, c and d, before and after the treatment with acid vapor.

Figure 4.9 shows the FT-IR spectra of the particles C, D, E and F before and after the treatment with the acid vapors. All the samples were characterized by the typical absorption band at 3250 cm^{-1} , relative to O-H stretching vibration⁶². The absorption bands between 1800 and 1500 cm^{-1} were relative to the vibration of the C=O group. In particular, the peak at 1740 cm^{-1} was referred to the stretching vibration of the methylated carboxylic group⁶³. This peak resulted low in all the samples because the pectin was low methoxylated, and therefore had a low degree of esterification. The peak occurring in the not treated sample in the range from 1590 to 1597 cm^{-1} was relative to the asymmetrical stretching of the unprotonated carboxylic group (COO^-). Furthermore, the shoulder at 1660 cm^{-1} was the asymmetrical stretching of the protonated carboxylic group (COOH)^{64,65}. By treating the particles with the acid vapors, the

contribution relative to the protonated carboxylic group increased in all the particle samples. This induced a clear shift of the peak to higher wavenumbers, suggesting the effective protonation of the carboxylic groups in the particles. Such modification can be also noticed by the sharpening and increasing of the O-H group peak, which was subjected to shift to higher wavenumbers as well.

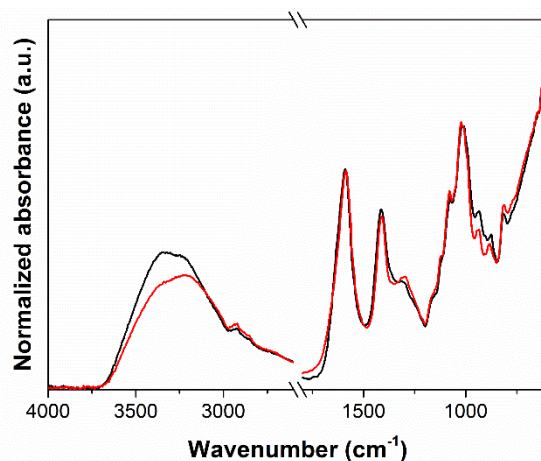


Figure 4.10 FT-IR spectra of the formulation G before and after the treatment with acid vapor. The black line is the spectrum measured before the treatment, while the red line after.

Finally, by analyzing the FT-IR spectrum relative to the formulation G, the protonation seems to not occur in those particles, in which only Alg is included (Figure 4.10). Therefore, the modification seemed to regard only the carboxylic groups of the pectin. The alginate has a range of pKa (1.5 to 3.5) lower than LMP. Therefore, if the acid vapors treatment is not sufficiently below those values, the alginate could not be modified.

4.5.6. Curcumin release from treated particles

After the treatment, curcumin release kinetic was characterized for each formulation with the same methods previously described. Briefly, particles were firstly immersed in the gastric simulated fluid for 2h. Successively, they were moved to the intestinal simulated medium and kept for 8h. The results were reported in Figure 4.11. As observed in previous paragraph, the releasing rate was slower in the gastric simulated medium, while it is faster in the intestinal

simulated medium, leading to a complete release of curcumin. Furthermore, the formulations C, D and G allowed a sustained release at neutral pH. In Table 4.5, the release kinetics obtained at pH 2 after 2h from pre-treated and post-treated particles were reported. From their comparison, it was noticed that curcumin was less released by the formulations that have been subjected to the acid vapors treatment. These results confirmed that the treatment can increase the retention of curcumin within the particles at low pH. In addition, they showed that the acid vapors treatment did not affect the capability of such formulations to sustain the release in the intestinal simulated medium.

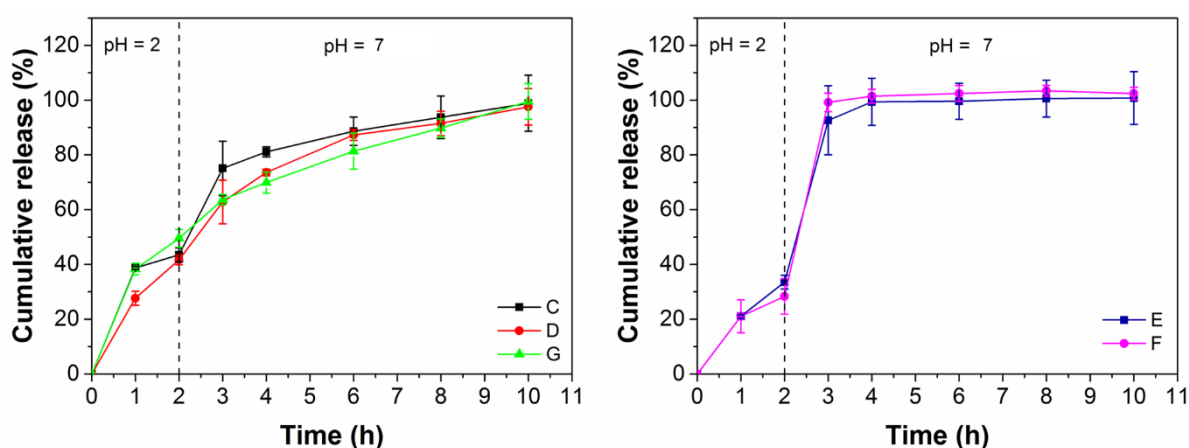


Figure 4.11 Release of curcumin from the acid vapors treated particles formulation C, D, G (left), E and F (right). The first 2h of the experiment were performed at pH = 2, while the next 8h at pH = 7. The two media were prepared as described in the experimental section.

Treatment	C	D	E	F	G
No acid	50±2%	49±4%	43±4%	35±1%	60±5%
Acid	43±3%	42±2%	34±2%	28±7%	50±3%

Table 4.5 Summary of the release kinetics of curcumin from not treated and treated particle samples after 2h (at pH = 2). The data are from graphs in Figure 4.8 and 4.11.

4.6 Conclusions

Curcumin is a nutraceutical molecule with several biological activity, such as antioxidant, anticancer, antiviral, antiarthritic, antiamyloid, and anti-inflammatory^{4,7,8}. However, this

molecule is characterized by insolubility in aqueous environment that make difficult the encapsulation in delivery system and its use as natural bioactive compound. Moreover, curcumin *in vivo* have shown to be poor bioavailable due to its low water solubility and high rate of metabolism. This entails that curcumin is subjected to a fast elimination from body²². Currently, the use of excipient food is one of the strategies that can help the solubility of nutraceutical molecules for increasing their bioaccessibility and, consequently, their bioavailability. In this chapter, the encapsulation of curcumin in polysaccharides-based particles through the electrospray have been described. The ability of CS and Alg solutions have been exploited to disperse curcumin and increase its solubility. Electro spraying LMP with different ratio of CS/curcumin and Alg/curcumin, different particles formulations were obtained. All the particles produced shown rounded-like shape, wrinkled surface and internal porosity. Particles with CS (A and B) were characterized by low EE and poor possibility to control the curcumin release at neutral pH. On the other hand, the inclusion of Alg in the formulation provided the particles C and D with high EE and granted a sustained release of curcumin in the intestinal simulated fluid. In addition, the possibility to treat the formulations with Alg, has improved the retention of curcumin at low pH within the particles, reducing the loss of curcumin in the gastric simulated medium. Therefore, such formulations have shown to be promising as system able to increase the bioaccessibility of curcumin.

4.7 Bibliography

1. Priyadarsini, K. The Chemistry of Curcumin: From Extraction to Therapeutic Agent. *Molecules* **19**, 20091–20112 (2014).
2. Yan, Y.-D. *et al.* Enhanced oral bioavailability of curcumin via a solid lipid-based self-emulsifying drug delivery system using a spray-drying technique. *Biol. Pharm. Bull.* **34**, 1179–86 (2011).
3. Hu, L. *et al.* Preparation and Enhancement of Oral Bioavailability of Curcumin Using Microemulsions Vehicle. *J. Agric. Food Chem.* **60**, 7137–7141 (2012).
4. Kurita, T. & Makino, Y. Novel curcumin oral delivery systems. *Anticancer Res.* **33**, 2807–2822 (2013).
5. Jovanovic, S. V, Boone, C. W., Steenken, S., Trinoga, M. & Kaskey, R. B. How curcumin works preferentially with water soluble antioxidants. *J. Am. Chem. Soc.* **123**, 3064–8 (2001).
6. Esatbeyoglu, T. *et al.* Curcumin-From Molecule to Biological Function. *Angew. Chemie Int. Ed.* **51**, 5308–5332 (2012).
7. Epstein, J., Sanderson, I. R. & MacDonald, T. T. Curcumin as a therapeutic agent: the evidence from in vitro, animal and human studies. *Br. J. Nutr.* **103**, 1545–1557 (2010).
8. Zhou, H., Beever, C. S. & Huang, S. The targets of curcumin. *Curr. Drug Targets* **12**, 332–47 (2011).
9. Plummer, S. M. *et al.* Inhibition of cyclo-oxygenase 2 expression in colon cells by the chemopreventive agent curcumin involves inhibition of NF- κ B activation via the NIK/IKK signalling complex. *Oncogene* **18**, 6013–6020 (1999).
10. Aggarwal, S., Takada, Y., Singh, S., Myers, J. N. & Aggarwal, B. B. Inhibition of growth and survival of human head and neck squamous cell carcinoma cells by curcumin via modulation of nuclear factor- κ B signaling. *Int. J. Cancer* **111**, 679–692 (2004).
11. Philip, S. & Kundu, G. C. Osteopontin Induces Nuclear Factor κ B-mediated Promatrix Metalloproteinase-2 Activation through κ B α /IKK Signaling Pathways, and Curcumin (Diferuloylmethane) Down-regulates These Pathways. *J. Biol. Chem.* **278**, 14487–14497 (2003).
12. Aggarwal, B. B., Kumar, A. & Bharti, A. C. Anticancer potential of curcumin: preclinical and clinical studies. *Anticancer Res.* **23**, 363–98
13. Bharti, A. C., Donato, N., Singh, S. & Aggarwal, B. B. Curcumin (diferuloylmethane) down-regulates the constitutive activation of nuclear factor-kappa B and Ikappa Balpha kinase in human multiple myeloma cells, leading to suppression of proliferation and induction of apoptosis. *Blood* **101**, 1053–1062 (2003).
14. Patel, B. B. *et al.* Curcumin targets FOLFOX-surviving colon cancer cells via

- inhibition of EGFRs and IGF-1R. *Anticancer Res.* **30**, 319–25 (2010).
15. Su, C.-C., Chen, G.-W., Lin, J.-G., Wu, L.-T. & Chung, J.-G. Curcumin inhibits cell migration of human colon cancer colo 205 cells through the inhibition of nuclear factor kappa B /p65 and down-regulates cyclooxygenase-2 and matrix metalloproteinase-2 expressions. *Anticancer Res.* **26**, 1281–8
 16. Dhillon, N. *et al.* Phase II Trial of Curcumin in Patients with Advanced Pancreatic Cancer. *Clin. Cancer Res.* **14**, 4491–4499 (2008).
 17. Capodice, J. L. *et al.* Zylflamend in men with high-grade prostatic intraepithelial neoplasia: results of a phase I clinical trial. *J. Soc. Integr. Oncol.* **7**, 43–51 (2009).
 18. Golombick, T., Diamond, T. H., Manoharan, A. & Ramakrishna, R. Monoclonal gammopathy of undetermined significance, smoldering multiple myeloma, and curcumin: A randomized, double-blind placebo-controlled cross-over 4g study and an open-label 8g extension study. *Am. J. Hematol.* **87**, 455–460 (2012).
 19. Chandran, B. & Goel, A. A Randomized, Pilot Study to Assess the Efficacy and Safety of Curcumin in Patients with Active Rheumatoid Arthritis. *Phyther. Res.* **26**, 1719–1725 (2012).
 20. Kuptniratsaikul, V. *et al.* Efficacy and safety of Curcuma domestica extracts compared with ibuprofen in patients with knee osteoarthritis: a multicenter study. *Clin. Interv. Aging* **9**, 451–8 (2014).
 21. Henrotin, Y., Priem, F. & Mobasheri, A. Curcumin: a new paradigm and therapeutic opportunity for the treatment of osteoarthritis: curcumin for osteoarthritis management. *Springerplus* **2**, 56 (2013).
 22. Sharma, R. A. *et al.* Effects of dietary curcumin on glutathione S-transferase and malondialdehyde-DNA adducts in rat liver and colon mucosa: relationship with drug levels. *Clin. Cancer Res.* **7**, 1452–8 (2001).
 23. Liu, W. *et al.* Oral bioavailability of curcumin: problems and advancements. *J. Drug Target.* **24**, 694–702 (2016).
 24. Lao, C. D. *et al.* Dose escalation of a curcuminoid formulation. *BMC Complement. Altern. Med.* **6**, 10 (2006).
 25. de Lima, A. C. S. *et al.* In vitro bioaccessibility of copper, iron, zinc and antioxidant compounds of whole cashew apple juice and cashew apple fibre (*Anacardium occidentale* L.) following simulated gastro-intestinal digestion. *Food Chem.* **161**, 142–147 (2014).
 26. Saura-Calixto, F., Serrano, J. & Goñi, I. Intake and bioaccessibility of total polyphenols in a whole diet. *Food Chem.* **101**, 492–501 (2007).
 27. Shoba, G. *et al.* Influence of piperine on the pharmacokinetics of curcumin in animals and human volunteers. *Planta Med.* **64**, 353–356 (1998).

28. Zhang, Z. *et al.* Encapsulation of curcumin in polysaccharide-based hydrogel beads: Impact of bead type on lipid digestion and curcumin bioaccessibility. *Food Hydrocoll.* **58**, 160–170 (2016).
29. Zou, L. *et al.* Enhancing nutraceutical bioavailability using excipient emulsions: Influence of lipid droplet size on solubility and bioaccessibility of powdered curcumin. *J. Funct. Foods* **15**, 72–83 (2015).
30. Zou, L., Liu, W., Liu, C., Xiao, H. & McClements, D. J. Designing excipient emulsions to increase nutraceutical bioavailability: emulsifier type influences curcumin stability and bioaccessibility by altering gastrointestinal fate. *Food Funct.* **6**, 2475–2486 (2015).
31. Zou, L., Liu, W., Liu, C., Xiao, H. & McClements, D. J. Utilizing Food Matrix Effects To Enhance Nutraceutical Bioavailability: Increase of Curcumin Bioaccessibility Using Excipient Emulsions. *J. Agric. Food Chem.* **63**, 2052–2062 (2015).
32. McClements, D. J. & Xiao, H. Excipient foods: designing food matrices that improve the oral bioavailability of pharmaceuticals and nutraceuticals. *Food Funct.* **5**, 1320–1333 (2014).
33. Kalasz, H. & Antal, I. Drug Excipients. *Curr. Med. Chem.* **13**, 2535–2563 (2006).
34. Hamman, J. & Steenekamp, J. Excipients with specialized functions for effective drug delivery. *Expert Opin. Drug Deliv.* **9**, 219–230 (2012).
35. Florence, A. T. (Alexander T. & Attwood, D. *Physicochemical principles of pharmacy: in manufacture, formulation and clinical use.* (2015). doi:10.1017/CBO9781107415324.004
36. Porter, C. J. H., Trevaskis, N. L. & Charman, W. N. Lipids and lipid-based formulations: optimizing the oral delivery of lipophilic drugs. *Nat. Rev. Drug Discov.* **6**, 231–248 (2007).
37. Burns, D. T., Brown, J. K., Dinsmore, A. & Harvey, K. K. Base-activated latent fingerprints fumed with a cyanoacrylate monomer. A quantitative study using Fourier-transform infra-red spectroscopy. *Anal. Chim. Acta* **362**, 171–176 (1998).
38. Borel, P. *et al.* Chylomicron β -Carotene and Retinyl Palmitate Responses Are Dramatically Diminished When Men Ingest β -Carotene with Medium-Chain Rather than Long-Chain Triglycerides. *J. Nutr.* **128**, 1361–1367 (1998).
39. Yáñez, J. A., Wang, S. W. J., Knemeyer, I. W., Wirth, M. A. & Alton, K. B. Intestinal lymphatic transport for drug delivery. *Adv. Drug Deliv. Rev.* **63**, 923–942 (2011).
40. Guo, J. & Kaletunç, G. Dissolution kinetics of pH responsive alginate-pectin hydrogel particles. *Food Res. Int.* **88**, 129–139 (2016).
41. Huang, X. *et al.* Enhancement of curcumin water dispersibility and antioxidant activity using core-shell protein-polysaccharide nanoparticles. *Food Res. Int.* **87**, 1–9 (2016).
42. Jaya, S., Durance, T. D. & Wang, R. Effect of alginate-pectin composition on drug

- release characteristics of microcapsules. *J. Microencapsul.* **26**, 143–153 (2009).
43. Bigucci, F., Luppi, B., Monaco, L., Cerchiara, T. & Zecchi, V. Pectin-based microspheres for colon-specific delivery of vancomycin. *J. Pharm. Pharmacol.* **61**, 41–46 (2009).
 44. Orsini Delgado, M. C., Tironi, V. A. & Añón, M. C. Antioxidant activity of amaranth protein or their hydrolysates under simulated gastrointestinal digestion. *LWT - Food Sci. Technol.* **44**, 1752–1760 (2011).
 45. Tokle, T., Mao, Y. & McClements, D. J. Potential Biological Fate of Emulsion-Based Delivery Systems: Lipid Particles Nanolaminated with Lactoferrin and β -lactoglobulin Coatings. *Pharm. Res.* **30**, 3200–3213 (2013).
 46. SHIMIZU, M. Interaction between Food Substances and the Intestinal Epithelium. *Biosci. Biotechnol. Biochem.* **74**, 232–241 (2010).
 47. Li, J., Shin, G. H., Lee, I. W., Chen, X. & Park, H. J. Soluble starch formulated nanocomposite increases water solubility and stability of curcumin. *Food Hydrocoll.* **56**, 41–49 (2016).
 48. Hjorth Tønnesen, H. Solubility and stability of curcumin in solutions containing alginate and other viscosity modifying macromolecules Studies of curcumin and curcuminoids. XXX. *Pharmazie* **61**, 696–700 (2006).
 49. Kawadkar, J., Chauhan Meenakshi, K. & Ram, A. Evaluation of potential of Zn-pectinate gel (ZPG) microparticles containing mesalazine for colonic drug delivery. *Daru* **18**, 211–20 (2010).
 50. Dongowski, G. & Anger, H. Metabolism of pectin in the gastrointestinal tract. *Prog. Biotechnol.* **14**, 659–666 (1996).
 51. Cummings, J. H. *et al.* The digestion of pectin in the human gut and its effect on calcium absorption and large bowel function. *Br. J. Nutr.* **41**, 477–85 (1979).
 52. Hajjali, H., Heredia-Guerrero, J. A., Liakos, I., Athanassiou, A. & Mele, E. Alginate Nanofibrous Mats with Adjustable Degradation Rate for Regenerative Medicine. *Biomacromolecules* **16**, 936–943 (2015).
 53. Ulleberg, E. K. *et al.* Human gastrointestinal juices intended for use in in vitro digestion models. *Food Dig.* **2**, 52–61 (2011).
 54. Jasim, F. & Ali, F. A novel and rapid method for the spectrofluorometric determination of curcumin in curcumin spices and flavors. *Microchem. J.* **46**, 209–214 (1992).
 55. Kunwar, A., Barik, A., Pandey, R. & Priyadarsini, K. I. Transport of liposomal and albumin loaded curcumin to living cells: an absorption and fluorescence spectroscopic study. *Biochim. Biophys. Acta* **1760**, 1513–1520 (2006).
 56. Barik, A., Priyadarsini, K. I. & Mohan, H. Photophysical studies on binding of curcumin to bovine serum albumins. *Photochem. Photobiol.* **77**, 597–603 (2003).

57. Sahu, A., Kasoju, N. & Bora, U. Fluorescence Study of the Curcumin–Casein Micelle Complexation and Its Application as a Drug Nanocarrier to Cancer Cells. *Biomacromolecules* **9**, 2905–2912 (2008).
58. Patra, D., El Khoury, E., Ahmadieh, D., Darwish, S. & Tafech, R. M. Effect of Curcumin on Liposome: Curcumin as a Molecular Probe for Monitoring Interaction of Ionic Liquids with 1,2-Dipalmitoyl-sn-Glycero-3-Phosphocholine Liposome. *Photochem. Photobiol.* **88**, 317–327 (2012).
59. Ashford, M., Fell, J., Attwood, D., Sharma, H. & Woodhead, P. Studies on pectin formulations for colonic drug delivery. *J. Control. Release* **30**, 225–232 (1994).
60. Skinner, M. & Hunter, D. *Bioactives in fruit : health benefits and functional foods*. (Wiley Blackwell, 2013).
61. Siddiqui, I. A., Adhami, V. M., Ahmad, N. & Mukhtar, H. Nanochemoprevention: Sustained Release of Bioactive Food Components for Cancer Prevention. *Nutr. Cancer* **62**, 883–890 (2010).
62. Samout, N. *et al.* Therapeutic effect of apple pectin in obese rats. *Biomed. Pharmacother.* **83**, 1233–1238 (2016).
63. Yang, X. *et al.* Low methoxyl pectin gelation under alkaline conditions and its rheological properties: Using NaOH as a pH regulator. *Food Hydrocoll.* (2017). doi:10.1016/j.foodhyd.2017.12.006
64. Neufeld, L. & Bianco-Peled, H. Pectin–chitosan physical hydrogels as potential drug delivery vehicles. *Int. J. Biol. Macromol.* **101**, 852–861 (2017).
65. Vityazev, F. V. *et al.* Pectin-silica gels as matrices for controlled drug release in gastrointestinal tract. *Carbohydr. Polym.* **157**, 9–20 (2017).

Chapter 5

Conclusions

5.1 Final remarks

Thanks to the versatility of the electrospinning procedures, ECA polymers was electrospun such to obtain highly aligned fibrous mats, by using a rotating collector. Electrospun aligned fibers were used to modified glass surfaces, through a thermal treatment. The partial melting of the ECA aligned fibers, left a coating on the glass surface, which derived from the electrospun fibers topography. When myoblast cells were seeded on the coating, the oriented topography demonstrated the ability to align the cells, modifying their morphology. Such device could be potentially used as substrate for the regeneration of the skeletal muscle tissue *in vitro*, since the myoblasts were able to sense to topographical cues of the coating, thereby enabling their oriented disposition. Moreover, the possibility to produce large mats by the electrospinning can eliminate the problems related to the size of the tissue to be replaced.

Next steps will be aimed at investigating the ability of the aligned substrates to support the differentiation of the myoblasts, analyzing the expression of the gene typical of this phase.

Electrospinning was used to encapsulate hPL in silk fibroin fibers, such to fabricate active wound dressing. In such device, the properties of the electrospun fibrous materials were combined with those of silk fibroin and hPL. In fact, electrospun fibers can be used as wound dressings that allow efficient gas exchange, to absorb wound exudate as well as support cell proliferation and migration. All the above-mentioned features successfully mimic the natural extracellular matrix, thus improving and sustaining the healing process of the wounds. Silk fibroin was able to control the release of proteins, depending on its crystallinity degree, and preserve the activity of sensitive molecules, improving their shelf life. More specifically, the crystallinity degree of silk fibroin was finely controlled by using water vapor treatment. Silk fibroin has also shown to increase the stability of the hPL upon a thermal treatment (60°C), confirming its preserving activity toward sensitive molecules. The hPL has important potential as therapeutic tool for chronic wound, but currently is used as a gel. Therefore, the proposed engineered fibers could facilitate the use of hPL for wound healing and in medical procedures. Electrospun patches are readily applicable to the wound site, similarly to a gauze. Furthermore, it could have a pre-determined release kinetic and could be prepared and store as ready-to-use devices thanks to the preservation of the hPL activity and the prolonged shelf life granted by the silk fibroin matrix. Future analysis will investigate the release of the growth factors and proteins that form the hPL. In this way, a complete characterization of the kinetic release will be obtained, and the release of each protein could be pre-determined, according to silk fibroin crystallinity.

Electrospray was used to fabricate particles able to encapsulate curcumin, by using CS, Alg and LMP. Electrospray provided the particle system with high loading of curcumin, rounded-like shape, wrinkled morphology and internal porosity. Then, the use of CS and Alg have

allowed the dispersion of curcumin. Comparing the results of the curcumin release assessment, respect to the LMP:CS, the particle system LMP:Alg have shown higher EE, a reduced loss of curcumin in gastric simulated fluid, upon acid vapors treatment, and a better control of the release in the intestinal simulated medium, allowing the sustained release of curcumin. An excipient food-based system with these characteristics would have a good impact on the bioaccessibility of the curcumin at intestinal tract. Therefore, the next investigations will regard the characterization of the absorption of curcumin *in vivo* and understand the efficiency of the system in increasing the bioavailability of curcumin.